2017

Higher-order modulation theory for resonant flow

Mohammed Daher Albalwi
University of Wollongong

Higher-order modulation theory for resonant flow

A thesis presented for the degree of

Doctor of Philosophy

Mohammed Daher Albalwi

Supervisors

Professor Timothy Marchant, University of Wollongong

Professor Noel Smyth, University of Edinburgh, UK

School of Mathematics and Applied Statistics

Faculty of Engineering and Information Sciences

University of Wollongong

Australia

2017

Abstract

The flow of a fluid over topography in the long wavelength, weakly nonlinear limit is considered, for both isolated obstacles and steps or jumps. The upstream flow velocity is assumed to be close to a linear long wave velocity of the unforced flow, so that the flow is near resonant. Higher order nonlinear, dispersive and nonlinear-dispersive terms beyond the Korteweg-de Vries approximation are included, so that the flow is governed by a forced extended Korteweg-de Vries equation.

For the isolated obstacle, modulation theory solutions for the undular bores generated upstream and downstream of the forcing are found and used to study the influence of the higher-order terms on the resonant flow, which increases for steeper waves. These modulation theory solutions are compared with numerical solutions of the forced extended Korteweg-de Vries equation for the case of surface water waves. Good comparison is obtained between theoretical and numerical solutions, for properties such as the upstream and downstream solitary wave amplitudes and the widths of the bores. They are also compared with numerical solutions of the forced extended Benjamin-Bona-Mahony equation, which is asymptotically equivalent to the forced extended Korteweg-de Vries equation, but is numerically stable for higher amplitude waves.

The usefulness of uniform soliton theory is also considered, for waves generated by an obstacle. It is based on the conservation laws of the extended Korteweg-de Vries equations for mass and energy and assumes that the upstream wavetrains is composed of solitary waves. We compare the solutions with theoretical and numerical solutions of the

forced extended Korteweg-de Vries equation and the forced extended Benjamin-Bona-Mahony equation, to fully assess this approximation method for upstream solitary wave amplitude and wave speed.

The flow of a fluid over a step or jump is also examined, and is a variation on the problem of flow over an isolated obstacle. Higher-order modulation theory solutions, based on the extended Korteweg-de Vries equation, for the undular bores generated upstream and downstream of the forcing are found. It is shown that an upstream propagating undular bore is generated by a positive step and formed by an elevation upstream of the step, and a downstream propagating undular bore is generated by a negative step and formed by a depression downstream of the step. An excellent comparison is obtained between the analytical and numerical solutions.

Certification

I, Mohammed Daher Albalwi, declare that this thesis, submitted in partial fulfilment of the requirements for the award of Doctor of Philosophy, in the School of Mathematics and Applied Statistics, University of Wollongong, is wholly my own work unless otherwise referenced or acknowledged. The document has not been submitted for qualifications at any other academic institution.

_____

March 2017

Mohammed Daher Albalwi

Acknowledgements

I would like to express the deepest appreciation to my supervisors, Professor Timothy Marchant and Professor Noel Smyth for their support, advice and encouragement and willing to share their wealth of knowledge during the time of my doctoral research.

I am also thankful to the Government of Saudi Arabia for through the awarding of a PhD Scholarship by King Abdullah bin Abdulaziz program.

Finally and most importantly, this thesis is especially dedicated to my beloved family. To my parents, lovely brothers and sisters, dearest wife and my lovely sons (Abdulellah, Abdulrahman and Omar) for their unfailing support and long patience, I am extremely grateful.

Table of Contents

Abstract ii

Certification iv

Acknowledgements v

Table of Contents vi

1 Introduction 1
- 1.1 Solitary waves and solitons . . . 2
- 1.2 The KdV equation and its extensions . . . 5
- 1.3 Modulation theory . . . 8
- 1.4 Undular bores . . . 10
- 1.5 Studies and observations of bores and resonant flow . . . 12
- 1.6 Objectives and thesis plan . . . 19

2 Higher-order modulation theory for resonant flow over an isolated topography 22
- 2.1 Introduction . . . 22
- 2.2 Derivation of forced eKdV equation . . . 27
- 2.3 Higher-order modulation theory . . . 33

3 Comparison of theoretical and numerical results for resonant flow over an isolated obstacle 50
- 3.1 Comparison with numerical results . . . 54
- 3.2 Conclusions . . . 67

4 Comparison of theoretical results and numerical solutions for the forced eBBM equation 69
- 4.1 Results and discussion . . . 71
- 4.2 Conclusions . . . 82

5 Uniform soliton theory 84
- 5.1 Introduction . . . 84
- 5.2 Mass and energy conservation law for the eKdV equation . . . 85
- 5.3 Results and discussion . . . 88

5.4 Conclusions 94

6 Resonant flow over a step **95**
6.1 Introduction 95
6.2 The steady-state solution, for flow over a step 97
6.3 Comparison with numerical results 114
6.4 Conclusions 121

7 Conclusions and future work **122**

Appendix **126**

A The numerical schemes **126**
A.1 The forced eKdV equation 126
A.2 The forced eBBM equation 127

Chapter 1

Introduction

Waves are disturbances that travel through space and time at finite velocity and transfer energy from one location to another. One well studied example is water waves, a ubiquitous phenomenon with applications that include ocean waves generated by tides, wind or earthquakes. Water waves can propagate on the water surface or within a density stratified ocean, and occur due to the forces of gravity and surface tension. The propagation of water over obstacles or shelves, such as occurs on the ocean floor, leads to the generation of solitary waves and undular bores. These bores occur in many applications ranging from oceans, the atmosphere to optical fibres. Moreover, a vast range of mathematical techniques and theories exist for studying these phenomena.

One of the first theoretical insights into water waves was by Isaac Newton who deduced the frequency of deep water waves in his Principia, Newton (1687). Pierre Laplace, Leonhard Euler, Joseph Lagrange, Siméon Poisson and Augustin Cauchy all followed and made theoretical improvements to the linear theory of water waves during the eighteenth and early nineteenth centuries, see Darrigol (2003); Craik (2004), for comprehensive reviews of these historical developments.

In 1755 Leonhard Euler derived the equations of motion (hydrodynamics) for an ideal fluid. Subsequently, Lagrange (1781, 1786) found the linearized governing equations for small amplitude waves. The Euler equations for inviscid flow together with the appropriate free surface boundary conditions describe the motion of water waves. The Euler water wave equations lead to various approximations for small amplitude and long waves, such as the Korteweg-de Vries (KdV) and Benjamin, Bona, and Mahony (BBM) equations.

1.1 Solitary waves and solitons

One key wave phenomenon is the solitary wave, which maintains its coherence and propagates with constant shape and speed. Solitary waves consist of an isolated pulse, which propagates without change of shape due to a balance between nonlinearity and dispersion (or diffraction).

In 1834, the British engineer, John Scott Russell, made the first recorded observations of solitary waves, which were created by a canal barge travelling along the Union canal in Edinburgh, UK, Russell (1844). He observed that a hump-like wave travelled along the canal without changing its shape or its speed over a large distance and he called it a "wave of translation". Before this time, the expectation was that all waves were oscillatory and existing wave theory was not able to explain this phenomenon. Russell deduced that a nonlinear effect must have caused this new type of wave.

Later, the problem caught the attention of scientists, which led to theoretical investigations by Boussinesq (1871, 1877). He derived an approximate nonlinear equation for weakly nonlinear, dispersive shallow water waves. Also, theoretical investigations were made by Rayleigh (1876) for weakly nonlinear, dispersive water waves. Both sets of

work confirmed Russell's observations. Not long after that, Diederik Korteweg and his Ph.D student, Gustav de Vries, derived a nonlinear partial differential equation governing the phenomenon, Korteweg and de Vries (1895). The so called KdV equation has since been used in many fields of physics and applied mathematics. The KdV equation can be derived from the Euler water wave equations by assuming long wavelength and small amplitude waves, see Marchant and Smyth (1990). The KdV equation in standard form is

$$\eta_t + 6\eta\,\eta_x + \eta_{xxx} = 0.$$

The KdV equation includes two competing effects: linear dispersion, η_{xxx}, that describes the spreading of the wave, and nonlinearity, $\eta\,\eta_x$, that accounts for the steepening of the wave. The balance between the effects of nonlinearity and dispersion results in a stable solitary wave.

Much later, Zabusky and Kruskal (1965) considered numerical simulations of the evolution of an initial condition into solitons and their interaction. The KdV equation is the continuum limit of a $1-D$ anharmonic lattice employed by Fermi et al. (1955) to explore the energy distributed between the many possible oscillations that can occur in a nonlinear lattice. Zabusky and Kruskal showed that KdV solitary waves have elastic properties as they interact with each other with no change in speed and shape. They coined the term "soliton" for the KdV solitary waves due to their elastic nature upon collision.

Gardner et al. (1967) discovered a method, termed the inverse scattering transform (IST), to find an exact solution of the initial value problem (IVP) for the KdV equation. The IST technique is considered to be the primary technique for the study of integrable equations such as the KdV equation. However, in practice it is extremely difficult to determine solutions via the IST and other methods are used. For example, the solution of the

IVP problem for the KdV equation was obtained on the semi-infinite line, for both constant and time dependent boundary values using a range of other techniques, Marchant and Smyth (1991). Hirota (1971) developed an important technique for integrable nonlinear evolution equations to construct multisoliton solutions that is relatively simple to use. He used his method to find the N-soliton solution for the KdV equation and many other equations such as sine-Gordon equation, Hirota (1972).

The nonlinear Schrödinger (NLS) equation is another universal weakly nonlinear wave model with applications that include water wave stability, see Zakharov (1968). Hirota (1973) used his method to find the N-soliton solution for the NLS equation. Besides describing water waves, it is highly relevant in many other physical applications, for example nonlinear optics, plasma physics, quantum condensates, hydrodynamics, nonlinear instability phenomena, nonlinear acoustics, the propagation of nonlinear waves in uniform media, see Zakharov and Shabat (1972); Hasegawa and Tappert (1973); Chen and Liu (1978).

Benjamin et al. (1972) considered a model equation for weakly nonlinear shallow water waves, which is asymptotically equivalent to the KdV equation, in the limit of small wave amplitude. The BBM equation or regularized long-wave (RLW) equation has superior numerical stability properties compared with the KdV equation, for which high wave numbers are unstable. It has superior stability properties are due to a bounded dispersion relation, for large wave numbers. The BBM equation only has three integrals of motion, while the KdV equation has an infinite number, indicating the non-integrability of the BBM equation compared with the KdV equation, see Olver (1979). The BBM equation can be obtained from the KdV equation by replacing the dispersive term η_{xxx},

with an asymptotically equivalent η_{xxt}, term. Bona et al. (1985) solved the BBM equation numerically to model the propagation of water waves in a channel. Marchant (2000) used an extended BBM (eBBM) equation to consider solitary wave interactions for the case of surface waves on shallow water.

1.2 The KdV equation and its extensions

The KdV equation is a generic nonlinear wave equation describing weakly nonlinear long waves. It is also an integrable equation possessing an inverse scatting solution, so that, in principle, its analytical solution is completely determined. Aside from the mathematical aspects, the KdV equation arises in a wide range of physical applications, including water wave theory and plasma physics, for which weak nonlinearity is balanced by weak dispersion, see Whitham (1974).

For some applications, the modified KdV (mKdV) equation, with cubic nonlinearity,

$$\eta_t + 6\alpha\eta^2\eta_x + \eta_{xxx} = 0,$$

is appropriate. Like the KdV equation it is integrable. It appears in many physically important nonlinear problems. For example, applications include electrohydrodynamics, Perel'man et al. (1974), elastic media, Matsutani and Tsuru (1991) and internal waves, Grimshaw et al. (1997).

The combined KdV-mKdV or Gardner equation (which combines quadratic and cubic nonlinearity),

$$\eta_t + 6(\eta + \alpha\eta^2)\eta_x + \eta_{xxx} = 0,$$

is also an important integrable model, as it describes many nonlinear phenomena such

as ocean waves and internal solitary waves in shallow seas, see Melville and Helfrich (1987), as it includes some higher order nonlinear effects. Besides being a model for water waves, the Gardner equation has a variety of other applications such as solid state physics and quantum field theory, Vassilev et al. (2011). In the field of plasma physics, Watanabe (1984) studied ion acoustic solitons theoretically using the Gardner equation and the modified KdV equation. In plasmas with negative ions, the propagation of nonlinear ion-acoustic waves is governed by the Gardner equation, see Ruderman et al. (2008).

The extended KdV equation (eKdV), which includes nonlinear and dispersive terms one order beyond the KdV approximation, was derived from the water wave equations by Marchant and Smyth (1990). This higher order model was shown to be asymptotically integrable, but no exact higher order soliton solutions are known. A third order extension to the KdV equation can be found, see Marchant (2002b), with corrections two orders beyond the KdV approximation. In follow up work, Marchant (2004) obtained asymptotic solitary wave interactions for this third order equation. For the case of non-zero surface tension, the second and third order equations are given in Burde (2011). Recently, a new KdV-type equation was derived by Karczewska et al. (2014a,b), which included topographical effects for a variable bottom.

The forced KdV equation describes the flow over an obstacle of small amplitude and is considered an universal model, and has been derived by many authors. This equation has several interesting physical applications, including quantum phenomena, hydrodynamics, oceanographic applications and electric currents. The forced KdV equation is derived from the water wave equations and the forcing function represents the bottom topography. A special case is the transcritical or resonant regime in which the background fluid

velocity is close to one of the linear long wave velocities of the underlying stratified flow. In this regime energy cannot escape from the vicinity of the forcing and the generated waves become nonlinear, Baines (1984, 1995). In particular, in the resonant regime it was found that a strongly nonlinear upstream propagating wavetrain was generated which resembled an undular bore, Baines (1984).

Akylas (1984) derived a forced KdV equation for water waves, which governs near-resonant flow in the long wavelength weakly nonlinear limit. In his numerical study he showed that a series of solitons are generated upstream of the obstacle. As well, the KdV equation with a forcing term was derived by Cole (1985) for water waves. Again, numerical results show that solitons are generated upstream of the forcing. Mei (1986) derived the forced KdV equation for water waves forced by slender bodies and he extended the theory by representing the forcing term as the sum of terms travelling in the channel at near critical speeds. Wu (1987) found a family of forced steady solitary waves in the analysis of the stability of solutions of the forced KdV equation and also derived relations based on mass, energy and momentum of the forced KdV equation, which gave results in good agreement with numerical results. Lee et al. (1989) derived the forced KdV equation for water waves and good agreement was obtained between experimental results and two theoretical models, the forced KdV equation and the generalized forced Boussinesq equation. They considered two types of forcing, a bottom topography and an external surface pressure. Furthermore, they found that a succession of solitary waves occurs, steadily advancing upstream of the disturbance, whereas a train of weakly dispersive nonlinear waves is generated downstream.

Grimshaw and Smyth (1986) derived a forced KdV equation for resonant internal

waves. They modelled the upstream flow by a series of equal amplitude KdV solitons and found their amplitude by mass and energy conservation. The downstream wave train was found using the undular bore solution of the KdV equation and excellent agreement with numerical solutions was found. Melville and Helfrich (1987) derived the forced KdV equation for internal waves. They examined the transcritical flow of a two-layer fluid over bottom topography and they showed that in a subcritical regime an undular bore is generated upstream rather than a train of solitons.

1.3 Modulation theory

Modulation theory is a well established method for studying slowly-varying oscillatory wavetrains by describing the evolution of its slowly varying parameters such as amplitude and mean level. Whitham (1965a,b, 1974) derived the modulation equations for the KdV equation, based on averaging its conservation laws. In addition, Whitham developed an elegant method to determine these modulation equations based on the use of averaged Lagrangians, with the method now referred to as averaged Lagrangian theory. Whitham derived the modulation equations of the cnoidal wave solution of the KdV equation, Whitham (1965b, 1974). These form a third order hyperbolic system for the amplitude, wavenumber and mean height of the cnoidal wave. When the underlying wavetrain is modulationally stable, the modulation equations are hyperbolic, see Whitham (1974) for further details. One special solution of hyperbolic partial differential equations is the centred simple wave solution, which is generated from an initial condition linking two levels via a discontinuous jump. Gurevich and Pitaevskii (1974) found that the simple wave solution of the modulation equations of the KdV equation, which physically de-

scribes an undular bore. This is the dispersive equivalent of a gas dynamic shock wave, an example of which is a tidal bore, Fornberg and Whitham (1978). In the framework of the Gardner equation, modulation theory was developed for undular bores by Kamchatnov et al. (2012). They used a reduced version of the finite-gap integration method in Riemann invariant form.

Theoretical work based on the forced KdV equation has used modulation theory to describe both the upstream and downstream propagating wavetrains that are generated, Smyth (1987). These wavetrains are described in terms of the simple wave solution of the modulation equations of the KdV equation, the undular bore solution. Smyth (1987) obtained a good estimate for the flow over isolated topography by using the undular bore solution of the KdV equation and showed that the modulated cnoidal wavetrain modelled both the upstream and downstream flows. Modulation theory for the forced eKdV equation, including second order terms, was derived by Marchant and Smyth (1990) as simple wave solutions for the eKdV modulation equations. In general, these simple wave solutions are not full undular bores as waves are continuously generated at the forcing, so that the bores do not fully develop to a constant level when they terminate at the forcing. These bores are termed partial bores, Smyth (1987).

Modulation theory solutions for resonantly forced flow was found to be in excellent agreement with numerical solutions, Grimshaw and Smyth (1986); Smyth (1987); Lee et al. (1989) and experimental results, Smyth (1988). Grimshaw et al. (2007b) derived modulation theory for transcritical flow over a step governed by the forced KdV equation, which also generates upstream and downstream undular bores. Transcritical flow of a stratified fluid was studied using the Gardner equation for higher amplitude flows over a

broad localised obstacle for both possible signs of the cubic nonlinear term, Kamchatnov et al. (2013).

Partial undular bores were subsequently found to occur for the solution of the initial boundary-value problem for the KdV equation, Marchant and Smyth (1991, 2002). They studied the initial boundary-value problem on the positive and negative quarter-plane. The positive quarter plane is for solutions in $x > 0$ and $t > 0$ while the negative quarter plane is for $x < 0$, $t > 0$. They found that five qualitatively different kinds of solution can occur with a good agreement with numerical solutions.

For the modified KdV equation, the modulation equations were derived by Driscoll and O'Neil (1976), based on Whitham's modulation theory. The modulation equations are based on the roots of the polynomial governing the periodic wave; for real roots the waves are stable, while for complex roots the waves are unstable. Marchant (2008) found a new type of undular bore, based on finite amplitude sinusoidal waves for the modified KdV equation. At the leading edge of the bore the algebraic mKdV soliton occurs.

Whitham modulation theory has been generalised to other integrable equations with many physical applications. Marchant and Smyth (2006b) developed modulation theory for the periodic peakon solution of the Camassa-Holm equation, and found the undular bore solution for this equation, which had turning points related to a minimum nonlinear group velocity.

1.4 Undular bores

An undular bore, also termed a dispersive shock wave, smoothly joins together two different mean levels. In an undular bore, dispersion rather than dissipation (damping) smooths

out an initial discontinuity, say in fluid level or density. A constantly expanding modulated wavetrain then links the two levels. The study of undular bores is highly relevant to many wave phenomena generated in the ocean and the atmosphere, see Smyth and Holloway (1988). Tidal bores occur at several well-known locations, such as the River Severn in the U. K., Qiantang river in China, Bay of Fundy in Canada and Cook Inlet in the U.S.A. The tide forces water upstream into a narrowing river or bay, for which the focussing effects outweigh frictional forces, leading to an undular bore. In coastal regions of the oceans, internal solitary waves of large amplitude are observed, which occur due to the interaction of the barotropic tide with the shelf break. The interaction of tidal forces and bottom topographies are a common mechanism for generating internal waves. Internal waves occur in many natural applications, such as in the atmosphere and in the ocean. The internal waves can move throughout the ocean for several hours and stretch tens of kilometres in length.

Apel et al. (1985) have detailed observations of internal solitary waves generated in the Sulu Sea in the Philippines and gave descriptions of their features. Figure 1.1 shows internal solitary waves propagating in the Sulu Sea between Malaysia and the Philippines, which are moving to the northeast toward Palawan Island. In this figure the waves are a few kilometres in length. Arvelyna and Oshima (2007) modelled internal waves by using a KdV model around Tsushima Strait. They predicted the generation of strong currents, associated with the internal waves, which were compared with observation from satellites with good agreement found. Figure 1.2 shows a satellite image of internal waves around Tsushima Island in the Korean Strait. The imaged area is 60 kilometres $\times$ 120 kilometres. It clearly shows two wave packets propagating toward Tsushima Island, one at the top and

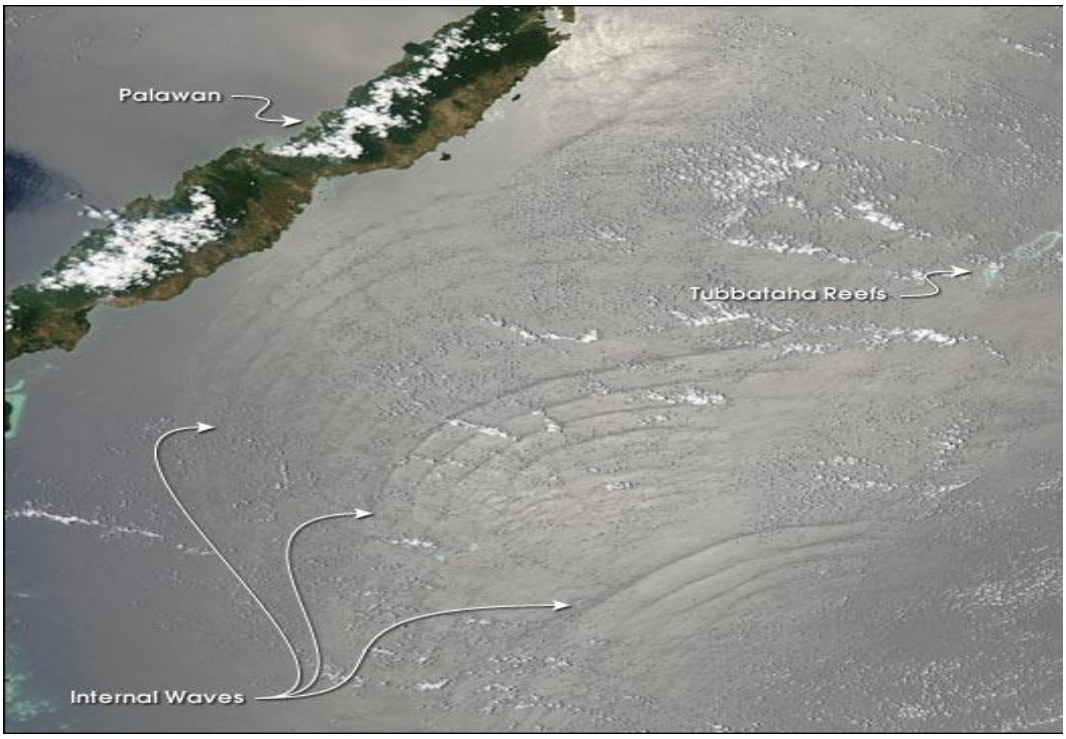

Figure 1.1: Internal waves in the Sulu Sea, image July 1, NASA (2003).

the other at the bottom of the image. It can be seen from the figure that the packet crest lengths range between 30 – 40 kilometres in length.

1.5 Studies and observations of bores and resonant flow

By the middle of the 20th century, laboratory observations of solitary waves had been made by many researchers. One of the earliest observations of solitary waves in a laboratory were published by Thews and Landweber (1935, 1936). They observed that a ship model proceeding steadily can generate upstream waves in towing tanks. Davis and Acrivos (1967) used a tank 2.5 m long, 10 cm wide and 40 cm deep and filled with a stratified solution of water and salt. They created two layers of constant density by floating fresh water onto the salt water, with an intermediate layer of 1 cm thickness, that

Figure 1.2: Internal waves in the the Korea Strait, ASTER falsecolor VNIR image acquired on 4 July 2000 at 0232 UTC. , NASA (2006).

led to the generation of solitary waves. In one propagation direction and for moderate amplitudes, the predictions of the KdV equation were tested experimentally in relatively shallow water of uniform depth, Hammack and Segur (1974). They showed that the KdV equation is a good model to describe the evolution of gravity waves of moderate amplitudes. Zhang et al. (2007) experimentally studied internal gravity waves over bottom topography represented by a semi-circular cylinder and described its features. The generation of internal solitary waves over variable topography was examined by the laboratory experiments of Chen (2007). Transcritical flow past a ship was studied experimentally by Gourlay (2010). He obtained experimental results, at ship speeds close to the critical speed, of the actual flow patterns that occur in open water or confined channels. Figure 1.3 displays a photograph of the upstream solitary wave produced by a ship model, in the confined channel used in their study.

Theoretical studies of internal solitary waves have been used to describe observations of waves in fjords and lakes, shallow coastal seas, and the atmospheric boundary layer, Grimshaw (2003). Ostrovsky and Stepanyants (2005) reviewed laboratory experiments of internal solitary waves and compared experimental results to theoretical models. The model equations including the KdV, Gardner, Benjamin-Ono and the Joseph-Kubota-Ko-Dobbs equations. They concluded that the KdV equation describe properties of solitary waves of moderate amplitude extremely well.

The study of internal waves, generated by the semi-diurnal tides on the Australian North West Shelf has been the subject of many papers over the last decades, and were observed from satellite data by Baines (1981). They occur due to interactions between the tide and the continental shelf break. The KdV equation was found to be a useful

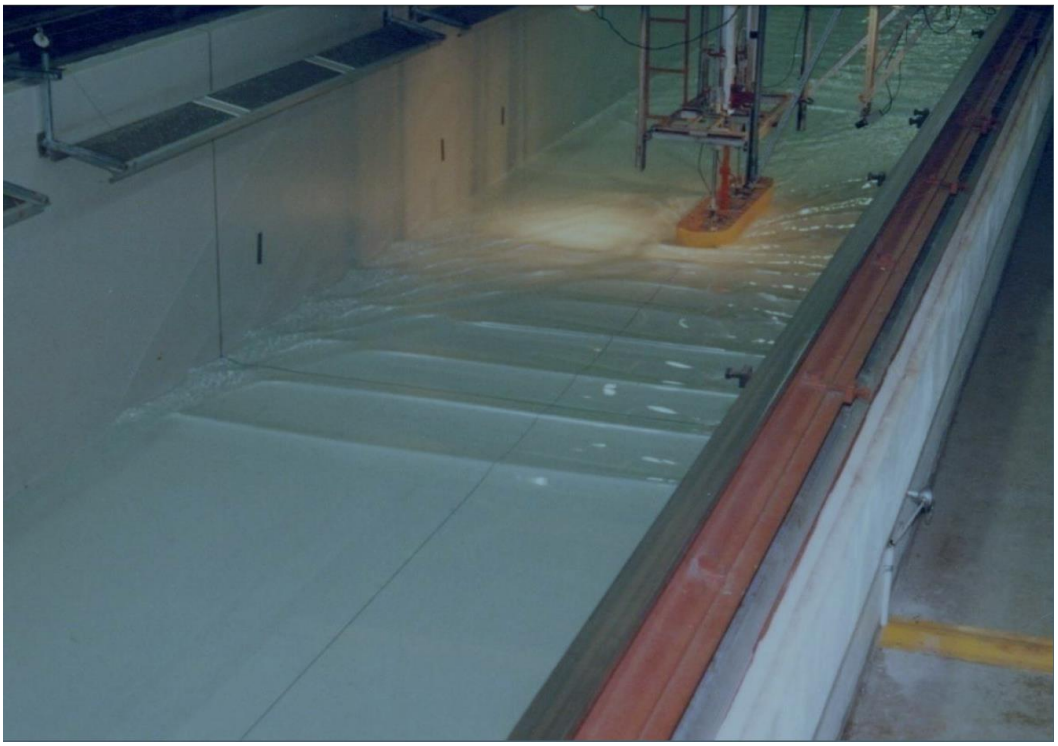

Figure 1.3: Experimental testing produce upstream solitary wave by a ship model, Gourlay (2010).

model for modeling these internal waves and hydraulic jumps, and undular bores on the North West Shelf, see Smyth and Holloway (1988). Holloway et al. (1997) used the KdV equation as a model to study the internal tide on the Australian North West Shelf. In their study, they showed that the form of the internal tide transformation is determined via the coefficient of the nonlinear term in the KdV equation as it changes from negative in deep water to positive in shallow water. In the atmosphere, a forced Benjamin-Ono equation is often the appropriate model, due to the upper atmospheric layer. Porter and Smyth (2002) used a modulation theory solution for the resonant flow of a two-layer fluid over topography, described by the Benjamin-Ono equation to describe the morning glory bores, which occur in Northern Australia. Their comparison showed good agreement between the theoretical solutions and observations.

El and Grimshaw (2002) showed that an undular bore is generated by the nonlinear evolution of flow over a shelf, which was described in terms of undular bore solutions to the Whitham modulation equations. Grimshaw et al. (2002a) derived an eKdV equation for internal solitary waves in a density and current stratified shear flow with a free surface. In addition, they considered two-layer shear flow with all coefficients of the eKdV equation represented in terms of integrals of the modal function. Helfrich and Melville (2006) gave an overview of the transient processes of wave generation and evolution, and the properties of steady internal solitary waves for weakly nonlinear theory described by the KdV equation. Apel et al. (2007) described internal solitary waves in the ocean by using the Boussinesq equation and the KdV equations.

Many studies based on KdV-type equations have used variable coefficients, such as Grimshaw et al. (2007a) who studied the shoaling of internal solitary waves over the continental shelf and slope. The propagation of nonlinear periodic waves and shallow-water solitary waves are governed by a KdV equation with variable coefficients, and can include bottom friction, El et al. (2007). They then used the Whitham averaging method to find perturbed modulation equations. El et al. (2012) studied the propagation of a shallow water undular bore over variable topography by using the variable-coefficient KdV equation (connecting two regions of constant depth). They obtained asymptotic solutions using modulation theory, which describes the evolution of this bore. A variable coefficient KdV-type equation was also used to describe the disintegration of internal solitary waves and their propagation, and deformation over the continental shelf and slope, Grimshaw et al. (2010). Marchant (2002a) studied solitary wave interaction for a higher order mKdV equation. He derived the higher order two-soliton solution using an asymptotically trans-

formation from the mKdV two-soliton solution and found the higher order phase shifts. His numerical solutions confirmed the theoretical predictions.

Grimshaw (1970) described the evolution and propagation of a solitary wave when the bottom topography is slowly varying by using the Boussinesq equations. He used a set of transport equations to describe the slow variations. Also, he found conservation of energy determines the variation of the wave amplitude. Grimshaw et al. (2009a) studied the stability of gravity-capillary waves using the forced KdV equation. They found that a small-amplitude wave of elevation is stable, while a depression wave, with a hollow at its crest, has variable stability. For a large amplitude depression, waves are unstable, whilst for the small amplitude depression, the waves are stable. Moreover, Grimshaw and Maleewong (2013) studied the stability of steady waves in water of finite depth generated by a moving localised pressure disturbance and gave descriptions of their features. They used a fully nonlinear boundary integral simulation, which was in good agreement with the forced KdV equation. The solution depended on three parameters, the magnitude and sign of the pressure distribution, and the Bond and Froude numbers.

Forced surface waves in a two-dimensional channel with a horizontal rigid flat bottom with a small positive bump were studied by Choi et al. (2008). In their study, the super-critical case was considered and the forced KdV equation used for both zero and nonzero initial conditions. In follow up work, Choi et al. (2010) considered a small negative or oscillatory bump. Gong and Shen (1994) proved that there are positive elevation solitary wave solutions of the forced KdV equation in the supercritical case. Additionally, both subcritical and supercritical cases, for free surface flow in a two-dimensional channel for a hydraulic fall over a bump were considered by Shen (1995).

The interaction of a solitary wave was investigated theoretically and numerically by using the forced KdV equation with an isolated moving external force of small amplitude, Grimshaw et al. (1994). They found that the theoretical predictions are in agreement with the numerical results. This work developed by Grimshaw and Pelinovsky (2002). They used the forced eKdV equation (the cubic nonlinear term only) with an isolated moving external force for the amplitude and position as a model for strongly nonlinear internal waves in the ocean.

The numerous theoretical studies of undular bores and resonant flow have been complemented by a vast array of numerical studies. The development of an undular bore that forms a transition between still water and a uniform flow were found numerically, using the KdV equation, by Peregrine (1966). He showed that the numerical results were consistent with experimental measurements. Wu and Wu (1982) presented numerical results for solitary waves in a current at near critical speed in shallow water flows forced by a bottom topography and an external surface pressure, by solving a long wave equation of the Boussinesq class. Direct numerical examination for the problem of steady free-surface flow of an ideal fluid over a step, was considered by King and Bloor (1987). They also investigated the problem analytically. Zhang and Chwang (1996) solved the Euler equations for inviscid free-surface flows numerically using a finite difference method and compared the results with numerical solutions of the forced KdV equation and the Boussinesq equations. Grimshaw et al. (2006) studied the evolution of internal solitary waves on the Australian North West Shelf using numerical solutions of the KdV equation.

More recently, Lee and Whang (2015) studied free surface flows in a two-dimensional channel over an obstacle (one and two bumps) by using the forced KdV equation. The

study focused on solitary wave solutions for the supercritical case. Between the two bumps, they observed that multiple trapped supercritical wave solutions occur. The forced KdV equation was used to examine free-surface flow over a spatially periodic channel bed topography, Binder et al. (2015). They demonstrated that solitary-type waves have periodic tails, by using the newly obtained theory of non autonomous dynamical systems. Grimshaw and Maleewong (2015) studied flow over two widely separated localised obstacles both analytically and numerically by using the forced KdV equation. They obtained two stages for the case of two obstacles. In the first stage, an upstream elevation shock and a downstream depression shock are generated for each obstacle, which are described by single obstacle theory. In the second stage, the first obstacle shock interacts with the downstream propagating depression whilst the second obstacle shock interacts with the upstream propagating elevation. Choi and Kim (2016) computed hydraulic falls and solitary wave-type solutions by solving the forced KdV equation using the relaxation method.

1.6 Objectives and thesis plan

One of the main objectives of this thesis is to study higher-order models for resonant flow over topography using the forced eKdV equation, which includes higher-order nonlinear, dispersive and nonlinear-dispersive terms beyond the forced KdV approximation. We derive the higher-order modulation theory solution for the resonant flow over both an obstacle and a step, and compare our theoretical results with numerical results of the KdV, eKdV and eBBM questions. The thesis aims to answer the following questions:

- Can higher-order modulation theory to describe resonant flow over a localized bump

and a step be derived?

- How do the forced eKdV results compare with the forced KdV results for wave properties such as solitary wave amplitudes, the width of the bores, and the resonant range?

- How does modulation theory compare with numerical solutions and how easily can these numerical solutions be calculated for the eKdV equation?

- How do these results compare for the asymptotically equivalent eBBM equation, particularly for steeper waves?

- Is uniform soliton theory a useful technique for predicting solitary wave amplitudes in the upstream undular bore?

This thesis consists of seven chapters. In Chapter 2 the derivation of the forced eKdV equation is considered for the flow of a stratified fluid over isolated topography. We also derive new modulation theory solutions by including the higher-order nonlinear, dispersive and mixed nonlinear-dispersive terms in an extended modulation theory for the eKdV equation. In Chapter 3 comparisons of the theoretical results of Chapter 2 with numerical simulations of the forced eKdV equation are made. We find the numerical solutions are stable only for small to moderate wave amplitudes. In Chapter 4 comparisons of the theoretical results of Chapter 2 with numerical simulations of the forced eBBM equation are made as the numerical scheme is stable for this equation, for all wave amplitudes. In Chapter 5 higher-order uniform soliton theory is derived. This theory assumes that the upstream waves are uniform train of solitary waves and their amplitude is found using mass and energy conservation. In Chapter 6 we present modulation theory solutions of the

forced eKdV equation describing the resonant flow over a step. This scenario is related to resonant flow over an isolated obstacle but there are key differences in the derivation of the theoretical solutions.

Finally, in Chapter 7 some conclusions are made with remarks and recommendations for future work.

Chapter 2

Higher-order modulation theory for resonant flow over an isolated topography

2.1 Introduction

This Chapter and Chapter 3 form the basis for the paper, Albalwi et al. (2017) with general higher-order coefficients. The waves generated by the flow of a fluid over topography or by a forcing, such as a ship, on the surface of a fluid or by submarine within a stratified fluid, is a classical topic in fluid mechanics and wave theory, Whitham (1974); Lamb (1997). The majority of this classical theory is based on small amplitude, linear waves, for which there exists a number of detailed accounts, Stoker (1957); McIntyre (1972); Whitham (1974); Baines (1984, 1995). However, when the speed of the imposed flow or the speed of the forcing is near the speed of a linear wave mode, energy accumulates at

the forcing, so that the flow becomes nonlinear with unsteady nonlinear wavetrains propagating upstream and downstream of the forcing. This flow regime is termed resonant, or transcritical, in the terminology of hydraulic theory, Baines (1995). Experimental work by Baines (1977, 1979, 1984) on the flow of a stratified fluid over topography found large amplitude upstream waves when the flow is near resonance. Baines (1984) also noted that the upstream wavetrain took the form of an undular bore. These experimental results for a stratified fluid were confirmed by ship tank experiments, Huang et al. (1982) and in wave tank experiments on the resonant forcing of surface waves by an obstacle, Lee et al. (1989). These experimental studies generated interest in theoretical and numerical analyses of resonant flow. In the weakly nonlinear, long wave regime it has been shown by a number of authors that in the resonant, or transcritical, regime the flow is governed by the forced KdV equation, with the forcing due to the topography or the imposed forcing, such as a pressure distribution (eg from a ship), Akylas (1984); Cole (1985); Grimshaw and Smyth (1986); Melville and Helfrich (1987); Lee et al. (1989). The study of resonant flow over topography is important in finding useful models for widely occurring phenomena in both oceanography and meteorology applications. The flow dynamics in stratified coastal waters and tidal flows over sills, which generate highly nonlinear internal waves, are two oceanographical applications.

As noted in the Introduction, in the resonant regime undular bores propagate upstream and downstream of the topography or forcing. In general, an undular bore is a modulated periodic wavetrain with solitons at one edge and linear dispersive waves at the other, Gurevich and Pitaevskii (1974); Fornberg and Whitham (1978); El and Hoefer (2016). While such modulated wavetrains are generally termed undular bores in fluids applications, the

term dispersive shock waves tends to be used in other nonlinear wave applications, El and Hoefer (2016). An undular bore differs from a compressive flow shock in that dispersion resolves the initial jump discontinuity between the two levels, while for compressible flow viscosity plays this role. Dispersion then results in an undular bore spreading as it evolves, while a compressive shock does not spread. Cnoidal waves are the nonlinear travelling wave solutions of the KdV equation and are expressed in terms of Jacobian Elliptic functions (see Page 38), Whitham (1974). In the limit in which the modulus squared m of the Elliptic function approaches unity, the cnoidal wave becomes the KdV soliton solution and in the limit as $m \to 0$ the cnoidal wave becomes a small amplitude, linear dispersive wave, Whitham (1974). One edge of the KdV undular bore then consists of solitons with $m = 1$ and the other edge consists of linear waves with $m = 0$, Gurevich and Pitaevskii (1974); Fornberg and Whitham (1978).

However, in general, the bore resulting from resonant flow has a variation from this general structure as the trailing edge of the bore can be fixed at the forcing, Grimshaw and Smyth (1986); Smyth (1987). For instance, near exact resonance, the upstream propagating bore is not a full undular bore, but a partial bore with a minimum modulus $m_0 > 0$ at the forcing, where the bore is generated, and $m = 1$ at its leading edge, Smyth (1987). A full upstream bore is not generated as part of this bore would then propagate downstream (see Figure 2.1 and the discussion on Page 32). As the minimum modulus m_0, which is related to the wavenumber of the modulated wave, is close to unity in this exact resonance case, the upstream undular bore can be approximated by a train of solitons, which has been a useful approximation, Grimshaw and Smyth (1986); Wu (1987); Lee et al. (1989). However, away from exact resonance, particularly as the flow becomes subcriti-

cal in hydraulic terminology, the upstream bore becomes detached from the forcing and propagates upstream. It is then a full undular bore with linear waves at its trailing edge, so that the train of solitons approximation ceases to be valid, Smyth (1987). The soliton approximation is less useful for the downstream propagating bore as it is a full undular bore for most of the resonant regime, Grimshaw and Smyth (1986); Smyth (1987). This issue of the different flow regimes in which the upstream bore is partial or full will be taken up in detail in this Chapter and Chapter 3.

The solution for resonant flow in the weakly nonlinear, long wave regime has then been fully developed in terms of the undular bore solution of the KdV equation and its generalisations. Whitham developed modulation theory to describe slowly varying modulated wavetrains, see Section 1.3. This weakly nonlinear, long wave theory based on the KdV equation has been successful in describing resonant flow. However, there is the question of the influence of higher order corrections to the KdV approximation on the solution for resonant flow, particularly in terms of relating these theoretical solutions to experimental results, Baines (1984); Lee et al. (1989). Lamb and Yan (1996) compared numerical solutions of the equations for internal waves in the Boussinesq approximation with solutions of the KdV equation and the eKdV equation with the next higher order nonlinear, dispersive and nonlinear-dispersive terms included. The initial condition was a depression which developed into an undular bore, so that this work has connections with resonant flow over topography. It was found that the inclusion of these higher order terms resulted in better agreement with full numerical solutions of the Boussinesq equations, except when the waves are of very high amplitude, as would be expected. Various studies of resonant flow in the weakly nonlinear, long wave limit have included higher

order corrections to the KdV equation under a number of different approximations. Resonant flow governed by the KdV equation with a third order nonlinearity correction, the Gardner equation, has been studied based on extended modulation equations, Marchant and Smyth (1990). Resonant flow based on this eKdV equation with third order nonlinearity, the Gardner equation, was also studied numerically and using hydraulic theory, Grimshaw et al. (2002b). Finally, a complete description of resonant flow as governed by the Gardner equation has been given, Kamchatnov et al. (2013) as the Gardner equation is integrable and its full Whitham modulation equations can be derived, from which its undular bore solution can be found, Kamchatnov et al. (2012). A study of fully nonlinear resonant flow was based on the Su-Gardner system, El et al. (2006, 2009). This system results from assuming a long wave approximation of the water wave equations, but with no small amplitude expansion in the wave amplitude, so that nonlinearity is included exactly, Su and Gardner (1969). This work confirmed the qualitative predictions of KdV theory, even for finite amplitude waves.

Here the resonant flow of a fluid over isolated topography will be considered in the weakly nonlinear, long wave limit. The next higher order nonlinear, dispersive and nonlinear-dispersive corrections to the KdV approximation will be included, so that the flow is governed by a forced eKdV equation. As for resonant flow governed by the forced KdV equation, the forcing generates undular bores which propagate upstream and downstream of it. This is balanced by a flat depression downstream of the forcing to which the downstream bore is attached, so that the total flow consists of a bore upstream of the forcing and a flat depression downstream, followed by the downstream bore. Solutions for the upstream and downstream flows are derived from the Whitham modulation

equations for the eKdV equation. These modulation equations are found via an approximate transformation which transforms the eKdV equation to the KdV equation, Marchant (1999a); Marchant and Smyth (2006a). This transformation is approximate in that it does not transform the eKdV to the KdV equation exactly, but the error is of higher order than the eKdV expansion. This transformation also means that the modulation equations for the eKdV equation can be found from those for the KdV equation. As discussed above, the upstream bore is either a full or partial undular bore, Smyth (1987). Unless the flow is sufficiently supercritical, part of the trailing edge of a full bore would flow downstream of the forcing, which is not observed, Grimshaw and Smyth (1986). This is resolved by making the upstream bore a partial undular bore, which is terminated at the forcing, Smyth (1987).

Similarly, if the flow is not sufficiently subcritical, part of a full downstream bore would propagate upstream. As for the upstream bore, this is resolved by making it a partial bore in this case, so that it is attached to the forcing. In the case of a partial downstream bore, there is no downstream depression. In Section 2.2 a derivation of the forced eKdV equation is made from the water wave equations. In Section 2.3 higher order modulation theory is developed for the forced eKdV equation.

2.2 Derivation of forced eKdV equation

Flow is described by the forced KdV equation in the weakly nonlinear regime, when the upstream flow speed is close to that of a linear long wave mode. An important parameter is the Froude number F, which is a non-dimensional flow velocity, as it characterises how close the flow is to exact resonance. When F is in a band about $F = 1$ the wave energy

cannot propagate from the obstacle, and these linear solutions fail. When F is not close enough to unity the flow is not critical and resonant flow does not occur. When the Froude number $F > 1$, supercritical flow occurs and when $F < 1$, subcritical flow occurs, Vanden-Broeck (1987). In order to derive the model equations, we shall use the Lagrangian for the water-wave equations derived by Luke (1967). Firstly, let us consider two-dimensional flow of a fluid over a localized topography, with long-wavelength, small-amplitude waves propagating on the surface of an irrotational, incompressible, inviscid and undisturbed fluid of constant depth h (away from the obstacle). We will use h to non-dimensionalize all space variables and $\sqrt{\frac{h}{a_g}}$ to non-dimensionalize time, where a_g is the acceleration due to gravity. Laplace's equation governs the two-dimensional motions of this fluid and the velocity potential will be denoted by $\Phi = (X, Y, T)$. We use a non-dimensional spatial variable X, scaled by the fluid depth h and a non-dimensional time T scaled by $\sqrt{ha^{-1}}$ and the surface elevation by $N = N(X, T)$. We assume that there are two small non-dimensional parameters $\alpha = ah^{-1}$ providing an estimate of the nonlinear effects, and $\beta = h^2\ell^{-2}$ giving a measure of dispersive effects where a and l are a typical wave amplitude and wavelength, respectively. Then we set

$$X = \beta^{-1/2}x, \qquad T = \beta^{-1/2}t, \qquad N = \alpha\eta, \qquad \Phi = \alpha\beta^{-1/2}\phi. \tag{2.2.1}$$

Let us consider the waves generated by the flow of a stratified flow over an isolated topographic feature, Grimshaw and Smyth (1986); Marchant and Smyth (1990), or by a moving pressure distribution with constant velocity on the surface of a fluid, Akylas (1984); Cole (1985); Lee et al. (1989). A special case of the flow of a stratified fluid over topography is the surface waves generated by the flow of a uniform fluid of finite depth over topography. In the case of the flow of a fluid over topography, we take the

upstream velocity to be U in the X direction, with the z direction upwards opposite to the direction of gravity. For waves generated by a surface forcing, we take the forcing to move at a velocity U in the negative X direction. The flow is considered in the weakly nonlinear, long wave limit so that the height of the topography is small compared to the fluid depth and the wavelength of the waves is much greater than the depth of the fluid. Let the amplitude of the topography be of the order $\alpha\beta = ahl^{-2}$ and a length scale for the wavelength of the generated waves be ε^{-1}, with $\varepsilon \ll 1$. The flow will be taken in the transcritical or resonant regime so that the imposed flow speed U is close to one of the linear long wave speeds c. If the amplitude and wavelength scales are such that $\varepsilon^2 = \frac{1}{\beta}$, then the flow is governed by a forced KdV equation, see Akylas (1984); Cole (1985); Grimshaw and Smyth (1986); Smyth (1987); Lee et al. (1989). In this scaling the parameter Δ, $U = c + \alpha\Delta$, measures how close the flow is to exact resonance, with $\Delta = 0$ corresponding to exact resonance. Let us take the topography or forcing to have the functional form $\alpha^2 G(x)$, $x = \varepsilon X$, due to the assumption about its length and amplitude scales. G is assumed to have its maximum at $x = 0$ and to have amplitude g_0, so that $G(0) = g_0$. Note that this implies that the topography is slowly varying.

The water wave equations and boundary conditions then can be written

$$\begin{aligned}
&\phi_{xx} + \frac{1}{\beta}\phi_{zz} = 0, && && \xi(x,t) < z < 1 + \alpha\eta \\
&\phi_z = \beta\phi_x\xi_x + \frac{\beta}{\alpha}\xi_t, && \text{for} && z = \xi(x,t) \\
&\eta_x = \frac{1}{\beta}\phi_z - \phi_x\eta_x, && \text{for} && z = 1 + \alpha\eta \\
&\phi_t + \frac{1}{2}\alpha\phi_x^2 + \frac{1}{2}\frac{\alpha}{\beta}\phi_z^2 + \eta = 0, && \text{for} && z = 1 + \alpha\eta,
\end{aligned} \tag{2.2.2}$$

see Grimshaw and Smyth (1986). Here, $\xi(x,t)$ is the bottom topography (assumed to be localized, so that $G(x) \to 0$ as $x \to \pm\infty$). Similar to Marchant (1999b), we assume the

bottom topography as

$$z = \xi(x,t) = \alpha\beta G(x - Ft), \tag{2.2.3}$$

where

$$F = 1 + \frac{1}{4}\alpha\Delta. \tag{2.2.4}$$

The detuning parameter Δ is measures the deviation from the exact resonance case of $\Delta = 0$. Note that at resonance the amplitude of the response is $O(\alpha)$, which is larger than the obstacle height, while for non-resonant cases the amplitude is $O(\alpha\beta)$, the same as the obstacle.

The velocity potential $\phi = (x,z,t)$ is expanded in the standard series form valid for long waves. It satisfies the boundary condition at $z = \xi(x,t)$ and the region of Laplace's equation in (2.2.2),

$$\begin{aligned}\phi = f - \frac{1}{2}\beta z^2 f_{xx} + \frac{1}{4!}\beta^2 z^4 f_{xxxx} - \frac{1}{6!}\beta^3 z^6 f_{xxxxxx} + \alpha\beta^2 z(G_x f_x + G f_{xx}) \\ + \frac{1}{8!}\beta^4 z^8 f_{xxxxxxxx} - \frac{1}{3!}\alpha\beta^3 z^3 (3G_{xx} f_{xx} + 3G_x f_{xxx} + G_{xxx} f_x + G f_{xxxx}) \\ - F\left(\beta^2 G_x z - \frac{1}{3!}\beta^3 z^3 G_{xxx} + \frac{1}{5!}\beta^4 z^5 G_{xxxxx}\right) + \ldots,\end{aligned} \tag{2.2.5}$$

where the unknown function $f(x,t)$ is the velocity potential to lowest order. Using the scalings (2.2.1), the Lagrangian for the water-wave equations, Luke (1967) and Whitham (1974), becomes

$$\frac{L}{phga} = \int_0^{1+\alpha\eta} \left[\phi_t + \frac{1}{2}\alpha(\phi_x)^2 + \frac{1}{2}\frac{\alpha}{\beta}(\phi_Y)^2\right] dY + \frac{1}{2}\alpha\eta^2. \tag{2.2.6}$$

The variational equations for this Lagrangian are

$$\begin{aligned}L_\eta = 0, \quad L_f - \frac{\partial}{\partial t}(L_{f_t}) - \frac{\partial}{\partial x}(L_{f_x}) + \frac{\partial^2}{\partial x^2}(L_{f_{xx}}) - \frac{\partial^3}{\partial x^2 \partial t}(L_{f_{xxt}}) - \frac{\partial^3}{\partial x^3}(L_{f_{xxx}}) \\ + \frac{\partial^4}{\partial x^4}(L_{f_{xxxx}}) - \frac{\partial^5}{\partial x^4 \partial t}(L_{f_{xxxxt}}) - \frac{\partial^5}{\partial x^5}(L_{f_{xxxxx}}) = 0.\end{aligned} \tag{2.2.7}$$

In the next steps we substitute $\phi(x,z,t)$ given by equation (2.2.5) into the Lagrangian for the water-wave equations (2.2.6). Then we neglect terms of order higher than second in the small parameters $O(\alpha,\beta)$. We obtain

$$\begin{aligned}\frac{L}{phga} &= f_t+\alpha\frac{1}{2}n^2+\alpha\eta f_t-\frac{1}{6}\beta f_{xxt}+\frac{1}{2}\alpha\left(f_x\right)^2+\frac{1}{2}\alpha^2\eta\left(f_x\right)^2+\frac{1}{40}\alpha\beta^2\left(f_{xxx}\right)^2\\ &+\frac{1}{6}\alpha\beta\left(f_{xx}\right)^2-\frac{1}{2}\alpha\beta\eta f_{xxt}+\frac{1}{120}\beta^2 f_{xxxxt}-\frac{1}{30}f_{xx}f_{xxxx}\\ &-\frac{1}{2}\alpha^2\beta\eta^2 f_{xxt}-\frac{1}{6}\alpha\beta f_x f_{xxx}+\frac{1}{24}\alpha\beta^2\eta f_{xxxt}-\alpha\beta G f_t\\ &+\frac{1}{120}\alpha\beta^2 f_x f_{xxxxx}-\frac{1}{2}\alpha^2\beta f_x f_{xxx}+\frac{1}{2}\alpha^2\beta\eta\left(f_{xx}\right)^2\\ &+\alpha^2\beta\frac{1}{2}\left(Gf_{xxt}+G_x f_{xx}-G\left(f_x\right)^2\right)+\alpha\beta^2 F\left(F\eta G_{xx}-G_{xx}f_x\right).\end{aligned} \tag{2.2.8}$$

Taking the variations of the Lagrangian (2.2.8) and $u=f_x$, we obtain a system of coupled differential equations for $\eta(x,t)$ and $u(x,t)$. This system of equations is related to the second order forced Boussinesq system. The first equation is

$$\begin{aligned}u_t+\eta_x+\alpha u u_x+\alpha\beta\left(\frac{1}{2}u_x u_{xx}-\frac{1}{2}u u_{xxx}-\eta_x u_{xt}-\eta u_{xxt}\right)-\beta\frac{1}{2}u_{xxt}\\ +\beta^2\left(F^2 G_{xxx}+\frac{1}{24}u_{xxxxt}\right)=0.\end{aligned} \tag{2.2.9}$$

The second equation is

$$\begin{aligned}&\eta_t+u_x+\alpha\left(\eta u_x+u\eta_x\right)-\beta\left(\frac{1}{2}\eta_{xxt}+\frac{2}{3}u_{xxt}-FG_x\right)+\beta^2\left(\frac{2}{15}u_{xxxxx}+\frac{1}{24}\eta_{xxxxt}-FG_{xxx}\right)\\ &-\alpha\beta\left(\frac{1}{2}u\eta_{xxx}\eta+4\eta_x u_{xx}+\frac{5}{2}u_x\eta_{xx}+2\eta_x\eta_{xt}+\eta_t\eta_{xt}+2\eta u_{xxx}+\eta\eta_{xxt}+Gu_x+uG_x\right)\\ &=0,\end{aligned} \tag{2.2.10}$$

to $O(\alpha^2,\alpha\beta,\beta)$. The KdV equation describes right-moving waves while the Boussinesq equation describes bidirectional waves. We use an unidirectional assumption to obtain the

KdV equation from the Boussinesq equations. Here, the horizontal velocity is

$$\begin{aligned} u &= \eta - \frac{1}{4}\alpha\eta^2 + \frac{1}{3}\beta\eta_{xx} + \frac{3}{16}\alpha^2(\eta_{xx})^2 + \frac{1}{2}\alpha^2\eta\eta_{xx} + \frac{1}{8}\alpha^2\eta^3 + \frac{1}{10}\alpha^2\eta_{xxxx} \\ &\quad - \frac{1}{2}\alpha G(1+\frac{1}{8}\alpha\Delta) + \frac{1}{2}\alpha^2 G\eta + \frac{15}{24}\alpha^2 G_{xx} + \ldots \end{aligned} \tag{2.2.11}$$

Substituting (2.2.11) into (2.2.9) and (2.2.10) yields the forced eKdV equation on retaining terms up to and including $O(\alpha\beta, \alpha^2, \beta^2)$,

$$\begin{aligned} &u_t + u_x + \frac{3}{2}\alpha u u_x + \frac{1}{6}\alpha u_{xxx} - \frac{3}{8}\alpha^2 u^2 u_x + \frac{23}{24}\alpha^2 u_x u_{xx} + \frac{5}{12}\alpha^2 u u_{xxx} + \frac{19}{360}\alpha^2 u_{xxxxx} \\ &= -\frac{1}{2}\alpha(1+\frac{3}{8}\alpha\Delta)G_x - \frac{7}{8}\alpha^2 G_x u - \alpha^2 G u_x - \frac{5}{24}\alpha^2 G_{xxx}. \end{aligned} \tag{2.2.12}$$

In this thesis, we shall be interested in the influence of the next order nonlinear, dispersive and mixed nonlinear-dispersive terms in the KdV approximation to the resonant flow, Grimshaw et al. (2002b); Marchant and Smyth (1990). Note that the eKdV equation (2.2.12) with $G = 0$, conserves mass exactly but only energy in as asymptotic sense, to $O(\alpha)$. At this order, the non-dimensional, normalised equation governing the resonant flow of a fluid over topography is the forced eKdV equation, Marchant and Smyth (1990)

$$\begin{aligned} &-u_t - \Delta u_x + 6uu_x + u_{xxx} - \alpha c_1 u^2 u_x + \alpha c_2 u_x u_{xx} + \alpha c_3 u u_{xxx} + \alpha c_4 u_{xxxxx} \\ &= -(1+\alpha c_8\Delta)G_x - \alpha c_6 u G_x - \alpha c_5 G u_x - \alpha c_7 G_{xxx}. \end{aligned} \tag{2.2.13}$$

Here, $\alpha \ll 1$ is the square root of a typical non-dimensional topography height. The flow is assumed to start from the rest state, so that $u(x,0) = 0$. The coefficients of the higher-order terms, c_i, $i = 1,\ldots,8$, are calculated from the background stratification and have been explicitly calculated for the case of surface water waves, Marchant and Smyth (1990), for which

$$c_1 = 1, \quad c_2 = \frac{23}{6}, \quad c_3 = \frac{5}{3}, \quad c_4 = \frac{19}{60}, \quad c_5 = -\frac{4}{3}, \quad c_6 = -\frac{7}{6}, \quad c_7 = \frac{5}{12}, \quad c_8 = \frac{1}{4}. \tag{2.2.14}$$

The full details of the resonant solution for the forced KdV equation have been given in previous work, Grimshaw and Smyth (1986); Smyth (1987), so only a detailed outline of the extension of this solution to the forced eKdV equation (2.2.13) will be given in this chapter.

Figure 2.1 shows a typical solution of the forced eKdV equation (2.2.13), for surface water waves (2.2.14). Shown are a perspective view of the solution in the $x-t$ plane (top) and the surface profile u and bathymetry G versus x at $t = 25$ (bottom). The numerical solution of (2.2.13) with the initial condition $u = 0$ is shown. The other parameters are $\Delta = 0$ and $\alpha = 0.15$, so that the flow is at exact resonance. The forcing function is the hyperbolic secant (3.1.1). The solution consists of three parts, a steady hydraulic flow over the topography, a partial undular bore which propagates upstream and a full undular bore downstream of the obstacle. Mass is transported upstream, so a flat depression occurs downstream of the obstacle to conserve mass overall. The downstream bore returns the mean level to zero downstream of the depression. Solutions for the flow in these three regions will be derived. Note that the numerical scheme for the forced eKdV equation is given in Appendix (A.1).

2.3 Higher-order modulation theory

The solution of the forced eKdV equation (2.2.13) displayed in Figure 2.1 shows that over the forcing the flow is steady and non-dispersive, as found by Grimshaw and Smyth (1986) and Smyth (1987). The flow over the forcing is then the solution of the non-dispersive form of the forced eKdV equation (2.2.13), which is

$$-u_t - \Delta u_x + 6uu_x - \alpha c_1 u^2 u_x + (1 + \alpha c_8 \Delta) G_x + \alpha c_6 u G_x + \alpha c_5 G u_x = 0. \qquad (2.3.15)$$

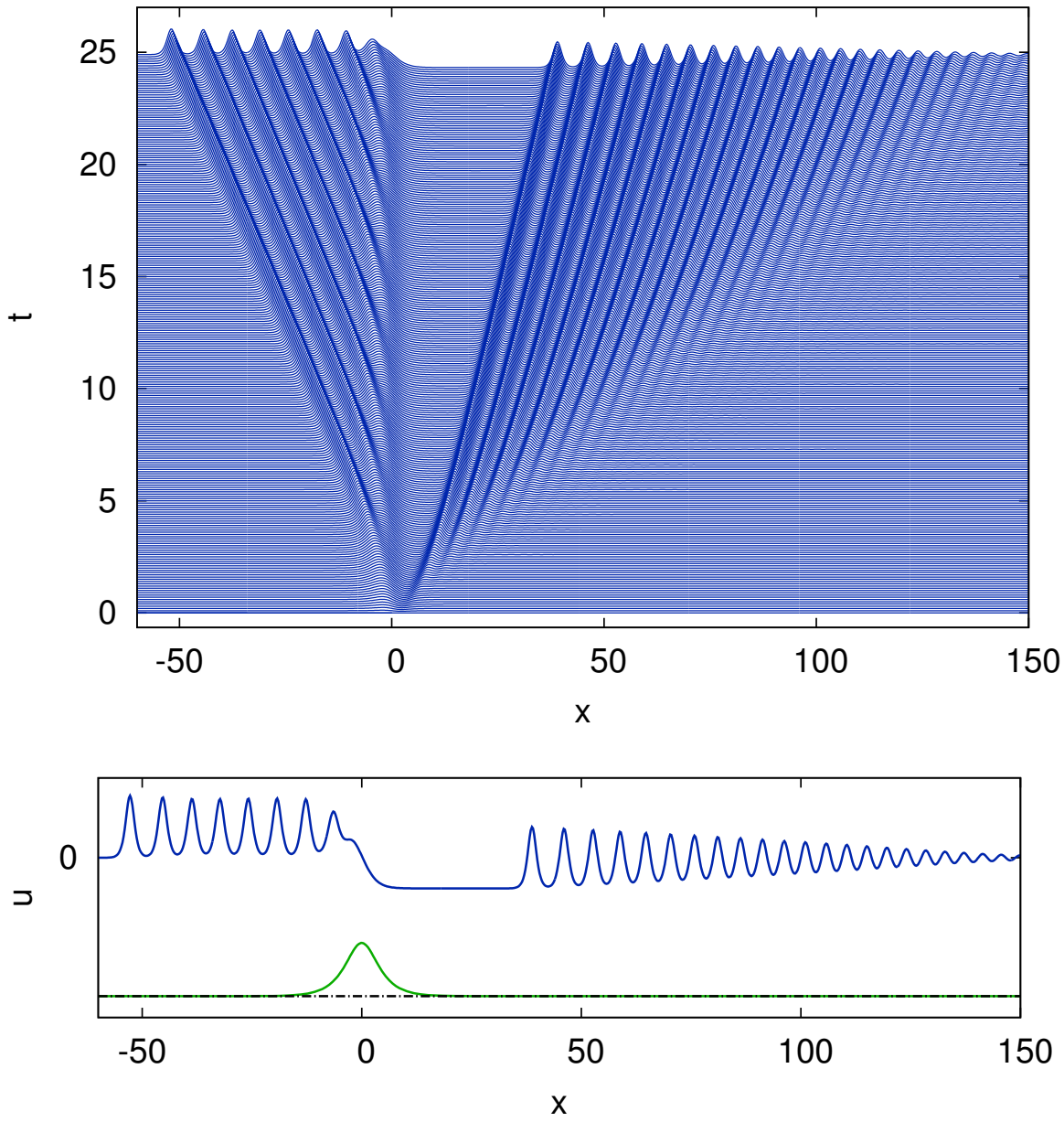

Figure 2.1: Solution of the forced eKdV equation (2.2.13), for surface water waves (2.2.14). Shown is a perspective view in the $x-t$ plane with time up to $t = 25$ (top) and the surface profile u and bathymetry G versus x at $t = 25$ (bottom). The numerical solution of (2.2.13) with the initial condition $u = 0$ is shown. The forcing function is (3.1.1). The other parameters are $\alpha = 0.15$ and $\Delta = 0$.

This hyperbolic equation has two steady solutions and the appropriate solution for the steady flow in this context is

$$u_s = \begin{cases} \frac{1}{6}[\Delta - \alpha c_5(g_0 - \frac{\Delta^2}{12}) + (1 + \frac{1}{2}\alpha c_8 \Delta)N(x)] + \frac{\alpha}{216}[M_1(\Delta^2 + \Delta N(x) + 4(g_0 - G))] \\ -\frac{\alpha}{36}[M_2(\Delta^2 + \frac{\Delta}{2}N(x))], \quad x < 0, \\ \frac{1}{6}[\Delta - \alpha c_5(g_0 - \frac{\Delta^2}{12}) - (1 + \frac{1}{2}\alpha c_8 \Delta)N(x)] + \frac{\alpha}{216}[M_1(\Delta^2 - \Delta N(x) + 4(g_0 - G))] \\ -\frac{\alpha}{36}[M_2(\Delta^2 - \frac{\Delta}{2}N(x))], \quad x > 0. \end{cases} \tag{2.3.16}$$

Here

$$N(x) = \sqrt{12(g_0 - G)}, \quad M_1 = c_1 + 3c_5 + 6c_6, \quad M_2 = c_5 + c_6. \tag{2.3.17}$$

This solution is comprised of the upper branch for negative x and the lower branch for positive x and is continuous at $x = 0$ at the peak of the forcing. It approaches a positive constant as $x \to -\infty$ and a negative constant as $x \to \infty$; this limiting behaviour is required so that the steady flow over the forcing matches with the bores propagating upsteam and downstream, for more details see Grimshaw and Smyth (1986); Smyth (1987); Marchant and Smyth (1990).

The steady solution (2.3.16) terminates in a positive jump upstream of the forcing and a negative jump downstream. As the eKdV equation (2.2.13) is a nonlinear, dispersive wave equation, these jumps are smoothed by evolving into undular bores, also termed dispersive shock waves, Gurevich and Pitaevskii (1974); Fornberg and Whitham (1978); Baines (1995); El and Hoefer (2016). It is this dispersive resolution of the discontinuities resulting from the resonant response of the flow over the forcing which generates the upstream and downstream propagating undular bores, Grimshaw and Smyth (1986); Smyth (1987).

To match with the upstream and downstream flows, we take the limiting forms of the

steady flow (2.3.16) as $x \to \pm\infty$, giving

$$u_s = \frac{1}{6}\left[\Delta - \alpha c_5\left(g_0 - \frac{\Delta^2}{12}\right) \pm \left(1 + \frac{1}{2}\alpha c_8 \Delta\right)\sqrt{12 g_0}\right] + \frac{\alpha}{216}\left[M_1\left(\Delta^2 \pm \Delta\sqrt{12 g_0} + 4 g_0\right)\right] - \frac{\alpha}{36}\left[M_2\left(\Delta^2 \pm \frac{\Delta}{2}\sqrt{12 g_0}\right)\right], \quad x \to \mp\infty. \tag{2.3.18}$$

These limiting values $u_s \to u_u$ as $x \to -\infty$ and $u_s \to u_d$ as $x \to \infty$ will be matched to the upstream and downstream bores in the next section. The resonant flow, characterised by strong upstream and downstream responses in the form of undular bores, only exists for a finite range of Δ around the exact resonance at $\Delta = 0$, Grimshaw and Smyth (1986); Smyth (1987). As Δ increases from zero, the flow eventually becomes supercritical with a localised trapped hump over the forcing and transient waves propagating upstream and downstream, Grimshaw and Smyth (1986); Smyth (1987); Baines (1995). On the other hand, as Δ decreases from zero, the flow eventually becomes subcritical with a localised trapped dip over the forcing, a steady lee wavetrain downstream and a transient propagating upstream, Grimshaw and Smyth (1986); Smyth (1987); Baines (1995). The range of the resonant regime can be quantified from the requirement of matching the steady flow (2.3.16) over the forcing to the upstream and downstream propagating bores. This is easiest to determine by looking at the limiting values u_s as $x \to \pm\infty$. The upstream and downstream states (2.3.18) are physically valid when $u_u > 0$ and $u_d < 0$. These requirements give that resonant flow will occur when Δ lies in the range

$$-\sqrt{12 g_0} + \alpha g_0 r_1 < \Delta < \sqrt{12 g_0} + \alpha g_0 r_1, \quad \text{where} \quad r_1 = 6c_8 - \frac{1}{9}c_1 + \frac{2}{3}c_5 + \frac{1}{3}c_6. \tag{2.3.19}$$

Note that at $O(\alpha)$ the width of the resonant band is unchanged from that given by the forced KdV equation, but is translated, by $\alpha g_0 r_1$, towards the supercritical regime. Also note that only the coefficients associated with the higher-order non-dispersive terms in (2.3.15) contribute to the correction to the resonant range, as given by $\alpha g_0 r_1$.

It was found by Marchant (1999a) and Marchant and Smyth (2006a) that solutions of the eKdV equation

$$-u_t - \Delta u_x + 6uu_x + u_{xxx} - \alpha c_1 u^2 u_x + \alpha c_2 u_x u_{xx} + \alpha c_3 u u_{xxx} + \alpha c_4 u_{xxxxx} = 0. \qquad (2.3.20)$$

This equation has the coefficients of the higher-order terms, c_i, $i = 1,\ldots,4$, which have been obviously calculated for the internal waves case by Marchant and Smyth (2006a), for which

$$\alpha c_1 = 0.191, \quad \alpha c_2 = 1.39, \quad \alpha c_3 = 0.186, \quad \alpha c_4 = 0.0573. \qquad (2.3.21)$$

Equation (2.3.20) can be transformed by

$$\begin{aligned} &u = \eta + \alpha c_9 \eta^2 + \alpha c_{10}\eta_{xx} + \alpha c_{11}\eta_x \int_{Ut}^{x} (\eta(p,t) - \beta)\, dx, \\ &\tau = t + \alpha \frac{c_4}{3} x, \quad \xi = x + \alpha c_{11}\beta(x - Ut) + \alpha c_{11} Dt \qquad (2.3.22) \\ &c_9 = \frac{1}{6}(c_1 + c_3 + 4c_4), \quad c_{10} = \frac{1}{12}(c_1 + c_2 - 6c_4), \quad c_{11} = \frac{1}{3}(8c_4 - c_3), \quad D = Uu - 3u^2 - u_{\xi\xi}, \end{aligned}$$

to solutions of the standard KdV equation

$$\frac{\partial \eta}{\partial \tau} + 6\eta \frac{\partial \eta}{\partial \xi} + \frac{\partial^3 \eta}{\partial \xi^3} = 0, \qquad (2.3.23)$$

when terms of $O(\alpha^2)$ are neglected. In this transformation β and U are the mean level and phase speed of the cnoidal wave solution of the KdV equation (2.3.23), Whitham (1974). This transformation will be used to derive the undular bore solution of the unforced eKdV equation from that of the KdV equation, Gurevich and Pitaevskii (1974); Fornberg and Whitham (1978).

Note that there is an exact transformation between the modulation equations of the KdV equation and of the Gardner equation, but which is non-invertible, Kamchatnov et al. (2013, 2012). The Gardner equation has a number of different solution types, such as

trigonometric bores and solibores, which have no KdV counterparts. In addition, Sprenger and Hoefer (2017) considered a fifth-order KdV equation and found new types of undular bore solutions due to a resonance between radiation and the bore. The eKdV equation (2.2.13) contains both the third order nonlinear term u^2u_x of the Gardner equation and the fifth order dispersive term u_{xxxxx} of the fifth order KdV equation. However, the near-identity transformation (2.3.22) only generates a classical KdV bore type solution for the eKdV equation as the amplitude parameter α is assumed small. Hence, the novel bore types which occur for the Gardner and fifth-order KdV equations cannot be found using the methods of the present work.

Modulation theory, Whitham (1965a,b, 1974), or the method of averaged Lagrangians, is based on finding differential equations for the parameters, such as the mean height, wavenumber and amplitude, of a slowly varying wavetrain. Modulation theory for the KdV equation, Whitham (1965b, 1974) is based on its periodic cnoidal wave solution, Whitham (1974)

$$\eta = \beta + \frac{2a}{m}\left[1 - m - \frac{E(m)}{K(m)} + m\,\mathrm{cn}^2\left(\frac{K(m)}{\pi}\theta, m\right)\right]. \tag{2.3.24}$$

Here the phase $\theta = k\xi - \omega\tau$. This travelling wave has wavenumber k, frequency ω, phase speed $U = \frac{\omega}{k}$, mean height β and amplitude a. $K(m)$ and $E(m)$ are complete elliptic integrals of the first and second kinds, respectively. The parameter m is the modulus squared. As $m \to 1$ the cnoidal wave solution (2.3.24) approaches the KdV soliton and as $m \to 0$ it approaches the linear travelling wave solution of the KdV equation.

A particular solution of the hyperbolic KdV modulation equations is a simple wave solution, which corresponds physically to the undular bore solution of the KdV equation, Gurevich and Pitaevskii (1974); Fornberg and Whitham (1978). This undular bore solu-

tion is a modulated cnoidal wave which joins the level A behind the bore to the level B in front of the bore, with $A > B$. The undular bore is then the modulated cnoidal wave

$$\eta = A - (A-B)m + 2(A-B)m\,\mathrm{cn}^2\left(\frac{K}{\pi}\theta, m\right), \tag{2.3.25}$$

with the modulated wave parameters given by

$$\begin{aligned} a &= 2(A-B)m, \qquad & \beta &= 2B - A + (A-B)\left(2\frac{E(m)}{K(m)} + m\right), \\ k &= K^{-1}\pi\sqrt{A-B}, \qquad & U &= 2A + 4B + 2(A-B)m, \\ p &= A + (A-B)m, \qquad & q &= A - (A-B)m, \end{aligned} \tag{2.3.26}$$

$$\text{on } \frac{\xi}{\tau} = \lambda = U - 4(A-B)\frac{m(1-m)K(m)}{E(m) - (1-m)K(m)}, \quad 12B - 6A \le \frac{\xi}{\tau} \le 4A + 2B. \tag{2.3.27}$$

In this undular bore solution the modulus squared $0 \le m \le 1$. At the leading edge, where $m = 1$ solitons of amplitude $2(A-B)$ with a mean level of $\beta = B$ occur, while at the trailing edge, where $m = 0$ there are sinusoidal waves of small amplitude exist on a mean level $\beta = A$. The bore has width $10(A-B)\tau$, and only exists if $A > B$. The quantities p and q are the peak and trough heights of the wave and represent the envelopes of the wavetrain.

The transformation (2.3.22) can now be used to transform the KdV undular bore solution (2.3.25) into the undular bore solution of the unforced eKdV equation, Marchant and Smyth (1990). The amplitude a, wavenumber k and mean height β of the eKdV undular bore are then

$$\begin{aligned} a &= (A-B)m + \alpha\left[(c_9 m + 2c_{10}(m^2 - 2m)\right](A-B)^2, \\ \beta &= 2B - A + (A-B)\left(2\frac{E(m)}{K(m)} + m\right) + \frac{\alpha}{3}c_9(A-B)^2\left[3m^2 - 5m + 2 + 2(2m-1)\frac{E(m)}{K(m)}\right] \\ &\quad + \frac{4}{3}\alpha c_{11}(A-B)^2\left[3\left(1 - \frac{E(m)}{K(m)}\right)^2 - 2\left(1 - \frac{E(m)}{K(m)}\right)(m+1) + m\right], \\ k &= \pi K^{-1}\sqrt{A-B}\left[1 + \alpha c_{11}(2A(A-B)m - (A-B)^2 m^2 - A^2 + 4AB)\right. \\ &\quad \left. - \alpha\frac{c_4}{3}(2A + 4B + 2(A-B)m) - \frac{1}{2}\alpha c_9(A+B)\right]. \end{aligned} \tag{2.3.28}$$

This is also the undular bore solution of the forced eKdV equation (2.2.13) if the sign of the characteristic λ (2.3.27) is reversed to account for $-u_t$ and a shift Δ is added to account for $-\Delta u_x$ in this equation. The undular bore solution of the forced eKdV equation (2.2.13) is then (2.3.28) with

$$\begin{aligned}
\frac{x}{t} &= \Delta - 2A - 4B - 2(A-B)m + 2(A-B)S \\
&\quad + \alpha c_9\left[2A^2 + 4B^2 + 2(A^2-B^2)m - 2(A^2-B^2)S\right] \\
&\quad - \frac{\alpha}{3}c_4\left[U - 2(A-B)S\right]^2 + \alpha c_{11}\left[2A(A-B)m - (A-B)^2m^2 - A^2 + 4AB\right] \\
&\quad - 2\alpha c_{11}(A-B)S\left[2B - A + (A-B)m + 2(A-B)\frac{E(m)}{K(m)}\right], \qquad (2.3.29) \\
&\quad \text{where } S(m) = \frac{2m(1-m)K(m)}{E(m) - (1-m)K(m)}.
\end{aligned}$$

Here the higher order phase speed is

$$\begin{aligned}
U &= 2A + 4B + 2(A-B)m - \alpha c_{11}\left[2A(A-B)m - (A-B)^2m^2 - A^2 + 4AB\right] \\
&\quad + \alpha\frac{c_4}{3}\left[2A + 4B + 2(A-B)m\right]^2 - \alpha c_9\left[6B^2 + 2\left(A^2 - B^2\right)(1+m)\right]. \qquad (2.3.30)
\end{aligned}$$

The envelopes p and q of this cnoidal wave are given by

$$\begin{aligned}
p &= A + (A-B)m + \alpha c_9\left[(A-B)^2m^2 + 2A(A-B)m - \left(A^2 - B^2\right)m\right] \\
&\quad - 4\alpha c_{10}(A-B)^2m, \qquad (2.3.31) \\
q &= A - (A-B)m + \alpha c_9\left[(A-B)^2m^2 - 2A(A-B)m + \left(A^2 - B^2\right)m\right] \\
&\quad + 4\alpha c_{10}(A-B)^2m(1-m). \qquad (2.3.32)
\end{aligned}$$

The extended undular bore solution can now be used to determine the bores propagating both upstream and downstream of the forcing. Let us first consider the upstream propagating bore, as seen in Figure 2.1. It is clear from matching with the steady solution over the forcing (2.3.18) that the upstream propagating bore has $B = 0$ to match with the initial

undisturbed flow. However, it can be seen from the characteristic velocity (2.3.29) that the linear trailing edge of the bore propagates downstream if $\Delta > -6A + O(\alpha)$ as $m \to 0$, which is unphysical and contradicts what is seen in the numerical solution of Figure 2.1. This is resolved by stopping the upstream undular bore solution at $x = 0$, so that the upstream undular bore is a partial bore, Smyth (1987). The partial bore then has modulus in the range $m_0 \le m \le 1$, with m_0 the characteristic velocity (2.3.29) which sets $\frac{x}{t} = 0$. Waves of modulus m_0 are then generated at the forcing, Smyth (1987), which is what is seen in Figure 2.1. This gives, on using the characteristic velocity (2.3.29), that the minimum modulus m_0 is the solution of

$$\begin{aligned}
&\Delta = 2A(1+m_0-S_0) + \alpha\frac{4}{3}c_4A^2(1+m_0-S_0)^2 - \alpha 2c_9A^2(1+m_0-S_0)\\
&+\alpha c_{11}A^2(1-2m_0+m_0^2) - 2\alpha c_{11}S_0A^2\left(1-m_0-2\frac{E(m_0)}{K(m_0)}\right), \qquad (2.3.33)\\
&\text{where } S_0 = \frac{2m_0(1-m_0)K(m_0)}{E(m_0)-(1-m_0)K(m_0)}.
\end{aligned}$$

The jump height A can then be found by setting the mean level β, given by (2.3.28), of the bore at the forcing $x = 0$, so its equal to the upstream limit u_u (2.3.18) of the steady solution over the forcing. This results in A being the solution of

$$\begin{aligned}
&\frac{1}{6}\left[\Delta - \alpha c_5\left(g_0 - \frac{\Delta^2}{12}\right) + \left(1+\frac{1}{2}\alpha c_8\Delta\right)\sqrt{12g_0}\right] + \frac{\alpha}{216}\left[M_1\left(\Delta^2 + \Delta\sqrt{12g_0} + 4g_0\right)\right]\\
&-\frac{\alpha}{36}M_2\left(\Delta^2 + \frac{\Delta}{2}\sqrt{12g_0}\right) \qquad (2.3.34)\\
&= m_0A - A + 2A\frac{E(m_0)}{K(m_0)} + \frac{\alpha c_9}{3}A^2\left[3m_0^2 - 5m_0 + 2 + 2(2m_0-1)\frac{E(m_0)}{K(m_0)}\right]\\
&+\frac{4}{3}\alpha c_{11}A^2\left[3\left(1-\frac{E(m_0)}{K(m_0)}\right)^2 - 2\left(1-\frac{E(m_0)}{K(m_0)}\right)(m_0+1) + m_0\right].
\end{aligned}$$

Equations (2.3.33) and (2.3.34) for the minimum modulus m_0 and the upstream jump

height A can be solved in the limit of small α to give

$$A = A_0 + \alpha A_1, \quad A_0 = \frac{\Delta + \sqrt{12g_0}}{6T}, \quad T = m_0 - 1 + 2\frac{E(m_0)}{K(m_0)}, \tag{2.3.35}$$

$$\begin{aligned} \text{where } A_1 = \frac{1}{216T}\Big[& M_1\left(\Delta^2 + \Delta\sqrt{12g_0} + 4g_0 + 18c_8\Delta\sqrt{12g_0}\right) \\ & -6M_2\left(\Delta^2 + \frac{\Delta}{2}\sqrt{12g_0}\right) - 36c_5\left(g_0 - \frac{\Delta^2}{12}\right)\Big] \end{aligned} \tag{2.3.36}$$

$$\begin{aligned} & -\frac{1}{108T^3}\left(\Delta + \sqrt{12g_0}\right)^2\Big[c_9\left(3m_0^2 - 5m_0 + 2 + 2(2m_0 - 1)\frac{E(m_0)}{K(m_0)}\right) \\ & +3c_{11}\left(3\left(1 - \frac{E(m_0)}{K(m_0)}\right)^2 - 2\left(1 - \frac{E(m_0)}{K(m_0)}\right)(m_0 + 1) + m_0\right)\Big]. \end{aligned}$$

On solving equation (2.3.33) for the minimum modulus m_0 it is found that when

$$\Delta = -\frac{1}{2}\sqrt{12g_0} + \alpha g_0 r_2, \quad \text{where} \quad r_2 = \frac{3}{2}c_8 + \frac{1}{36}c_1 - \frac{1}{12}c_3 + \frac{5}{3}c_4 + \frac{1}{3}c_5 - \frac{1}{12}c_6, \tag{2.3.37}$$

$m_0 = 0$, so that the partial upstream undular bore becomes a full bore with $A = u_u$. For Δ below the value (2.3.37), a full undular bore propagates upstream.

The upstream propagating partial and full undular bores have now been determined. On noting the resonant range (2.3.19), we have that for

$$-\sqrt{12g_0} + \alpha g_0 r_1 < \Delta \leq -\frac{1}{2}\sqrt{12g_0} + \alpha g_0 r_2, \tag{2.3.38}$$

a full undular bore propagates upstream, while for

$$-\frac{1}{2}\sqrt{12g_0} + \alpha g_0 r_2 < \Delta < \sqrt{12g_0} + \alpha g_0 r_1, \tag{2.3.39}$$

a partial undular bore propagates upstream. As the upper resonant bound in (2.3.39) is approached, $m_0 \to 1$ and the partial bore becomes a train of solitary waves. Even at exact resonance $\Delta = 0$, $m_0 = 0.64 + O(\alpha)$, Smyth (1987), so that the upstream undular bore can be well approximated by a train of solitary waves, Grimshaw and Smyth (1986); Smyth (1987). For this reason, the upstream wavetrain is often termed a train of solitons, Wu

(1987); Lee et al. (1989), even though this is just an approximation which in fact breaks down as the lower limit of the resonant range is approached.

The downstream propagating bore seen in Figure 2.1 can be determined in a similar manner. In this case, to match with the undisturbed flow downstream of the forcing we have $A = 0$ with $B < 0$. In the case of the downstream propagating undular bore, the trailing soliton edge of the bore with $m \to 1$ matches with the downstream level u_d of the steady flow given by (2.3.18), as seen from Figure 2.1. The mean level (2.3.28) then gives

$$\begin{aligned} B &= \frac{1}{6}\left[\Delta - \alpha c_5\left(g_0 - \frac{\Delta^2}{12}\right) - \left(1 + \frac{1}{2}\alpha c_8\Delta\right)\sqrt{12g_0}\right] + \frac{\alpha}{216}M_1\left(\Delta^2 - \Delta\sqrt{12g_0} + 4g_0\right) \\ &\quad - \frac{\alpha}{36}M_2\left(\Delta^2 - \frac{\Delta}{2}\sqrt{12g_0}\right). \end{aligned} \tag{2.3.40}$$

Finally, the general undular bore solution (2.3.28) and (2.3.29) gives that the amplitude, mean height and wavenumber of the downstream propagating undular bore in the range (2.3.19) are given by

$$\begin{aligned} a &= |B|m + \alpha\left[c_9 m + 2c_{10}\left(m^2 - 2m\right)\right]B^2, \\ \beta &= 2B - B\left(2\frac{E(m)}{K(m)} + m\right) + \alpha\frac{c_9}{3}B^2\left[3m^2 - 5m + 2 + 2(2m-1)\frac{E(m)}{K(m)}\right] \\ &\quad + \alpha\frac{4c_{11}}{3}B^2\left[3\left(1 - \frac{E(m)}{K(m)}\right)^2 - 2\left(1 - \frac{E(m)}{K(m)}\right)(m+1) + m\right], \\ k &= \frac{\pi\sqrt{|B|}}{K(m)}\left[1 - \alpha c_{11}B^2m^2 - \alpha\frac{1}{3}\alpha c_4(4B - 2Bm) - \frac{1}{2}\alpha c_9 B\right], \end{aligned} \tag{2.3.41}$$

on the characteristics

$$\begin{aligned} \frac{x}{t} &= \Delta - 2B(2 - m + S) - \alpha\frac{4}{3}c_4B^2(2 - m + S)^2 + \alpha 2c_9B^2(2 - m + S) \\ &\quad - \alpha c_{11}B^2m^2 + 2\alpha c_{11}SB^2\left(2 - m - 2\frac{E(m)}{K(m)}\right). \end{aligned} \tag{2.3.42}$$

This downstream undular bore is a full bore, so that $0 \le m \le 1$. The extent of the bore is

$$\Delta - 2B - \alpha B^2\left(\frac{4}{3}c_4 - 2c_9 + c_{11}\right) \leqslant \frac{x}{t} \leqslant \Delta - 12B - \alpha B^2\left(\frac{144}{3}c_4 - 12c_9\right). \tag{2.3.43}$$

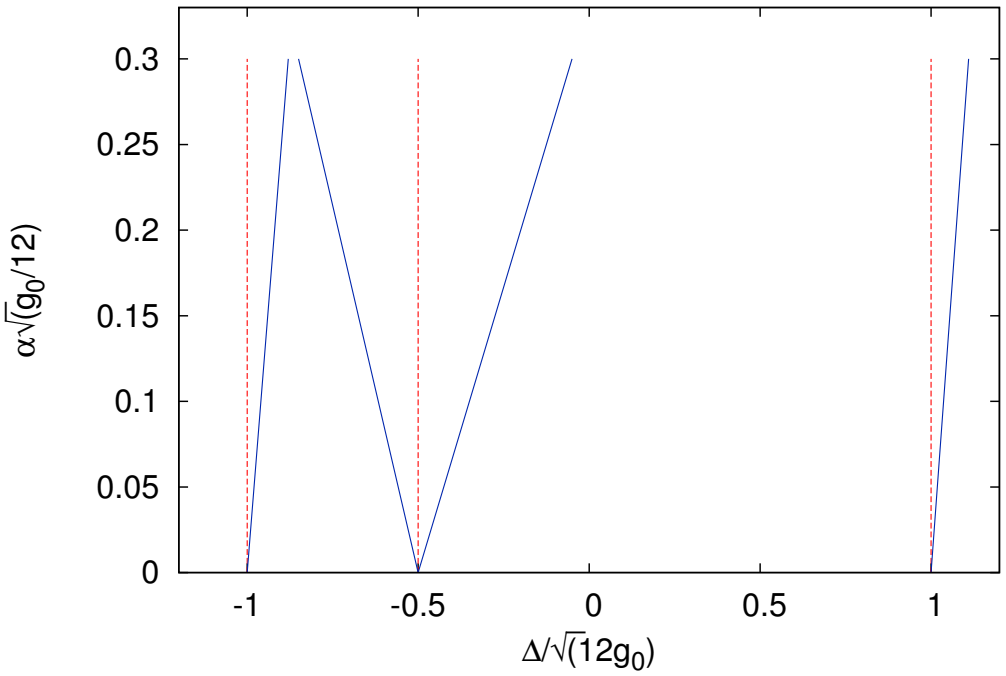

Figure 2.2: The parameter ranges in the $\Delta(12g_0)^{-\frac{1}{2}}$ versus $\alpha(\frac{12}{g_0})^{\frac{1}{2}}$ plane for full and partial undular bores, for surface water waves (2.2.14). Compared are eKdV (blue solid line) and KdV (red dashed lines) modulation theory.

This solution gives the full downstream undular bore seen in Figure 2.1.

However, the downstream undular bore cannot fully propagate downstream if the flow is not sufficiently supercritical. It can be found from the characteristic velocity (2.3.42) that when

$$\Delta = -\frac{1}{2}\sqrt{12g_0} + \alpha g_0 r_3, \quad \text{where} \quad r_3 = \frac{3}{2}c_8 - \frac{7}{36}c_1 - \frac{3}{4}c_3 + 3c_4 - \frac{1}{3}c_5 + \frac{7}{12}c_6, \tag{2.3.44}$$

the solitary wave, trailing edge of the bore with $m = 1$ is stationary and attached to the forcing. For subcritical Δ less than this value, the solitary wave edge of the downstream bore would propagate upstream. For example, at the subcritical limit of the resonant range for the KdV case $\Delta = -\sqrt{12g_0}$ and the trailing edge of the full bore has the negative

velocity $-\frac{1}{3}\sqrt{12g_0}$. This is resolved by making the downstream bore a partial bore in this highly subcritical range. The downstream bore is then a full undular bore for Δ in the range

$$-\frac{1}{2}\sqrt{12g_0}+\alpha g_0 r_3 < \Delta < \sqrt{12g_0}+\alpha g_0 r_1 \tag{2.3.45}$$

and it is a partial bore for

$$-\sqrt{12g_0}+\alpha g_0 r_1 < \Delta \leq -\frac{1}{2}\sqrt{12g_0}+\alpha g_0 r_3. \tag{2.3.46}$$

In the subcritical regime, the solution must match to the linear lee wave solution, which is a stationary wavetrain attached to the forcing, preceded by a transient front Smyth (1987).

Figure 2.2 shows the parameter ranges in the $\Delta(12g_0)^{-\frac{1}{2}}$ versus $\alpha(\frac{12}{g_0})^{\frac{1}{2}}$ plane for full and partial undular bores, for surface water waves. Compared are eKdV and KdV modulation theory. The figure illustrates the ranges (2.3.38) and (2.3.39) for the upstream bore and (2.3.45) and (2.3.46) for the downstream bore. Moving from left to right, the three sets of curves show the subcritical limit of the bore, the transition between the partial and full bore and the supercritical limit of the bore. The upstream and downstream bores have the same subcritical and supercritical resonant limits; as α increases these limits move toward the supercritical range. A full upstream bore is predicted by KdV theory for strongly subcritical flows and a partial bore for weakly subcritical and all supercritical flows. The transition point in KdV theory between full and partial bores occurs at $\Delta = -\frac{1}{2}\sqrt{12g_0}$. For the downstream bore the KdV transition point is the same, but the regimes are reversed. It appears from the figure that the eKdV subcritical limit and eKdV downstream bore boundaries cross at large α. However, it should be noted that the extended theory is only valid for small α and the exact curves will deviate from the small α predictions as α increases.

A partial downstream bore is predicted by KdV theory for strongly subcritical flows and a full bore for weakly subcritical and all supercritical flows. In the eKdV theory the transition point between the full and partial bores is no longer the same for the upstream and downstream bores. For the upstream bore the transition point moves towards the supercritical range as α increases, while for the downstream bore it moves towards the subcritical range.

The downstream solution in the range of Δ given by (2.3.46) is then a stationary cnoidal wavetrain of modulus m_{0d} preceded by a partial bore with modulus squared in the range $m_{0d} > m > 0$ to match with this stationary wavetrain at its trailing edge. The details of this downstream lee wave limit are given in Smyth (1987). In particular, the phase velocity of the waves of the partial bore does not approach 0 as the upper limit (2.3.46) of the partial bore range is approached, so that a partial bore as for the upstream case is not possible. The stationary cnodial wavetrain then as mean level β_l and phase velocity U_l given by

$$\begin{aligned}
\beta_l &= 2B - B\left(2\frac{E(m_{0d})}{K(m_{0d})} + m_{0d}\right) + \alpha\frac{c_9}{3}B^2\left[3m_{0d}^2 - 5m_{0d} + 2 + 2(2m_{0d}-1)\frac{E(m_{0d})}{K(m_{0d})}\right] \\
&+ \alpha\frac{4c_{11}}{3}B^2\left[3\left(1-\frac{E(m_{0d})}{K(m_{0d})}\right)^2 - 2\left(1-\frac{E(m_{0d})}{K(m_{0d})}\right)(m_{0d}+1) + m_{0d}\right], \qquad (2.3.47) \\
U_l &= 2B(2-m_{0d}) + \alpha c_{11}B^2 m_{0d}^2 + \alpha\frac{4}{3}c_4B^2(2-m_{0d})^2 - \alpha 2c_9B^2(2-m_{0d}),
\end{aligned}$$

where the mean level of the stationary wavetrain is the same as the leading edge of the partial undular bore and is equal to the downstream limit of the steady hydraulic flow, i.e. $\beta_l = u_s$. Also, the wavetrain must be stationary, so that $U = \Delta$. Equations (2.3.47) form a pair of equations determining the parameters m_{0d} and B for the partial downstream undular bore. The modulation theory solutions for the full and partial undular bores upstream and downstream of the forcing are now complete.

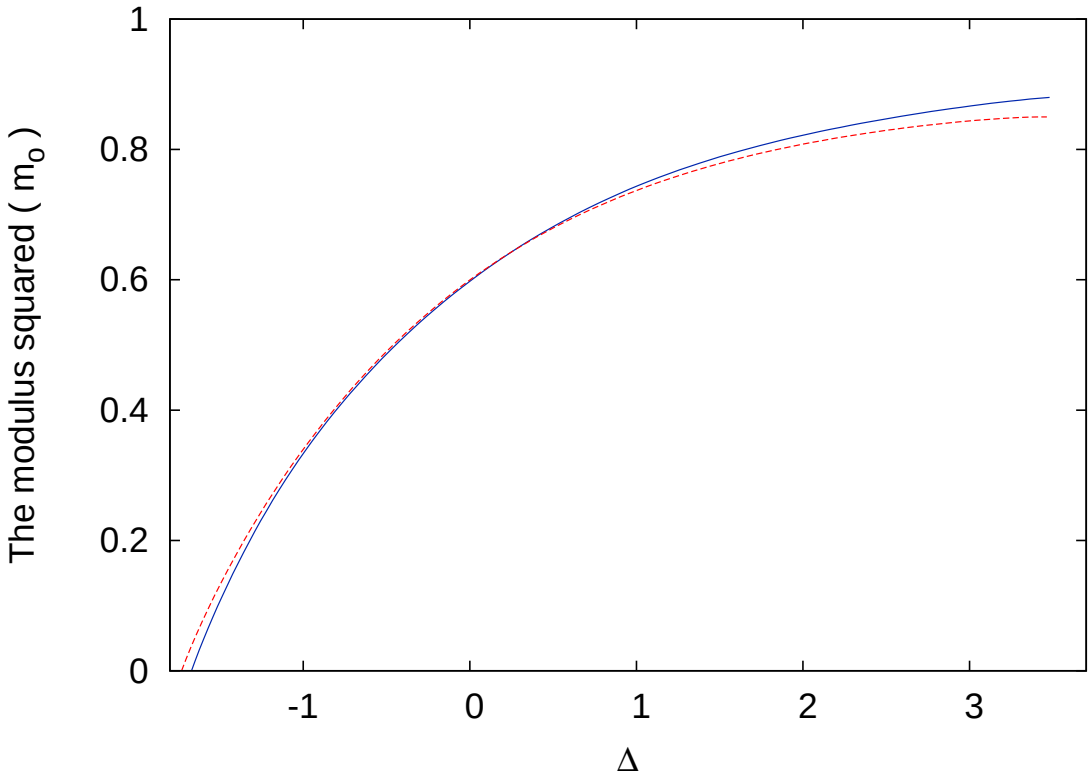

Figure 2.3: The modulus squared m_0 versus the detuning parameter Δ, for surface water waves (2.2.14). Compared are modulation theory for the forced eKdV equation (2.2.13) (blue solid line) and the forced KdV equation (red dashed line). The amplitude parameter is $\alpha = 0.15$.

Figure 2.3 shows the modulus squared, m_0, versus the detuning parameter Δ, for surface water waves. Compared are modulation theory for the forced eKdV and KdV equations. The amplitude parameter is $\alpha = 0.15$. The upstream undular borelies in the range $m_0 \le m \le 1$. If $m_0 = 0$ a full bore occurs upstream, while as $m_0 \to 1$ the bore becomes a train of solitary waves. At exact resonance $\Delta = 0$, the modulus squared, $m_0 = 0.64$, is approximately the same for both the eKdV and the KdV theories.

In the supercritical case, for positive Δ, the modulus squared m_0 of the eKdV theory is slightly greater than that for KdV theory. For example at $\Delta = 3$, $m_0 = 0.87$ and 0.84 for

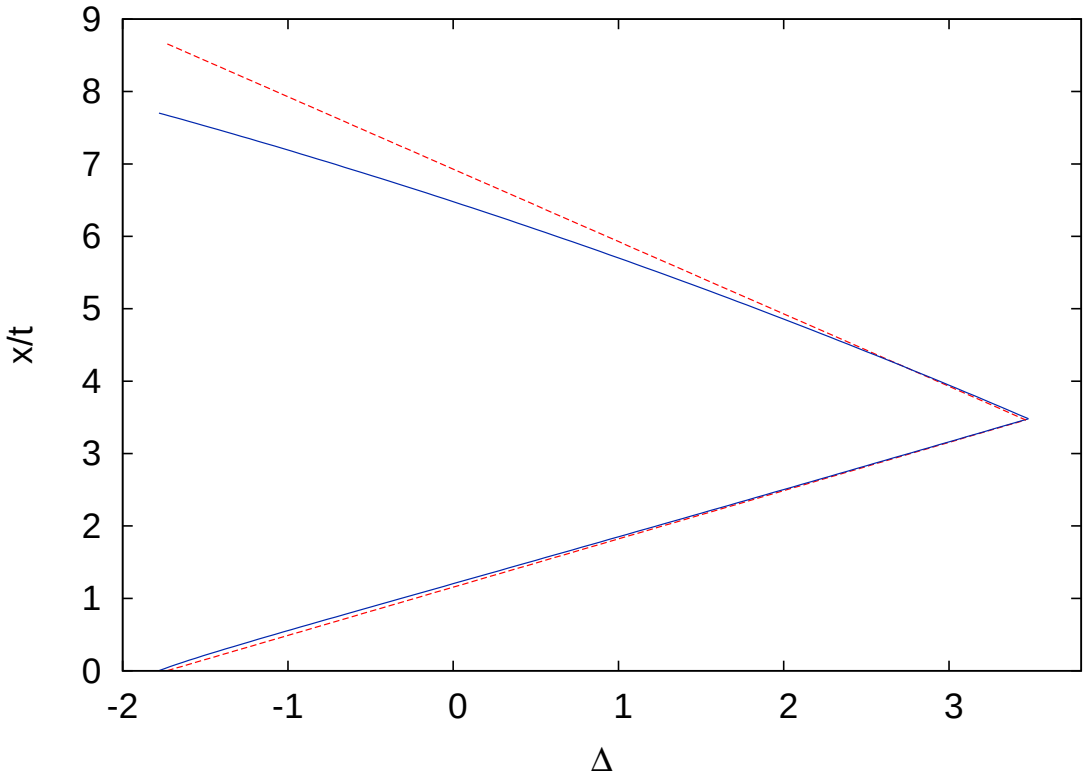

Figure 2.4: The leading and trailing edges of the downstream undular bore versus the detuning parameter Δ, for surface water waves (2.2.14). Compared are modulation theory for the forced eKdV equation (2.2.13) (blue solid line) and the forced KdV equation (red dashed line). The amplitude parameter is $\alpha = 0.15$.

eKdV and KdV theories, respectively. For the subcritical case, for negative Δ, the modulus squared m_0 of the eKdV theory is slightly lower than for the KdV theory. For example, at $\Delta = -0.5$, $m_0 = 0.53$ and 0.54 for the eKdV and KdV theories, respectively. Also, the resonant regimes for a partial upstream bore, are slightly different, $-1.73 < \Delta < 3.46$ and $-1.67 < \Delta < 3.48$ for the KdV and eKdV cases, respectively. The differences between the two theories are fairly slight and the KdV results provide a good approximation.

Figure 2.4 shows the leading and trailing edges of the downstream undular bore, $\frac{x}{t}$

versus the detuning parameter Δ, for surface water waves. Compared are modulation theory for the forced eKdV and KdV equations. The amplitude parameter is $\alpha = 0.15$. The comparison is given for ranges of the full downstream bore, which are $-1.73 < \Delta < 3.46$ and $-1.78 < \Delta < 3.48$ for the KdV and eKdV equations, respectively. The trailing edge has zero velocity and is at the forcing when $\Delta = -1.73$ and $\Delta = -1.78$ for the KdV and eKdV cases, respectively. Modulation theory shows that the eKdV bore is up to 12% narrower than the KdV bore and that the velocity of the leading edge of the eKdV bore (at which linear waves occur) is significantly lower. This result of a narrower downstream bore is in qualitative agreement with those based on using the fully nonlinear Su-Gardner equation, El et al. (2006) and the internal wave bore considered by Lamb and Yan (1996). Hence the result obtained here, of a narrower downstream bore, is confirmed by a range of other results.

Partial downstream bores occur in the ranges $-3.46 < \Delta < -1.73$ and $-3.44 < \Delta < -1.78$ for the KdV and eKdV equations, respectively. In these ranges the trailing edge is a steady cnoidal wave of modulus squared m_{0d}. Solving equations (2.3.47) gives $m_{0d} = 1$ at the transition between a full and partial bore, with $m_{0d} > 0.99$ over the whole range of Δ, for which the bore is partial. Hence the stationary wavetrain is composed of near solitary waves.

Chapter 3

Comparison of theoretical and numerical results for resonant flow over an isolated obstacle

The intent of this Chapter is to present numerical results and comparisons with theoretical solutions of the forced eKdV equation for resonant flow over an isolated topography. The results of this Chapter and Chapter 2 appear in Albalwi et al. (2017) with general higher-order coefficients.

The forced eKdV equation including second order terms beyond the KdV approximation has been studied numerically by a number of authors. For example, numerical simulations of the eKdV equation for stratified flow over topography have been investigated for a two-layer stratification by Melville and Helfrich (1987). Good agreement was found between the laboratory experiments and the numerical solutions. Hanazaki (1992) presented numerical results for resonant flow of a stratified fluid over topography

by using the forced eKdV equation. This study proved that the waves with an upstream propagation speed larger than the background flow speed. Grimshaw et al. (2002b) generated upstream and downstream in the transcritical solution and they found many forms of the solitary waves in transcritical internal wave flows, some of them were observed in Melville and Helfrich (1987).

The theoretical results of Chapter 2 are compared with numerical simulations of the forced eKdV equation (2.2.13), see Appendix (A.1) for details of the numerical scheme. Figure 3.1 shows the evolution of the solution of the forced eKdV equation (2.2.13), for surface water waves (2.2.14). Shown are a perspective view of the solution in the $x-t$ plane (top) and the surface profile u and bathymetry G versus x at $t = 25$ (bottom). The numerical solution of (2.2.13) with the initial condition $u = 0$ is shown. The other parameters are $\Delta = 1$ and $\alpha = 0.15$, so that the flow is supercritical. The forcing function is the hyperbolic secant (3.1.1). The solution consists of three parts, a steady hydraulic flow over the topography, and bores which propagates upstream and downstream wavetrains.

Figure 3.2 shows a typical solution of the forced eKdV equation (2.2.13), for surface water waves (2.2.14). Shown are a perspective view of the solution in the $x-t$ plane (top) and the surface profile u and bathymetry G versus x at $t = 20$ (bottom). The other parameters are $\Delta = -0.5$ and $\alpha = 0.15$, so that the flow is subcritical. The forcing function is the hyperbolic secant (3.1.1). Again, the solution consists of three parts, a steady hydraulic flow over the topography, the upstream partial undular bore and a full undular bore downstream of the obstacle. Figures 2.1; 3.1; 3.2 and 3.4- 3.6, that display bore profiles, all have parameters that correspond to the Figure 2.2 regime of partial upstream and full downstream undular bores.

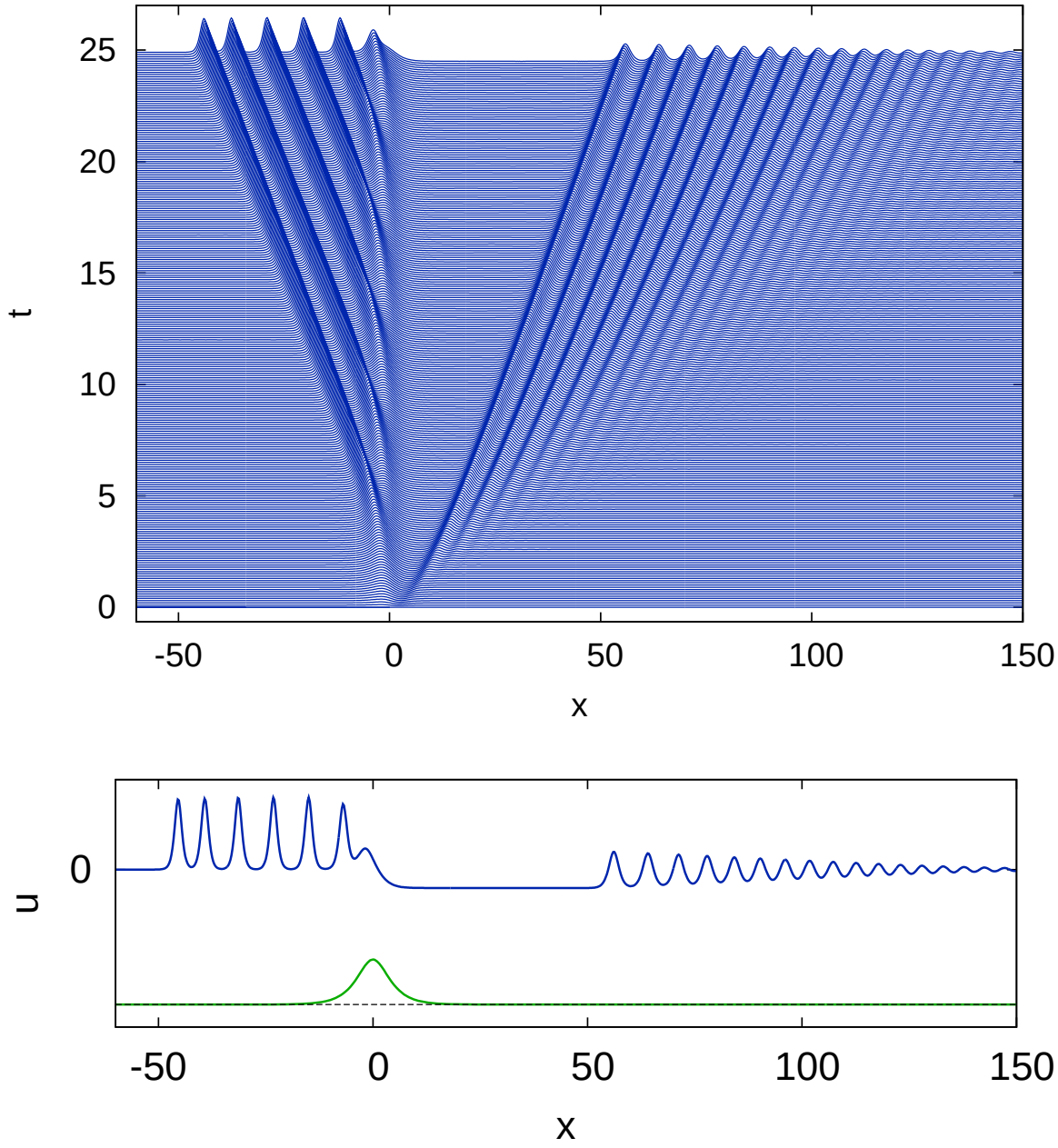

Figure 3.1: Solution of the forced eKdV equation (2.2.13), for surface water waves (2.2.14). Shown is a perspective view in the $x-t$ plane with time up to $t = 25$ (top) and the surface profile u and bathymetry G versus x at $t = 25$ (bottom). The numerical solution of (2.2.13) with the initial condition $u = 0$ is shown. The forcing function is (3.1.1). The other parameters are $\alpha = 0.15$ and $\Delta = 1$.

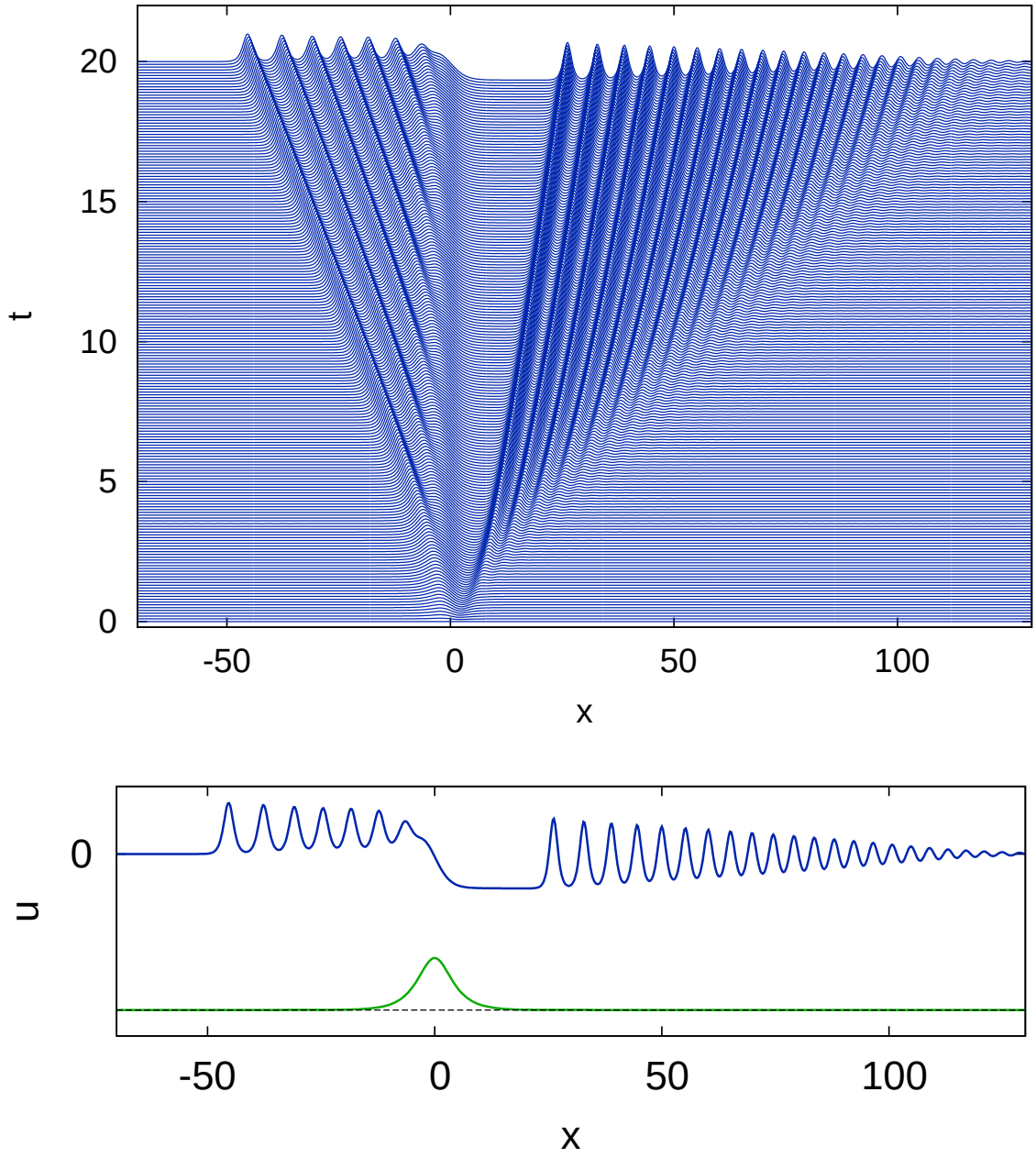

Figure 3.2: Solution of the forced eKdV equation (2.2.13), for surface water waves (2.2.14). Shown is a perspective view in the $x-t$ plane with time up to $t = 20$ (top) and the surface profile u and bathymetry G versus x at $t = 20$ (bottom). The numerical solution of (2.2.13) with the initial condition $u = 0$ is shown. The forcing function is (3.1.1). The other parameters are $\alpha = 0.15$ and $\Delta = -0.5$.

In Section 3.1 the higher order modulation theory is compared with numerical solutions and excellent agreement is found. The eKdV equation is also used to quantify the effect of the higher order nonlinear, dispersive and nonlinear-dispersive terms on resonant flow. The effect of only certain of these higher order terms has been studied in the past by Marchant and Smyth (1990); Grimshaw et al. (2002b); Kamchatnov et al. (2013). In Section 3.2 conclusions are given.

3.1 Comparison with numerical results

In this section the extended modulation theory solution will be compared with numerical solutions of the forced eKdV equation (2.2.13). The forced eKdV equation was solved numerically by an extension to the classical explicit leapfrog method of Zabusky and Kruskal (1965), which has truncation error $O(\Delta t^2, \Delta x^2)$ and is stable for small $\Delta t = O(\Delta x^5)$. See Appendix (A.1) for details of the numerical scheme. Note that this scheme together with the BBM results of Chapter 4 provide numerical results for both low and high amplitude waves.

The forcing functions used were either

$$G(x) = g_0 \operatorname{sech}^2(Wx), \tag{3.1.1}$$

or

$$G(x) = g_0 \exp(-W^2 x^2), \tag{3.1.2}$$

see Grimshaw and Smyth (1986). Furthermore, we used delta function forcing, which is

$$G(x) = g_0 \delta(x-a), \quad \text{where} \quad \delta(x-a) = \lim_{z\to\gamma} \frac{1}{2z} \operatorname{sech}^2\left(\frac{W(x-a)}{z}\right). \tag{3.1.3}$$

The parameter values $g_0 = 1.0$, $W = 0.3$, $a = 0.0$ and $\gamma = 0.5$ were used for the numerical solutions of the present work. These values give solutions which are representative of the general behaviour, Grimshaw and Smyth (1986); Smyth (1987). As well, the higher-order coefficients (2.2.14) for surface water waves are used for all the examples, except last one, we used the higher-order coefficients (2.3.21) for internal waves.

Figure 3.3 shows the upstream (a) and downstream (b) solitary wave amplitudes versus the detuning parameter Δ, for surface water waves (2.2.14). Compared are the eKdV and KdV modulation theories and the corresponding numerical results. The amplitude parameter is $\alpha = 0.15$. The forcing function is the hyperbolic secant (3.1.1). The upstream solitary wave amplitudes as predicted by eKdV modulation theory are greater than the KdV predictions. The predictions are similar in the subcritical regime, but the difference between the theoretical predications increases in the supercritical regime, with a difference of 10% at $\Delta = 3.46$. The variations between the numerical and theoretical results are small for the strongly subcritical and supercritical cases, but are slightly larger in the middle of the resonant band, with errors up to 10%. Overall, the amplitude results as given by modulation theory are in agreement with the numerical values. The downstream solitary wave amplitudes as predicted by the eKdV theory are similar to the KdV theory for supercritical flows and higher than KdV theory for subcritical flows, by up to 3%. There are small variations between the theoretical and numerical results for both theories, with a maximum error of 3%. The results show that for lower amplitude waves, the KdV and eKdV predictions are very similar, as expected. However, as wave amplitudes increase, for upstream solitary waves when the flow is supercritical, and for downstream solitary waves when the flow is subcritical, then the higher-order terms included in the eKdV

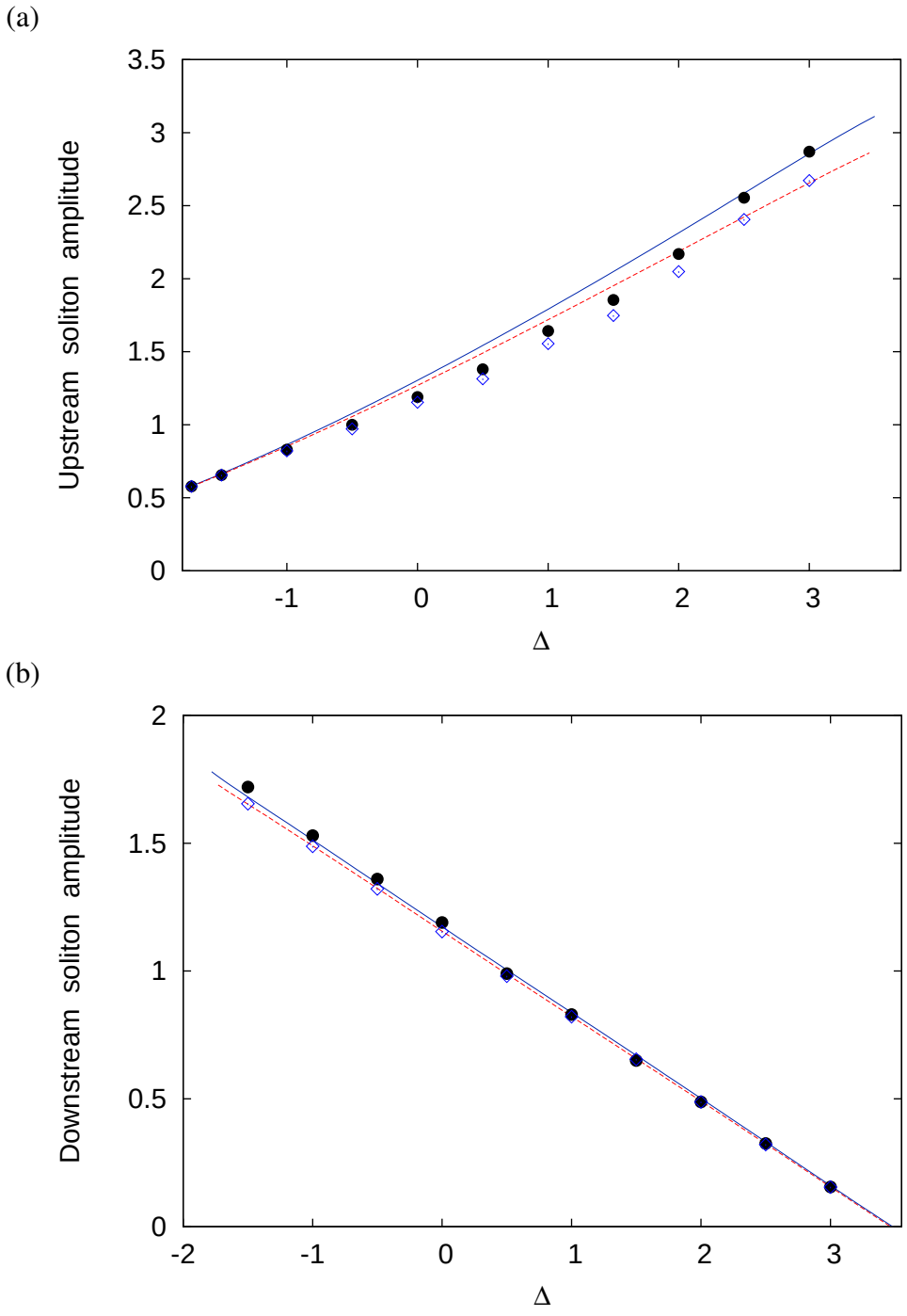

Figure 3.3: The upstream (a) and downstream (b) solitary wave amplitudes versus the detuning parameter Δ, for surface water waves (2.2.14). Compared are eKdV (blue solid line) and KdV (red dashed lines) modulation theory and eKdV ($\bullet$) and KdV ($\diamond$) numerical solutions. The forcing function is (3.1.1). The amplitude parameter is $\alpha = 0.15$.

model play a more significant role, with the eKdV predictions higher than the KdV ones. Note that the numerical results are consistent with their respective theoretical predictions, so the differences between eKdV and KdV numerics are real effects, and not the result of numerical error.

Marchant and Smyth (1990) drew similar comparisons for the case when only the higher-order nonlinear term $c_1 u^2 u_x$ was included in their Gardner-type eKdV equation, see their Figure 3. They found that the upstream eKdV solitary wave amplitudes were higher than KdV theory for supercritical cases, which is qualitatively similar to the results found here for the eKdV theory which includes the full set of higher-order terms. For the downstream solitary wave amplitude, they found their eKdV results to be higher (lower) for supercritical (subcritical) cases, which is different to the results obtained here. Hence the full set of higher-order terms included in the eKdV theory results in qualitatively different results to those for the Gardner equation, which only includes the higher-order nonlinear term.

Figure 3.4 shows the solution u versus x at $t = 30$, for surface water waves (2.2.14). Compared are numerical solutions of the forced eKdV and KdV equations and the wave envelopes for the upstream and downstream KdV and eKdV modulation theory wavetrains. The other parameters are $\Delta = 0$ and $\alpha = 0.15$. The forcing function is the hyperbolic secant (3.1.1). The upstream solitary wave amplitude from eKdV modulation theory is $A = 1.29$, compared with the numerical value of $A_n = 1.19$. For KdV theory, $A = 1.25$ and $A_n = 1.15$. The eKdV results are about 3% higher than the KdV results for both the theoretical and the numerical solutions, while the variation between the theoretical and the numerical results is about 8%.

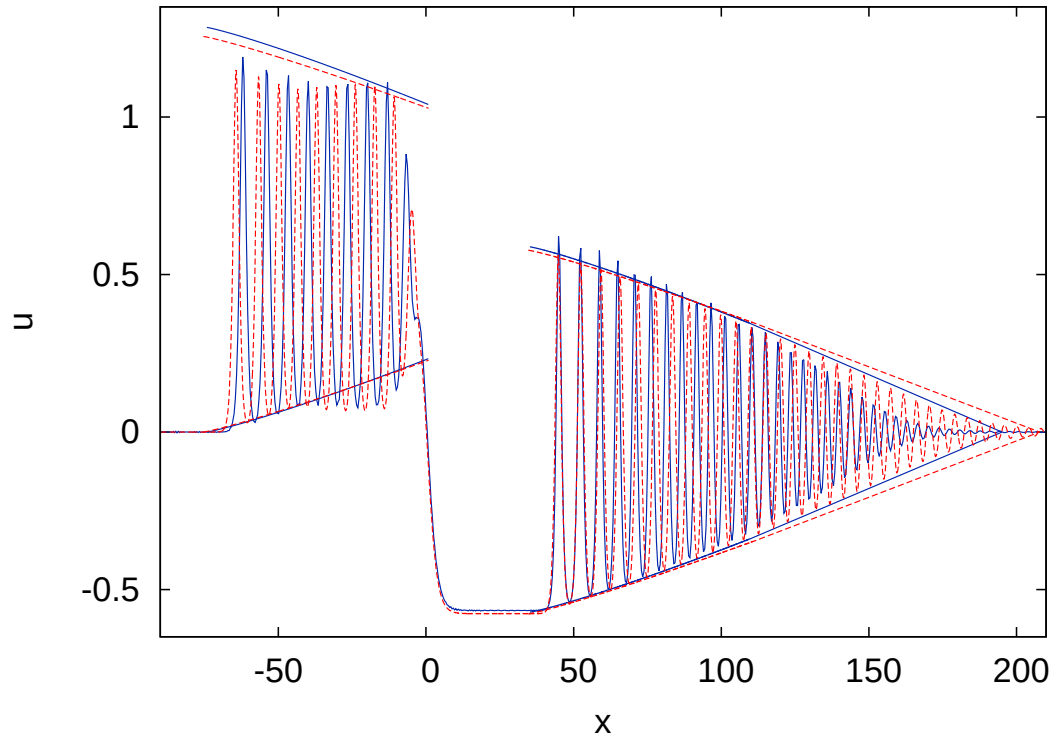

Figure 3.4: The solution u versus x at $t = 30$, for surface water waves (2.2.14). Compared are numerical solutions of the forced eKdV equation (blue solid line) and KdV equation (red dashed line). The other parameters are $\alpha = 0.15$ and $\Delta = 0$. The forcing function is (3.1.1). Also shown are the wave envelopes for the upstream and downstream undular bores for eKdV (blue solid line) and KdV (red dashes) modulation theories.

It should be noted for the comparison shown in Figure 3.4 that the approach of the upstream bore to the steady state is slow. This affects both the amplitude and the profile of the upstream bore when compared with modulation theory. If the upstream bore is propagated until its leading edge amplitude settles to its steady state, it is found that this amplitude is $A_n = 1.24$ for the eKdV equation (at $t = 100$) and $A_n = 1.17$ for the KdV equation. There is then a 4% and a 6% difference between the modulation theory and numerical amplitudes for the eKdV and KdV equations, respectively. The downstream

trailing edge solitary wave amplitude as given by the eKdV modulation theory is $B = 1.16$, while the steady numerical value is $B_n = 1.19$. Furthermore, the downstream solitary wave amplitude given by KdV modulation theory is $B = 1.15$, whereas the numerical value is $B_n = 1.15$. The errors for the downstream solitary wave amplitude as given by the eKdV and KdV modulation theories are then 3% and 0%, respectively. The eKdV theory predicts that the downstream bore is located in the region $36 < x < 195$ and has width $w = 159$, while KdV theory gives $35 < x < 208$ and $w = 173$. The eKdV numerical solution lies in the region $44 < x < 184$ with width $w = 140$, while the KdV numerical solution lies in $44 < x < 224$ with width $w = 180$. It is noted that the width of the downstream eKdV bore is significantly smaller than that of the KdV bore by more than 10%, again in agreement with the results of fully nonlinear theory based on the Su-Gardner equation, El et al. (2006). Lamb and Yan (1996) compared results for KdV and eKdV internal wave undular bores. The higher-order coefficients are different to those for surface water waves, but their eKdV results indicate a much narrower bore, in agreement with the results found here.

Figure 3.5 shows a supercritical solution u versus x at $t = 30$, for surface water waves (2.2.14). Shown are numerical solutions for the forced eKdV and KdV equations. Also shown are the wave envelopes for the upstream and downstream modulated wavetrains as given by the eKdV and KdV modulation theories. The parameters are $\alpha = 0.15$ and $\Delta = 1$. The forcing function is the hyperbolic secant (3.1.1). The upstream solitary wave amplitude for the eKdV modulation theory is $A = 1.79$, compared with the numerical value of $A_n = 1.65$. For the KdV theory, $A = 1.72$ and the numerical value is $A_n = 1.56$. The eKdV amplitudes are then 5% higher than the KdV amplitudes, indicating that the higher

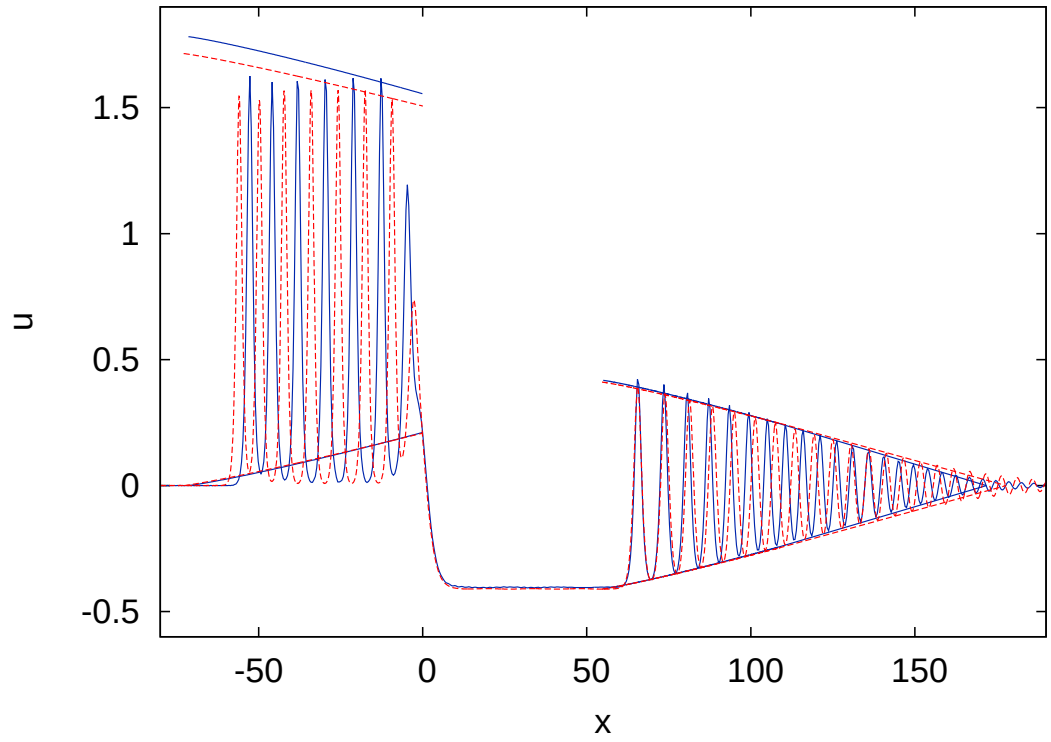

Figure 3.5: A supercritical solution u versus x at $t = 30$, for surface water waves (2.2.14). Compared are numerical solutions of the forced eKdV equation (blue solid line) and KdV equation (red dashed line). The other parameters are $\alpha = 0.15$ and $\Delta = 1$. The forcing function is (3.1.1). Also shown are the wave envelopes for the upstream and downstream undular bores for eKdV (blue solid line) and KdV (red dashes) modulation theories.

order corrections to the KdV equation have a moderate effect on the upstream wavetrain. The difference between the theoretical and the numerical results is about 8%. As for the results for exact resonance $\Delta = 0$ shown in Figure 3.4 the upstream bore is slow in approaching the steady state. The steady upstream leading edge amplitude is $A_n = 1.70$ (at $t = 100$) for the eKdV equation, which reduces the difference between modulation theory and the numerical solution to 5%. For the KdV equation the steady upstream leading edge amplitude is $A_n = 1.61$, a difference of 6% with the KdV modulation theory. The

downstream trailing edge solitary wave amplitude given by eKdV modulation theory is $B = 0.81$, compared with the numerical value $B_n = 0.82$. The value for the KdV equation given by both modulation theory and the numerical solution is $B = 0.82$. There is then only a 2% difference between the downstream trailing wave amplitudes as given by the eKdV and KdV equations, so that the higher order corrections to the KdV equation do not have a great effect on the downstream wave amplitude, in the supercritical regime. Modulation theory for the eKdV equation gives that the downstream bore lies in $55 < x < 168$ with width $w = 113$, while modulation theory for the KdV equation gives $55 < x < 178$ and width $w = 123$. These are compared with the eKdV numerical results $65 < x < 181$ with width $w = 116$ and KdV numerical results $64 < x < 192$ with width $w = 128$. Higher order effects again result in a narrowing of the bore, Lamb and Yan (1996); El et al. (2006).

Figure 3.6 shows a subcritical solution u versus x at $t = 30$, for surface water waves (2.2.14). Compared are numerical solutions for the forced eKdV and KdV equations. Also shown are the wave envelopes for the upstream and downstream modulated wavetrains from the eKdV and the KdV modulation theories. The other parameters are $\alpha = 0.15$ and $\Delta = -0.5$. The forcing function is the hyperbolic secant (3.1.1). The amplitude of the lead solitary wave of the upstream bore as given by eKdV modulation theory is $A = 1.07$ compared with the numerical value $A_n = 1.01$. These amplitudes given by the KdV theory are a modulation amplitude $A = 1.04$ and a numerical amplitude $A_n = 0.97$. The eKdV theory then gives amplitudes which are 3% higher than the KdV results, indicating the effect of higher order corrections to the KdV equation. The steady state upstream amplitudes are $A_n = 1.03$ for the eKdV equation and $A_n = 0.98$ for the KdV equation. The downstream trailing edge solitary wave amplitude as given by eKdV modulation theory is $B = 1.34$,

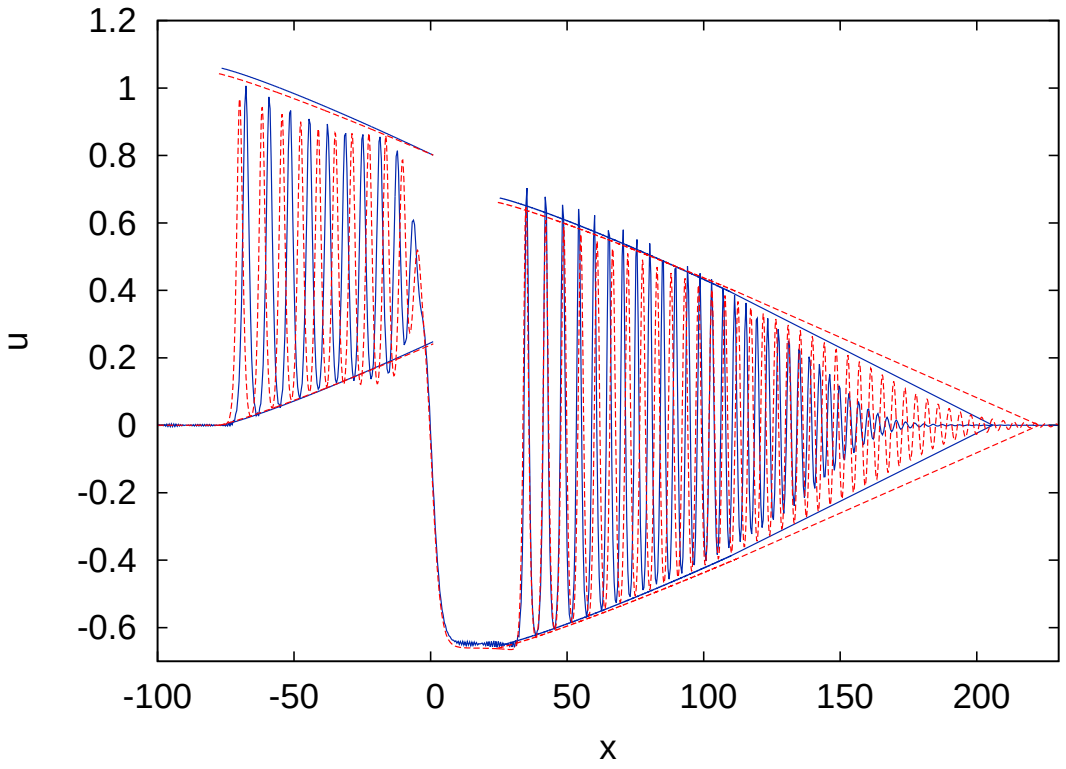

Figure 3.6: A subcritical solution u versus x at $t = 30$, for surface water waves (2.2.14). Compared are numerical solutions of the forced eKdV equation (blue solid line) and KdV equation (red dashed line). The other parameters are $\alpha = 0.15$ and $\Delta = -0.5$. The forcing function is (3.1.1). Also shown are the wave envelopes for the upstream and downstream undular bores for eKdV (blue solid line) and KdV (red dashes) modulation theories.

while the numerical amplitude is $B_n = 1.36$. Numerical solutions and modulation theory for the KdV equation give the equivalent amplitude $B = B_n = 1.32$. Again, the higher order corrections to the KdV equation give small changes in the upstream and downstream amplitudes, 3% from numerical solutions and 1% from modulation theory. In addition, modulation theory gives that the downstream eKdV bore lies in $27 < x < 207$ with width $w = 180$ and the KdV bore lies in $25 < x < 223$ with width $w = 198$, as compared with the numerical values $34 < x < 181$ with width $w = 147$ for the eKdV equation and $35 < x < 208$

with width $w = 173$ for the KdV equation. As for the previous exactly resonant and supercritical examples, higher order effects again result in a narrower bore, Lamb and Yan (1996); El et al. (2006).

Figure 3.7 shows the upstream (a) and downstream (b) solitary wave amplitudes versus the detuning parameter Δ, for surface water waves (2.2.14). Compared are the eKdV modulation theory and the corresponding numerical results for different forcing functions. The amplitude parameter is $\alpha = 0.15$. The forcing functions are hyperbolic secant function (3.1.1), exponential function (3.1.2) and delta function (3.1.3). The upstream solitary wave amplitudes of the numerical results of the forcing exponential function (3.1.2) are in good agreement with the numerical results of the forcing hyperbolic secant function (3.1.1) at the supercritical case. The delta function (3.1.3) results show a slight decrease in the solitary wave amplitudes compared to the other forcing functions results. For the subcritical case, the numerical results given by all the forcing functions are similar and corresponding with the modulation theory. For instance, the upstream solitary wave amplitude of numerical solution for both the forcing function hyperbolic secant and exponential is $A_n = 1.19$, compared with the numerical amplitude of the delta function, $A_n = 1.17$ at $\Delta = 0$. This is some 9% lower than the modulation theory amplitude for the delta function, whilst, 8% for the other forcing functions. The downstream solitary wave amplitudes of the numerical results of the forcing exponential function (3.1.2) are in agreement with the numerical results of the forcing hyperbolic secant function (3.1.1), and are closer to the modulation theory results than the numerical results given by the delta function (3.1.3) at the supercritical case. However, for the subcritical case, the agreement is excellent between the modulation theory and the numerical results given by the delta function. Over

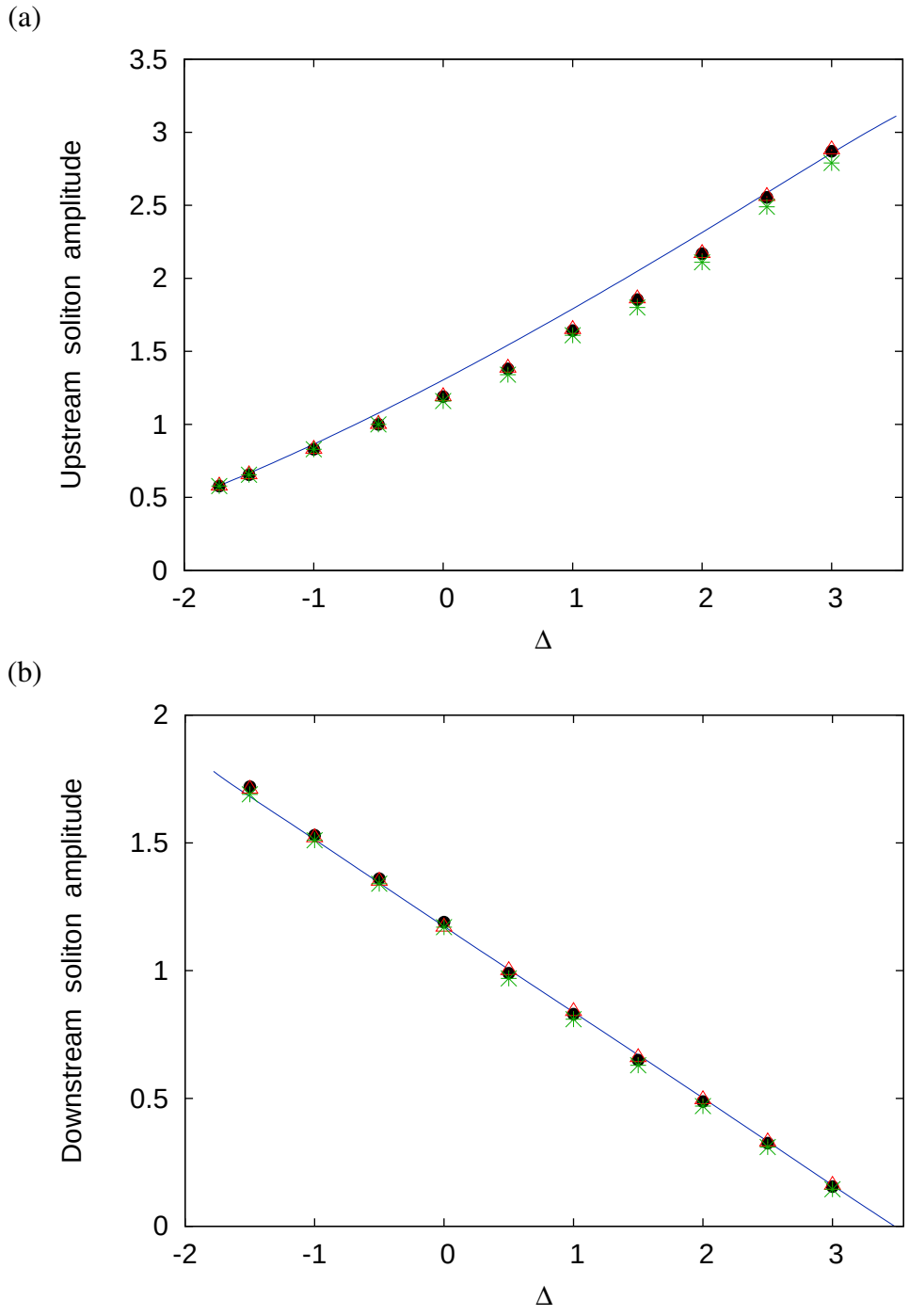

Figure 3.7: The upstream (a) and downstream (b) solitary wave amplitudes versus the detuning parameter Δ, for surface water waves (2.2.14). Compared are eKdV modulation theory (blue solid line) and numerical solutions for different forcing functions. The amplitude parameter is $\alpha = 0.15$. The forcing functions are hyperbolic secant (3.1.1) ($\bullet$), exponential (3.1.2) ($\triangle$) and delta (3.1.3) ($*$).

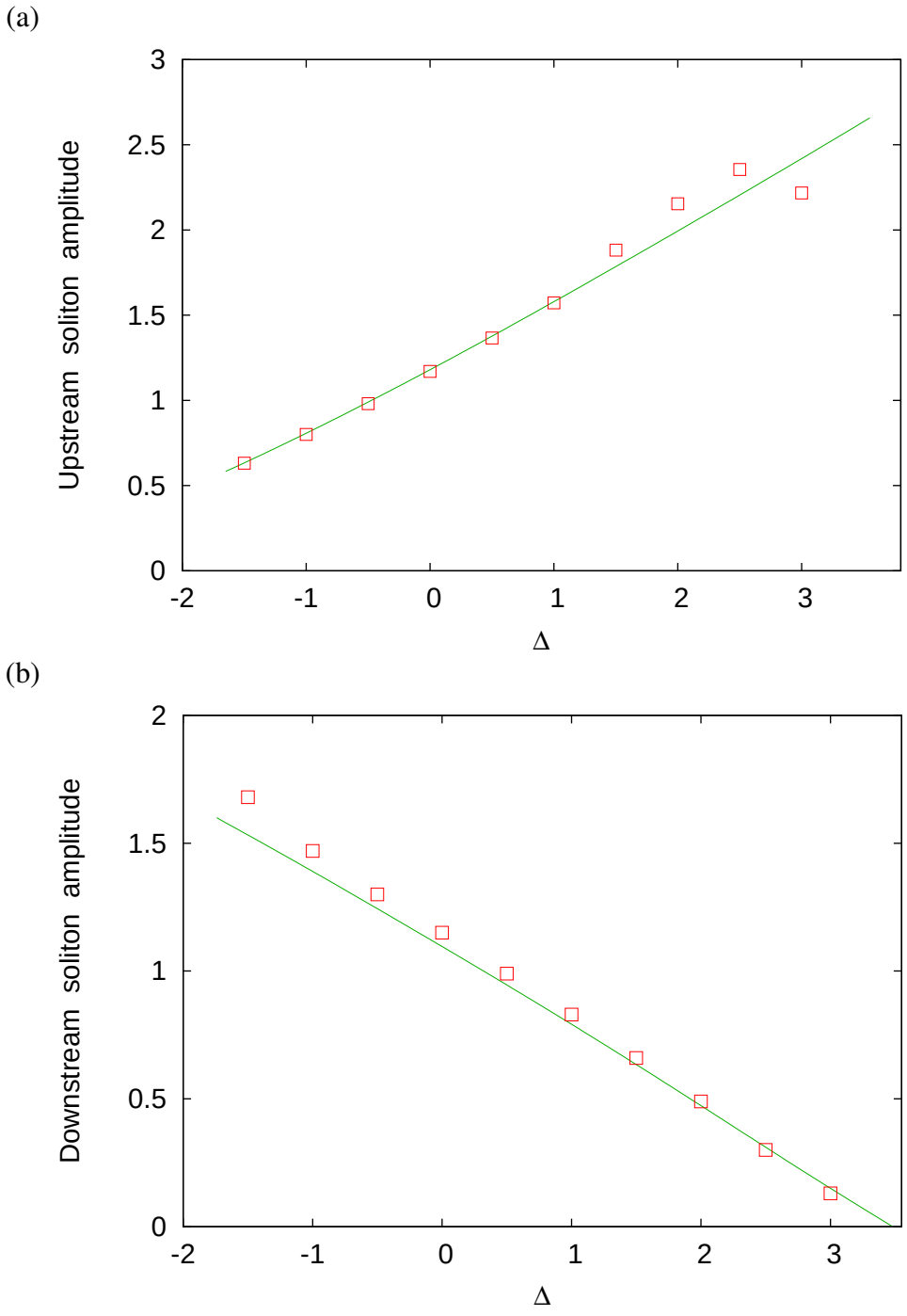

Figure 3.8: The upstream (a) and downstream (b) solitary wave amplitudes versus the detuning parameter Δ, for internal waves coefficients (2.3.21). Compared are eKdV modulation theory (green solid line) and numerical solution (□). The forcing function is (3.1.1). The other parameters are $\alpha c_5 = \alpha c_6 = \alpha c_7 = \alpha c_8 = 0$ and $\alpha = 0.15$.

all the shape of the forcing function does not make much difference to the resonant flow, and only the amplitude of the forcing is important.

Figure 3.8 shows the upstream (a) and downstream (b) solitary wave amplitudes versus the detuning parameter Δ, for internal waves coefficients (2.3.21). Compared are the eKdV modulation theory and the corresponding numerical results. The other parameters are $\alpha c_5 = \alpha c_6 = \alpha c_7 = \alpha c_8 = 0$ and $\alpha = 0.15$. The forcing function is the hyperbolic secant (3.1.1). The upstream solitary wave amplitudes as predicted by the eKdV modulation theory are in agreement with the numerical results in the most of resonant range, with a difference of 16% at $\Delta = 3$. The agreement between the modulation theory and the numerical results is excellent except for very steep waves. The downstream solitary wave amplitudes as predicted by the eKdV modulation theory are similar to the numerical results for supercritical flows and has slightly lower amplitude than the numerical results for subcritical flows, with a maximum error of 19%. The internal wave amplitudes are smaller than those for the surface water waves. For example, at $\Delta = 0$ and $\alpha = 0.15$, the upstream solitary wave amplitude as predicted by the eKdV modulation theory and the numerical solution for internal waves coefficients (2.3.21) is $A_n = 1.11$. This is less than the results given by the surface water waves (2.2.14), which are $A = 1.29$ as predicted by modulation theory and $A_n = 1.19$ the numerical value. Also, the downstream solitary wave amplitude as predicted by the eKdV modulation theory gives $B = 1.11$, whilst the numerical solution gives $B_n = 1.15$ for the internal waves. These results are lower than those for the surface water waves, which is $B = 1.16$ as predicted by modulation theory, while the steady numerical value is $B_n = 1.19$.

3.2 Conclusions

In Chapter 2 and this Chapter we have studied resonant flow over topography using the framework of the forced eKdV equation (2.2.13) in order to gauge the effect of higher order corrections to the standard KdV approximation for weakly nonlinear long waves. Our results are presented for transcritical, supercritical and subcritical flows over the obstacle. These results show that the eKdV predictions, which include these higher order terms, vary from the KdV predictions when the wave amplitudes are large. This occurs in the supercritical regime for upstream waves and the subcritical regime for downstream waves; in both cases the eKdV predictions are higher than the KdV ones. Numerical solutions have confirmed these theoretical predictions. The widths of the eKdV downstream undular bores are significantly reduced compared with KdV theory, in agreement with results based on the higher-order internal wave bore, Lamb and Yan (1996). This reduction is predicted in both flow settings even though the internal wave bore has different higher-order coefficients to those for surface water waves. The numerical comparisons show that a hyperbolic secant and an exponential forcing functions are similar and closer to modulation theory for upstream case more than a delta function, however, it is to be preferred to other forcing functions for downstream in both the extent of bore and the solitary wave amplitude only in the end of subcritical resonant case. The comparison between the theoretical and the numerical solutions were excellent for the internal waves case. It was further found that the inclusion of higher order corrections to the KdV approximation has greater effects on the upstream bore than on the downstream bore. For the amplitude scale $\alpha = O(0.1)$ the effects of the higher order corrections are up to 10%. These differences can be significant when comparisons are made with solutions of the full

water wave equations and with experimental and observational results.

Chapter 4

Comparison of theoretical results and numerical solutions for the forced eBBM equation

In this chapter we compare the theoretical results of extended modulation theory with numerical simulations of the forced eBBM equation. The forced eBBM equation is considered here because its numerical scheme has superior stability properties compared with that of the forced eKdV equation. This equation is asymptotically equivalent (in the limit of small α) to the forced eKdV equation and allows us to explore the accuracy of the extended modulation theory for steeper waves (larger α) as the numerical scheme for the forced eKdV equation is stable up to $\alpha \approx 0.15$. Marchant (1999b) developed a numerical scheme for the forced eBBM equation and found the appropriate higher-order coefficients so that it is asymptotically equivalent to the forced KdV and eKdV equations. The numerical stability properties of the forced eKdV and eBBM equations can be seen

by examining their linearized dispersion relations, which are

$$\omega = (1+\alpha\Delta)k - \alpha k^3 + \alpha^2 c_4 k^5, \quad \omega = \frac{k(1+\alpha\Delta)}{1+\alpha(1-\alpha\Delta)k^2 + \alpha^2 c_4 k^4}, \tag{4.0.1}$$

respectively. For the eKdV equation the wave speed is not bounded for large wavenumber k, which leads to numerical instabilities. As long as $c_4 > 0$ the wave speed for the eBBM equation is bounded. Hence it is numerically stable, see Marchant (2000). The forced eBBM equation is

$$\begin{aligned} &u_t + (1+\alpha\Delta)u_x + 6\alpha u u_x - (1-\alpha\Delta)u_{xxt} + \alpha^2 c_1 u^2 u_x + \alpha^2 c_2 u_x u_{xx} + \alpha^2 c_3 u u_{xxx} \\ &+ \alpha^2 c_4 u_{xxxxt} = -\alpha(1+\alpha c_8\Delta)G_x - \alpha^2 c_5 G u_x - \alpha^2 c_6 G_x u - \alpha^2 c_7 G_{xxx}. \end{aligned} \tag{4.0.2}$$

In this equation the linear dispersive terms contain a time derivative. The appropriate coefficients for (4.0.2) so that is asymptotically equivalent to the forced eKdV equation are

$$c_1 = -\frac{3}{2}, \quad c_2 = \frac{49}{4}, \quad c_3 = \frac{7}{2}, \quad c_4 = \frac{21}{40}, \quad c_5 = 2, \quad c_6 = \frac{7}{4}, \quad c_7 = \frac{3}{8}, \quad c_8 = \frac{3}{8}, \tag{4.0.3}$$

while the appropriate coefficients so that the eBBM equation (4.0.2) is asymptotically equivalent to the forced KdV equation for surface water waves are

$$c_1 = 0, \quad c_2 = 18, \quad c_3 = 5, \quad c_4 = 1, \quad c_5 = 0, \quad c_6 = 0, \quad c_7 = -1, \quad c_8 = 0, \tag{4.0.4}$$

see, Marchant (1999b). See Appendix (A.2) for details of the numerical scheme used for solving the eBBM equation (4.0.2). The forcing $G(x)$ was chosen as

$$G(x) = g_0 \operatorname{sech}^2(W(x-t)). \tag{4.0.5}$$

In Section 4.1 comparisons are made between the extended modulation theory and numerical solutions of the forced eBBM equation. In Section 4.2 conclusions are given.

4.1 Results and discussion

We show that the results for the forced eKdV and eBBM equations are qualitatively similar, for resonant flow over an obstacle, for waves of low to moderate steepness. Numerical results of the eKdV equation are not available for large α, due to numerical instability.

Figure 4.1(a) shows the upstream solitary wave amplitude versus the detuning parameter Δ. Compared are the extended modulation theory, for surface water waves (2.2.14) and the numerical solutions of the forced eBBM equation, for surface water waves (4.0.3). The forcing function is the hyperbolic secant (4.0.5) with $g_0 = 1.0$ and $W = 0.3$. The other parameters are $\alpha = 0.15$ and $t = 30$. The results show good agreement for the upstream solitary wave amplitudes. In general, the extended modulation theory predicts amplitudes greater than the numerical results of the eBBM model, over most of the resonant range. The difference between the extended modulation theory and the numerical solutions increases in the supercritical regime, with a difference of 11% at $\Delta = 3$, but is low for other values of Δ, with a 8% difference at $\Delta = 0$. The large differences near $\Delta = 3$ are due to large upstream solitary wave amplitudes there.

Figure 4.1(b) shows the downstream solitary wave amplitude versus the detuning parameter Δ, for surface water waves. Shown are the extended modulation theory and the numerical solutions of the forced eBBM equation. As for the upstream case, the extended modulation theory results are slightly higher than the eBBM numerical results over most of the resonant range. The difference between the extended modulation theory and numerical solution is fairly small, with errors of up to 12%.

Figure 4.2 shows the upstream and downstream solitary wave amplitudes versus the wave amplitude α. Compared are the extended modulation theory, for surface water

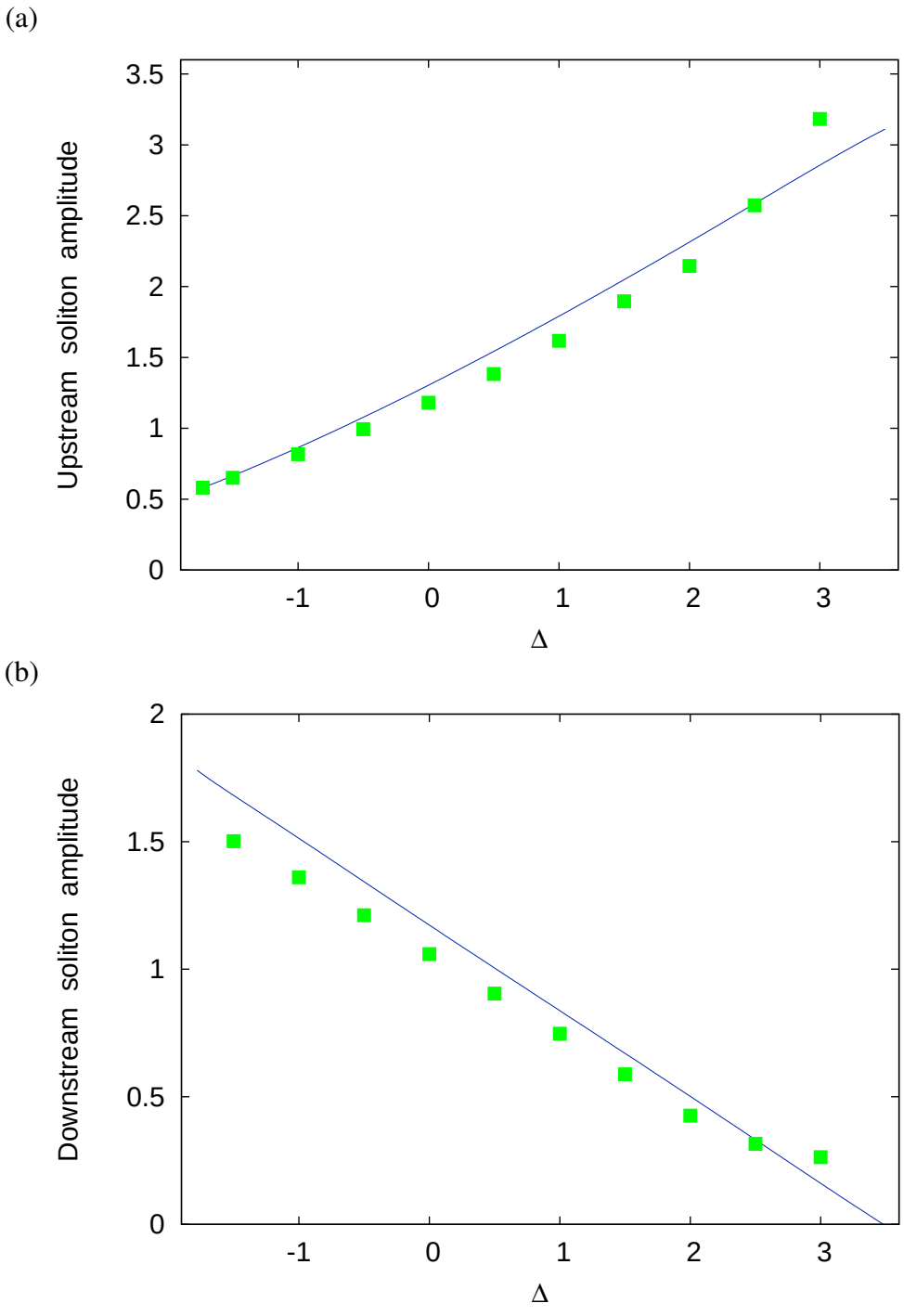

Figure 4.1: The upstream (a) and the downstream (b) solitary wave amplitudes versus the detuning parameter Δ. Compared are the extended modulation theory, for surface water waves (2.2.14) (blue line) and the numerical solutions for the forced eBBM equation, for surface water waves (4.0.3) (■). The forcing is (4.0.5) with $g_0 = 1.0$ and $W = 0.3$. The amplitude parameter is $\alpha = 0.15$.

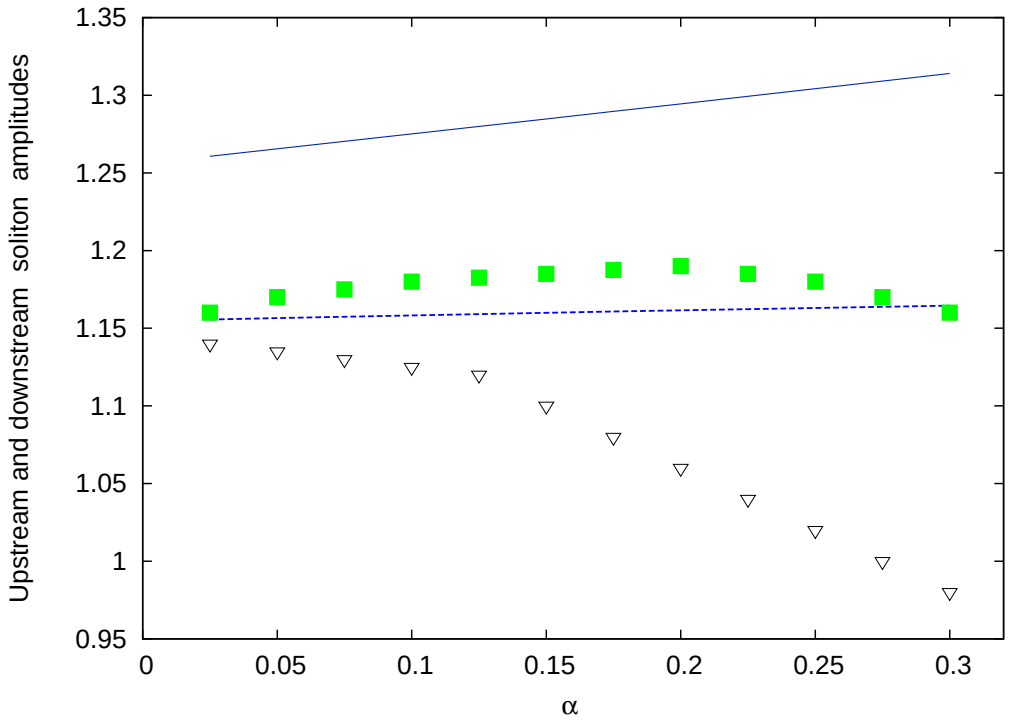

Figure 4.2: The upstream and downstream solitary wave amplitudes versus the amplitude α. Compared are the upstream (blue solid line) and the downstream (blue dashes) soliton amplitudes from the extended modulation theory, for surface water waves (2.2.14) and the numerical solution of the forced eBBM equation, for surface water waves (4.0.3) (■ upstream) and (▽ downstream). The forcing is (4.0.5) with $g_0 = 1.0$ and $W = 0.3$. The detuning parameter is $\Delta = 0$.

waves (2.2.14) and the numerical solution of the forced eBBM equation, for surface water waves (4.0.3). The detuning parameter is $\Delta = 0$. The forcing function is the hyperbolic secant (4.0.5) with $g_0 = 1.0$ and $W = 0.3$. Note that numerical results for the eKdV equation are only available for $\alpha \leq 0.15$, so this figure allows us to explore the comparison between numerical solutions and theory for steeper waves. The upstream and downstream solitary wave amplitudes from the extended modulation theory are greater than those of the numerical solutions over the whole range for α. For the upstream amplitudes, both extended modulation theory results and numerical solutions are fairly constant, with the errors of

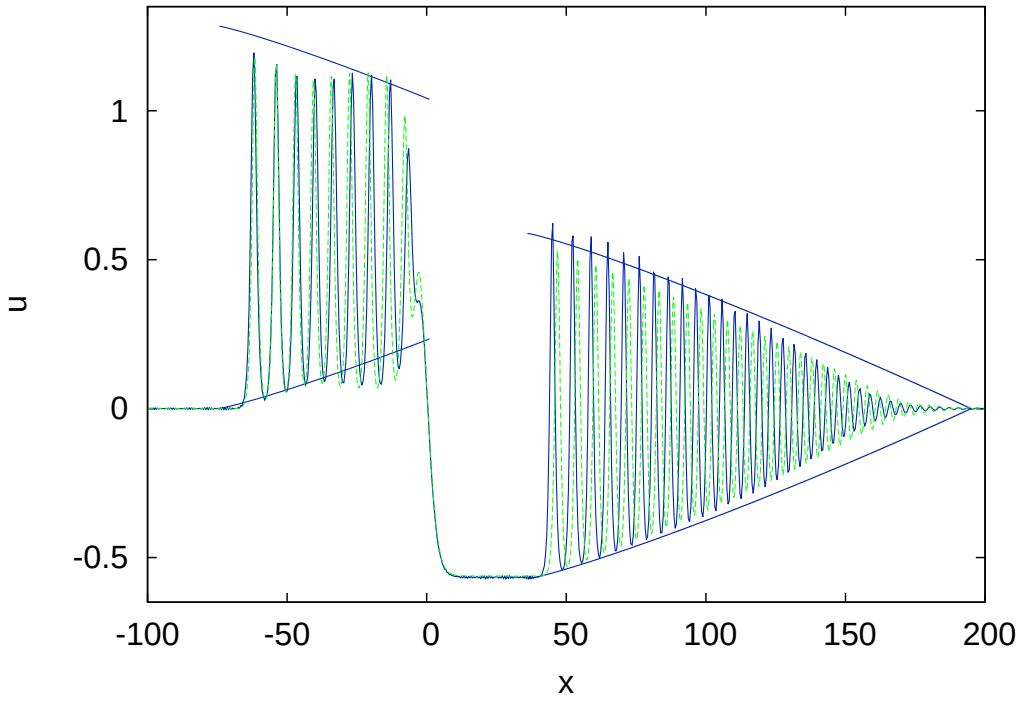

Figure 4.3: The elevation u versus x at $t = 30$. Compared are the numerical solutions of the forced eKdV equation, for surface water waves (2.2.14) (blue solid line) and the forced eBBM equation, for surface water waves (4.0.3) (green dashed). Also shown are the wave envelope for the upstream and downstream cnoidal wavetrains from extended modulation theory (blue solid line). The forcing functions are (3.1.1) for eKdV and (4.0.5) for eBBM with $g_0 = 1.0$ and $W = 0.3$. The other parameters are $\Delta = 0$ and $\alpha = 0.15$.

up to 13%, even for large α. For the downstream amplitudes, the error increases as α increases. This is to be expected as the differences between the eBBM equation and the extended modulation theory are $O(\alpha^2)$, which increases as α increases.

Figure 4.3 shows the elevation u versus x at $t = 30$. Compared are numerical solutions for both the forced eBBM equation, for surface water waves (4.0.3) and the forced eKdV equation, for surface water waves (2.2.14). Also shown are the wave envelopes for the upstream and downstream cnoidal wavetrains from the extended modulation theory. The

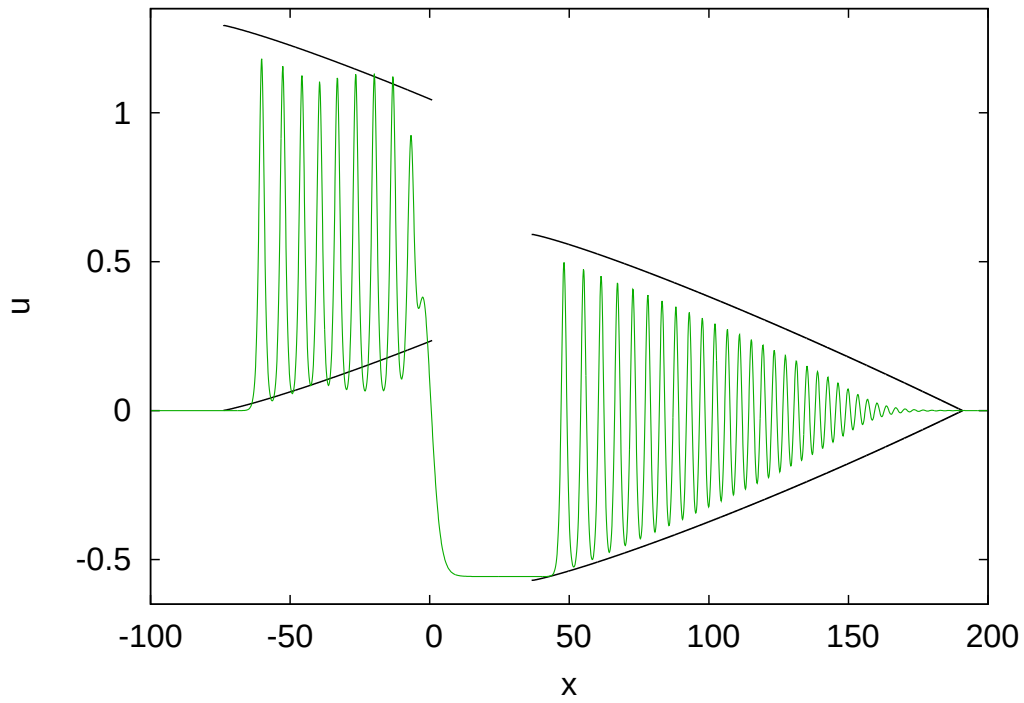

Figure 4.4: The elevation u versus x at $t = 30$, for surface water waves. Compared are the numerical solution of the forced eBBM equation (green solid line) and the wave envelope for the upstream and downstream cnoidal wavetrains from extended modulation theory (black solid line). The forcing is (4.0.5) with $g_0 = 1.0$ and $W = 0.3$. The other parameters are $\Delta = 0$ and $\alpha = 0.2$.

forcing functions are the hyperbolic secant (3.1.1) for the forced eKdV equation and the hyperbolic secant (4.0.5) for the forced eBBM equation. The other parameters are $\Delta = 0$, $\alpha = 0.15$, $g_0 = 1.0$ and $W = 0.3$. The upstream solitary wave amplitude as predicted by the extended modulation theory is $A = 1.29$, compared with the numerical solution of the eBBM model gives $A_{bbm} = 1.18$, while the numerical solution of the eKdV model is $A_n = 1.19$. The variation between the theoretical and the numerical results is about 8%. However, this difference decreases if the long time numerical solutions is used. For example, the upstream solitary wave amplitudes become $A_{bbm} = 1.20$ and $A_n = 1.24$, and the variation between the extended modulation theory results and the eBBM model is

reduced to 7%. The downstream solitary wave amplitude as predicted from the extended modulation theory is $B = 1.16$, while the numerical solution gives $B_{bbm} = 1.06$ and $B_n = 1.19$. Here the eBBM amplitude is significantly lower than the other predictions, with a difference of about 9%. For long time, the downstream eBBM solitary wave amplitude is $B_{bbm} = 1.09$, with a slightly reduced error of 6%. It is also worthwhile to compare the width of the downstream bore. The downstream eBBM bore occurs between $46 < x < 187$ and has width $w = 141$ and the eKdV bore has $44 < x < 184$ and width $w = 140$. The extended modulation theory bore occurs between $36 < x < 195$ and has width $w = 159$. Both numerical results are very similar and the difference with the extended modulation theory is about 11%. For waves of moderate steepness, $\alpha = 0.15$, the results of the eBBM and eKdV models are remarkably consistent.

Figure 4.4 shows the elevation u versus x at $t = 30$. Compared are the forced eBBM equation, for surface water waves (4.0.3) and the extended modulation theory, for surface water waves (2.2.14). The forcing function is the hyperbolic secant (4.0.5) with $g_0 = 1.0$ and $W = 0.3$. The other parameters are $\Delta = 0$ and $\alpha = 0.2$. The upstream solitary wave amplitude from the extended modulation theory is $A = 1.30$, whilst the numerical solution gives $A_{bbm} = 1.19$, a 8% difference. For this example no eKdV results are available as α is too large and the numerical scheme is unstable. The difference decreases for long time, with the upstream solitary wave amplitude, $A_{bbm} = 1.22$, a difference of about 6%. The downstream eBBM solitary wave amplitude, $B_{bbm} = 1.01$, and the extended modulation theory amplitude is $B = 1.16$. The variation between the numerical results of the extended BBM and the extended modulation theory is approximately 13%. In this example, the downstream bore from the extended modulation theory occurs between $36 < x < 191$

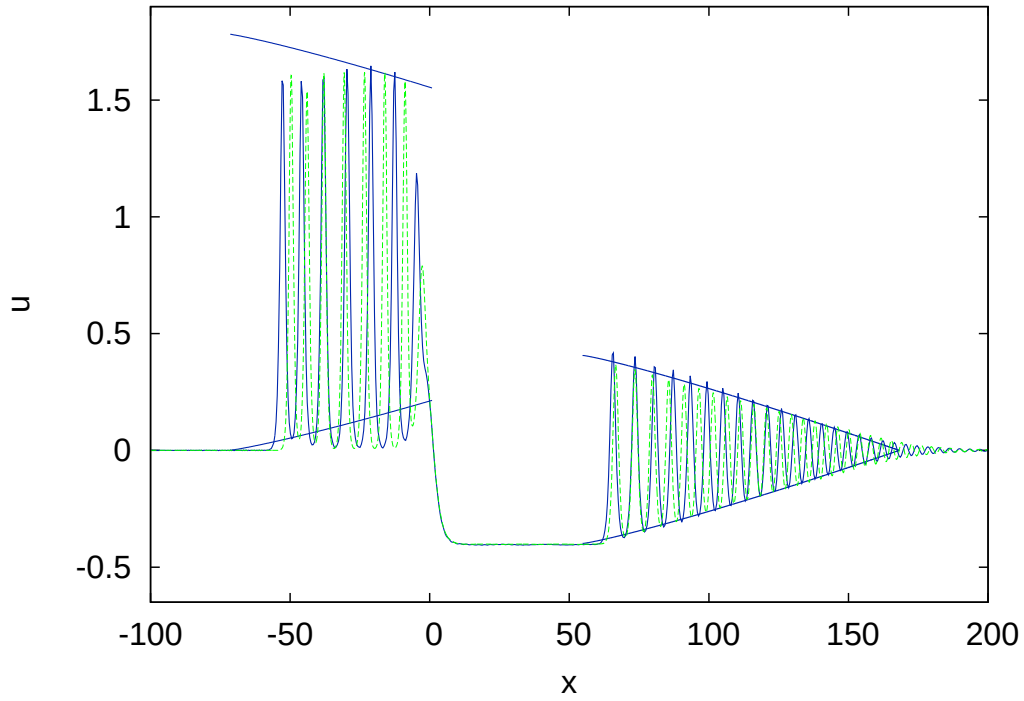

Figure 4.5: The elevation u versus x at $t = 30$, for surface water waves. Compared are the numerical solutions of the forced eKdV equation (blue solid line) and the forced eBBM equation (green dashed). Also shown are the wave envelope for the upstream and downstream cnoidal wavetrains from extended modulation theory (blue solid line). The forcing functions are (3.1.1) for eKdV and (4.0.5) for eBBM with $g_0 = 1.0$ and $W = 0.3$. The other parameters are $\Delta = 1$ and $\alpha = 0.15$.

with width $w = 155$ and the numerical bore between $47 < x < 181$ with width $w = 134$, a difference of about 13%. So for steeper waves the comparison between the extended modulation theory and eBBM numerical results is still good, with differences of up to 13%.

Figure 4.5 shows a supercritical case u versus x at $t = 30$, for surface water waves. Compared are the numerical solutions for both the forced eBBM and eKdV equations. Also shown are the wave envelopes for the upstream and downstream cnoidal wavetrains given by the extended modulation theory. The forcing functions are the hyperbolic secant

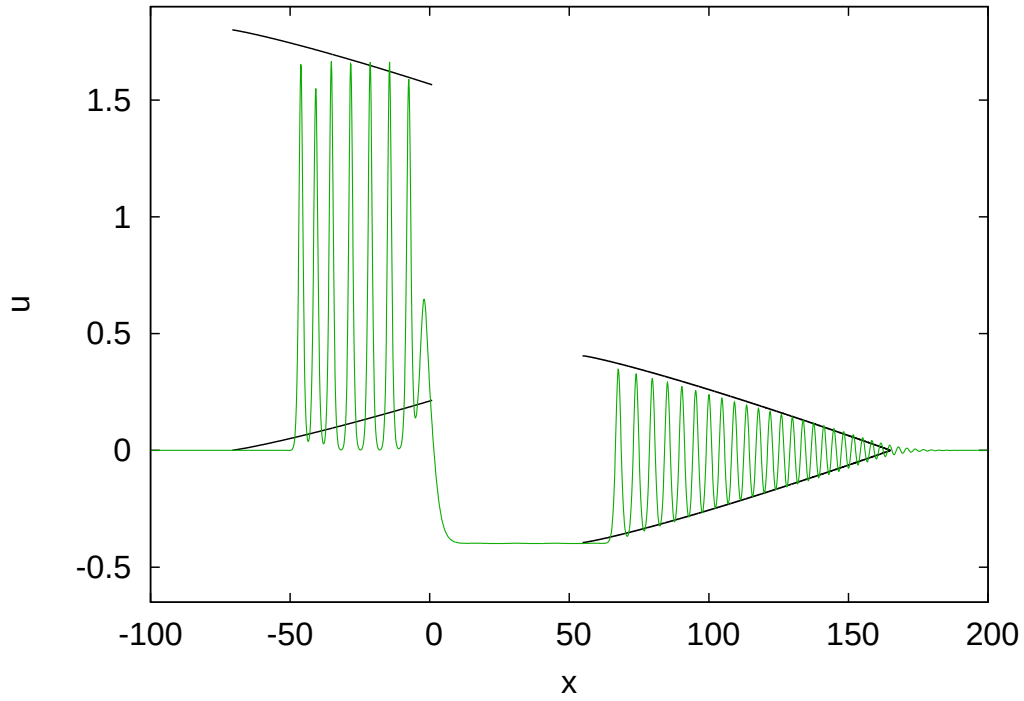

Figure 4.6: The elevation u versus x at $t = 30$, for surface water waves. Compared are the numerical solution of the forced eBBM equation (green solid line) and the wave envelope for the upstream and downstream cnoidal wavetrains from extended modulation theory (black solid line). The forcing functions are (3.1.1) for eKdV and (4.0.5) for eBBM with $g_0 = 1.0$ and $W = 0.3$. The other parameters are $\Delta = 1$ and $\alpha = 0.2$.

(3.1.1) for the forced eKdV equation and the hyperbolic secant (4.0.5) for the forced eBBM equation. The other parameters are $\Delta = 1$, $\alpha = 0.15$, $g_0 = 1.0$ and $W = 0.3$. The upstream solitary wave amplitude as predicted by the extended modulation theory is $A = 1.79$, compared with the numerical solution of the eBBM model, $A_{bbm} = 1.66$, and the eKdV value of $A_n = 1.65$. Again, the numerical results are very consistent to each other, with a error of 7% when compared with the extended modulation theory. Nevertheless, this difference decreases if the long time numerical solutions are used, for example, the upstream solitary wave amplitudes become $A_{bbm} = 1.68$ and $A_n = 1.70$, with errors of about

6%. The downstream solitary wave amplitude as predicted by the extended modulation theory is $B = 0.81$, while the numerical solutions give $B_{bbm} = 0.73$ and $B_n = 0.82$. As for the $\Delta = 0$ case the eBBM downstream amplitude is lower than the eKdV value The error between the extended modulation theory and the numerical result of the eBBM equation is about 10%. For long time, the downstream solitary wave amplitude of the numerical solution for the eBBM model is $B_{bbm} = 0.75$, with difference of 7%. In this example, the downstream numerical bore of the eBBM model lies between $65 < x < 187$ with width $w = 122$ and for the eKdV model it lies in $65 < x < 181$ with width $w = 116$, whilst the downstream bore as predicted by the extended modulation theory occurs between $55 < x < 168$ with width $w = 113$. There are only small variations for the width, of about 7%.

Figure 4.6 shows a supercritical solution u versus x at $t = 30$, for surface water waves. Compared are the forced eBBM equation and the extended modulation theory. The forcing function is the hyperbolic secant (4.0.5) with $g_0 = 1.0$ and $W = 0.3$. The other parameters are $\Delta = 1$ and $\alpha = 0.2$. The upstream solitary wave amplitude as predicted by the extended modulation theory is $A = 1.80$, whilst the numerical solution gives $A_{bbm} = 1.67$, a difference of 7%. The difference decreases for long time. The steady upstream solitary wave amplitude is $A_{bbm} = 1.70$, a variation of 6%. The downstream solitary wave amplitude given by the numerical solution of the eBBM equation is $B_{bbm} = 0.71$, and the extended modulation theory gives $B = 0.83$, a variation of 14%. The extended modulation theory predicts that the downstream bore is located in $55 < x < 165$ with width $w = 110$ and the numerical solution of the eBBM equation gives that the bore lies in $66 < x < 182$ and width $w = 116$. The variation is approximately 5%. The comparisons between the extended modulation theory and the eBBM results are very good for this example of steeper

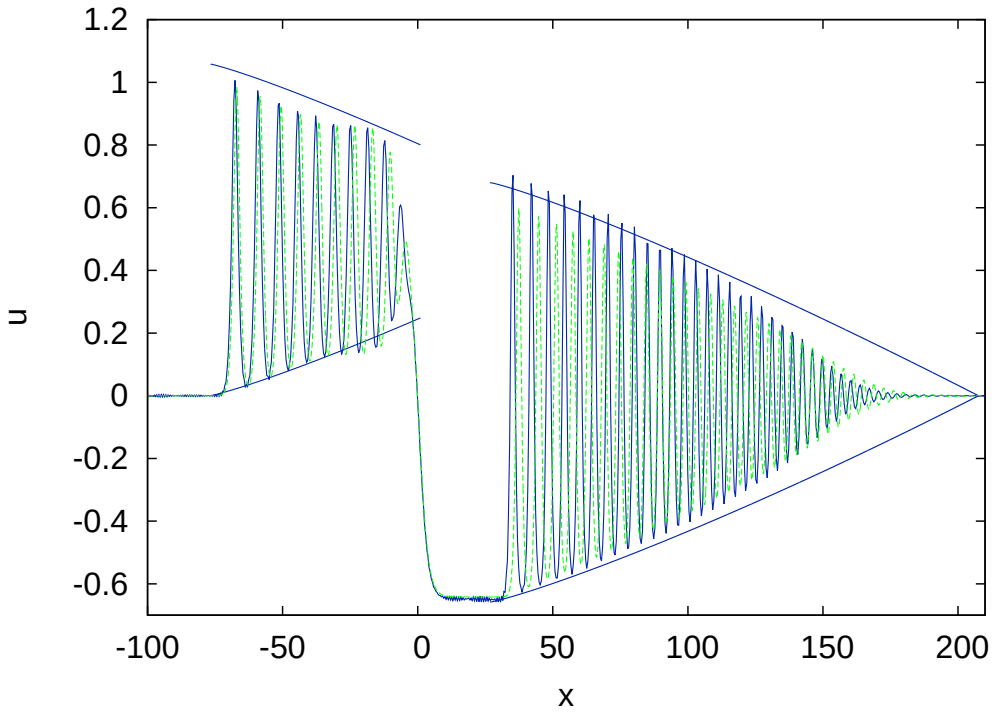

Figure 4.7: The elevation u versus x at $t = 30$, for surface water waves. Compared are the numerical solutions of the forced eKdV equation (blue solid line) and the forced eBBM equation (green dashed). Also shown are the wave envelope for the upstream and downstream cnoidal wavetrains from extended modulation theory (blue solid line). he forcing functions are (3.1.1) for eKdV and (4.0.5) for eBBM with $g_0 = 1.0$ and $W = 0.3$. The other parameters are $\Delta = -0.5$ and $\alpha = 0.15$.

waves in the supercritical regime.

Figure 4.7 shows a subcritical solution u versus x at $t = 30$, for surface water waves. Compared are numerical solutions for both the eBBM and eKdV equations. Also shown are the wave envelopes for the upstream and downstream cnoidal wavetrains given by the extended modulation theory. The forcing functions are the hyperbolic secant (3.1.1) for the forced eKdV equation and the hyperbolic secant (4.0.5) for the forced eBBM equation. The other parameters are $\Delta = -0.5$, $\alpha = 0.15$, $g_0 = 1.0$ and $W = 0.3$. The upstream solitary wave amplitude as predicted by the extended modulation theory is $A = 1.07$ compared

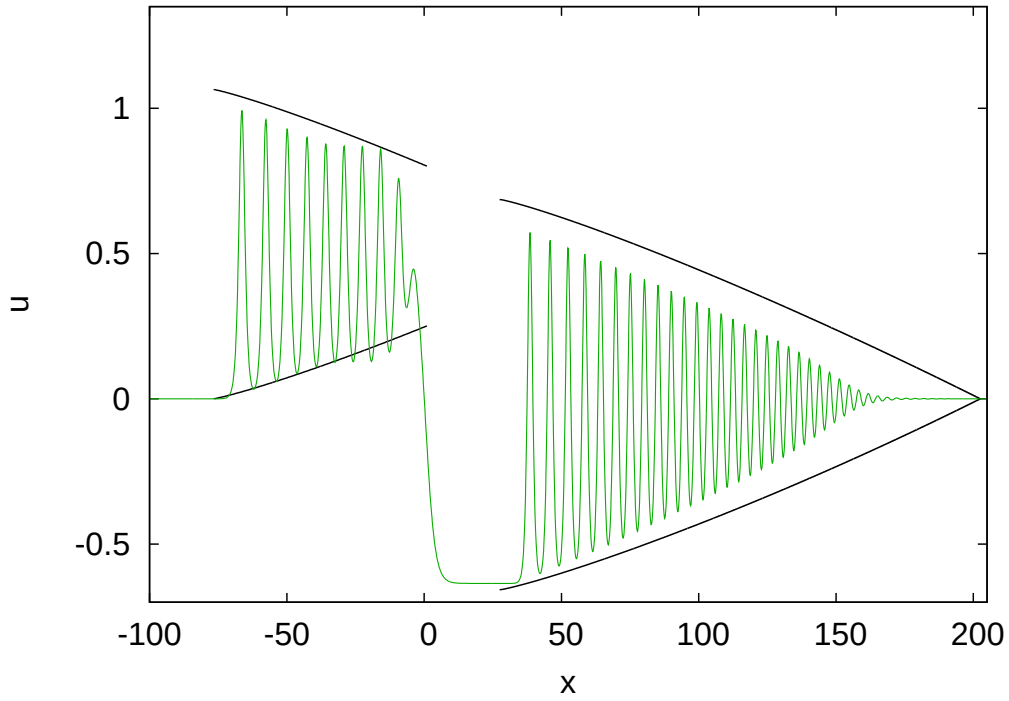

Figure 4.8: The elevation u versus x at $t = 30$, for surface water waves. Compared are the numerical solution of the forced eBBM equation (green solid line) and the wave envelope for the upstream and downstream cnoidal wavetrains from extended modulation theory (black solid line). The forcing is (4.0.5) with $g_0 = 1.0$ and $W = 0.3$. The other parameters are $\Delta = -0.5$ and $\alpha = 0.2$.

with the numerical solution of the eBBM equation, $A_{bbm} = 0.99$, while the eKdV model is $A_n = 1.01$. The difference between the extended modulation theory and the numerical solution of the eBBM equation is approximately 6%.

However, this difference decreases if the long time numerical solution is used, for example, the upstream solitary wave amplitudes become $A_{bbm} = 1.02$ with error about 4% whilst $A_n = 1.03$. The downstream steady solitary wave amplitude as predicted by the extended modulation theory is $B = 1.34$, while the numerical solution gives $B_{bbm} = 1.26$ and $B_n = 1.36$. Again, the eBBM model predicts lower downstream amplitudes. The difference between the theoretical results and the numerical solutions of the eBBM

equation is about 6%. For long time, the steady downstream solitary wave amplitude of numerical solution for the eBBM model is $B_{bbm} = 1.27$ with error of 5%. Extended modulation theory predicts that the downstream bore lies in $27 < x < 207$ with width $w = 180$, whilst the eBBM equation gives the bore lies in $36 < x < 198$ with width $w = 162$. For the eKdV equation $34 < x < 181$ and width $w = 147$. The variation between the theoretical predictions and the numerical solution of the eBBM equation for the width is about 10%.

Figure 4.8 shows a subcritical solution u versus x at $t = 30$, for surface water waves. Compared are the numerical solution of the forced eBBM equation and the extended modulation theory. The forcing function is the hyperbolic secant (4.0.5) with $g_0 = 1.0$ and $W = 0.3$. The other parameters are $\Delta = -0.5$ and $\alpha = 0.2$. The upstream solitary wave amplitude given by the extended modulation theory is $A = 1.07$, whilst the numerical solution gives $A_{bbm} = 1.00$. The upstream solitary wave amplitude error between the theoretical and the numerical results is approximately 6%. The difference decreases for long time. The steady upstream solitary wave amplitude is $A_{bbm} = 1.02$, the difference is about 5%.

The downstream solitary wave amplitude given by the numerical solution of the eBBM equation is $B_{bbm} = 1.23$, and the the extended modulation theory result is $B = 1.35$, a variation of 9%. The downstream bore as predicted by the extended modulation theory lies in $28 < x < 202$ with width $w = 174$. The eBBM equation bore lies in $38 < x < 179$ with width $w = 141$, a difference of 19%.

4.2 Conclusions

Numerical solutions from the eKdV and eBBM equations were compared for waves of moderate steepness for the subcritical, critical and supercritical cases. In each case the

two numerical solutions predict very similar results, except for the downstream solitary wave amplitude, for which the eBBM solution is lower than the eKdV value. The comparison with the extended modulation theory is also good. It can be concluded that there is a good qualitative agreement between the numerical solutions of the forced eBBM and eKdV equations, and the extended modulation theory. For steeper waves, the comparison between the extended modulation theory and the numerical solutions of the eBBM equations is reasonable, but differences occur due to neglected terms at $O(\alpha^2)$, particularly for the width of the downstream bore, in subcritical cases, and for the downstream solitary wave amplitude. In summary, the extended modulation theory is quite accurate for moderate to large α, in comparison with solutions of both the eKdV and eBBM equations. Hence the eBBM equation can be considered a suitable alternative to the eKdV equation for calculating numerical solutions, especially for waves of low to moderate steepness.

Chapter 5

Uniform soliton theory

5.1 Introduction

It was shown in Chapter 2 that the extended modulation theory solution for the upstream wavetrain consists of a modulated cnoidal wavetrain with modulus varying between $m = m_0$ and 1. In this chapter we will extend the theory of Grimshaw and Smyth (1986) by assuming that the resonant flow generates a uniform train of solitary waves (of modulus $m = 1$). So the uniform soliton theory applies when $m \to 1$, or in the supercritical range (see Figure 2.3). The uniform soliton theory predicts the amplitude of the solitary waves that are generated upstream by using mass and energy conservation. Wu (1987) developed uniform soliton theory for the critically resonant case $\Delta = 0$, with that work extended by Lee et al. (1989) to cover all resonant flows.

Marchant and Smyth (2012) developed an approximate method to describe the amplitude of the lead solitary waves in an undular bore, using mass and energy conservation, for general nonlinear wave equations, such as KdV, modified KdV, Benjamin-Ono and NLS equations. Smyth (1990) found approximate values of the upstream amplitude waves

by using energy conservation and the solution of modulation theory for the forced KdV equation derived by Smyth (1987). He compared these values with experimental and numerical results, the agreement is good for subcritical case and less good in supercritical case.

In a similar manner to the theoretical solutions of Grimshaw and Smyth (1986), they found the solitary wave amplitudes and spacings by using a balance of mass and energy. In Section 5.2 uniform soliton theory for the forced eKdV equation is derived. In Section 5.3 comparisons are made between uniform soliton theory and numerical solutions for both the forced eKdV and eBBM equations. In Section 5.4 conclusions are given.

5.2 Mass and energy conservation law for the eKdV equation

We assume that a finite number N of solitary waves are generated upstream of the forcing, in $-\infty < x < x_c$. Then, the conservation law for mass of the forced eKdV equation (2.2.13) can be written as

$$\begin{aligned}\frac{d}{dt}\int_{-\infty}^{x_c} u\,dx \;=\; & \left[-\Delta u + 3u^2 + \frac{\partial^2 u}{\partial x^2} + (1+\alpha c_8\Delta)G(x)\right]_{-\infty}^{x_c} \\ & + \alpha\left[-\frac{c_1}{3}u^3 + \frac{c_2}{2}\frac{\partial^2 u}{\partial x^2} + c_3\left(u\frac{\partial^2 u}{\partial x^2} - \frac{1}{2}\frac{\partial^2 u}{\partial x^2}\right) + c_4\frac{\partial^4 u}{\partial x^4}\right]_{-\infty}^{x_c} \\ & + \alpha\int_{-\infty}^{x_c}\left(c_5 G\frac{\partial u}{\partial x} + c_6\frac{\partial G(x)}{\partial x}u + c_7\frac{\partial^3 G(x)}{\partial x^3}\right)dx. \qquad (5.2.1)\end{aligned}$$

The position x_c is chosen to lie for enough away from the obstacle and $u = u_u$ with derivatives zero. Hence

$$\frac{d}{dt}\int_{-\infty}^{x_c} u dx = -\Delta u_u + 3u_u^2 - \frac{1}{3}\alpha c_1 u_u^3, \qquad (5.2.2)$$

where the value of u_u is given by (2.3.18). The eKdV solitary wave solution (2.3.20) was derived by Marchant and Smyth (1996) as

$$\begin{aligned} u = A_c \operatorname{sech}^2\theta + \alpha A_c^2\left(\frac{1}{6}c_1 + \frac{1}{6}c_2 + \frac{2}{3}c_3 - 5c_4\right)\operatorname{sech}^2\theta \\ + \alpha A_c^2\left(-\frac{1}{12}c_1 - \frac{1}{4}c_2 - \frac{1}{2}c_3 + \frac{15}{2}c_4\right)\operatorname{sech}^4\theta, \\ \text{where} \quad \theta = k(x - V_c t), \quad k = \sqrt{\frac{A_c}{2}}, \quad V_c = \Delta - 2A_c - \alpha 4 c_4 A_c^2. \end{aligned} \tag{5.2.3}$$

For surface water waves on shallow water, the coefficients c_i, $i = 1,8$ have the values (2.2.14). As $t \to \infty$, $N \sim -\frac{V_c}{h}t$, where h is the distance between solitary waves. The single solitary wave solution for the eKdV equation (2.3.20) has mass

$$M_s = \int_{-\infty}^{\infty} u dx = 2\sqrt{2A_c}\left(1 + \frac{1}{9}\alpha A_c(c_1 + 3c_3)\right). \tag{5.2.4}$$

The rate at which mass generated in the upstream wavetrain is given by (5.2.2). At time t, N solitary waves of mass M_s are generated so

$$-\sqrt{2A_c}\left[1 + \frac{1}{9}\alpha A_c(c_1 + 3c_3)\right]\frac{V_c}{h} = -\Delta u_u + 3u_u^2 - \frac{1}{3}\alpha c_1 u_u^3. \tag{5.2.5}$$

In a similar manner for mass, the conservation law for energy of the forced eKdV equation (2.2.13) can be written as

$$\begin{aligned} \frac{d}{dt}\int_{-\infty}^{x_c}\frac{1}{2}u^2\,dx &= \left[-\frac{1}{2}\Delta u^2 + 2u^3 + u\frac{\partial^2 u}{\partial x^2} - \frac{1}{2}\frac{\partial^2 u}{\partial x^2} - \alpha\frac{c_1}{4}u^4\right]_{-\infty}^{x_c} \\ &+ \alpha\int_{-\infty}^{x_c}\left(c_2 u\frac{\partial u}{\partial x}\frac{\partial^2 u}{\partial x^2} + c_3 u^2\frac{\partial^3 u}{\partial x^3} + (\frac{1}{\alpha} + c_8\Delta)uG(x)\right)dx \\ &+ \alpha\int_{-\infty}^{x_c}\left(c_4 u\frac{\partial^5 u}{\partial x^5} + c_5 Gu\frac{\partial u}{\partial x} + c_6\frac{\partial G(x)}{\partial x}u^2 + c_7 u\frac{\partial^3 G(x)}{\partial x^3}\right)dx. \end{aligned} \tag{5.2.6}$$

Again, the limits of the steady state solution $u_s \to u_u$ at $x = x_c$ and $G(x) \to 0$ as $x \to -\infty$ is used (with derivatives zero). So, we obtain

$$\frac{d}{dt}\int_{-\infty}^{x_c}\frac{1}{2}u^2 dx = -\frac{1}{2}\Delta u_u^2 + 2u_u^3 - \frac{1}{4}\alpha c_1 u_u^4. \tag{5.2.7}$$

A single eKdV solitary wave has the energy

$$E_s = \int_{-\infty}^{\infty} \frac{1}{2}u^2 dx = \frac{1}{3}(2A_c)^{\frac{3}{2}}\left(1 + \frac{1}{15}\alpha A_c(3c_1 - c_2 + 8c_3 + 30c_4)\right). \tag{5.2.8}$$

A similar matching, as for mass conservation, between the energy generated upstream (5.2.7) and (5.2.8) gives

$$-\frac{1}{3}A_c(\sqrt{2A_c})\left[1 + \frac{1}{15}\alpha A_c(3c_1 - c_2 + 8c_3 + 30c_4)\right]\frac{V_c}{h} = -\frac{\Delta}{2}u_u^2 + 2u_u^3 - \frac{1}{4}\alpha c_1 u_u^4. \tag{5.2.9}$$

Taking the ratio of (5.2.5) and (5.2.9) eliminates $\frac{V_c}{h}$ and leads to a single equation for the upstream solitary wave amplitude A_c in terms of u_u. Expanding in α gives

$$A_c = A_{c_0} + \alpha A_{c_1}, \quad \text{where} \quad A_{c_0} = \frac{3u_u(4u_u - \Delta)}{2(3u_u - \Delta)}, \tag{5.2.10}$$

$$A_{c_1} = \frac{3u_u^2(4u_u - \Delta)}{2(3u_u - \Delta)^2}\left[(4u_u - \Delta)\left(\frac{1}{10}c_2 - \frac{2}{15}c_1 - \frac{3}{10}c_3 - 3c_4\right) + c_1 u_u\left(\frac{1}{3} - \frac{3u_u - \Delta}{2(4u_u - \Delta)}\right)\right].$$

The solitary wave speed V_c can be found by using equations (5.2.3) and (5.2.10), which gives

$$V_c = -V_{c0} - \alpha V_{c1}, \tag{5.2.11}$$

where

$$V_{c0} = \frac{3u_u^2 + (3u_u - \Delta)^2}{(3u_u - \Delta)}, \tag{5.2.12}$$

and

$$V_{c_1} = \frac{3u_u^2(4u_u - \Delta)}{(3u_u - \Delta)^2}\left[(4u_u - \Delta)\left(\frac{1}{10}c_2 - \frac{2}{15}c_1 - \frac{3}{10}c_3 - 4c_4\right) + c_1 u_u\left(\frac{1}{3} - \frac{3u_u - \Delta}{2(4u_u - \Delta)}\right)\right].$$

The solution is physical as the amplitude $A_c > 0$, velocity $V_c < 0$ and spacing $h > 0$, as $3u_u - \Delta > 0$. We use the expression for u_u (2.3.18) to give

$$A_{c_0} \approx \frac{(\Delta + \sqrt{12g_0})(\frac{1}{3}\sqrt{12g_0} - \frac{1}{6}\Delta)}{\sqrt{12g_0} - \Delta},$$

$$A_{c_1} \approx \frac{1}{\sqrt{12g_0}-\Delta}\Big[(\frac{2}{3}\sqrt{12g_0}+\frac{1}{6}\Delta))S_1+(\Delta+\sqrt{12g_0})^2S_2-(\Delta+\sqrt{12g_0})(\frac{1}{3}\sqrt{12g_0} -\frac{1}{6}\Delta)\Big(-\frac{1}{54}c_1(\Delta+\sqrt{12g_0})+\frac{1}{15}(3c_1-c_2+8c_3+30c_4)(\frac{\sqrt{12g_0}}{3}-\frac{\Delta}{6})\Big)\Big],$$

where

$$S_1 = \frac{1}{2}c_8\Delta\sqrt{12g_0}-c_5(g_0-\frac{\Delta^2}{12})+\frac{1}{36}M_1(\Delta^2+\Delta\sqrt{12g_0}+4g_0)-\frac{1}{6}M_2(\Delta^2+\frac{1}{2}\Delta\sqrt{12g_0}),$$
$$S_2 = -\frac{1}{144}c_1(\Delta+\sqrt{12g_0})+\frac{1}{9}(c_1+3c_3)\frac{(\frac{1}{3}\sqrt{12g_0}-\frac{1}{6}\Delta)^2}{(\sqrt{12g_0}-\Delta)}.$$

This gives the upstream solitary wave amplitude in terms of g_o and Δ. Note that in the case $\alpha = 0$ the KdV result of Grimshaw and Smyth (1986) is obtained. Also note that the amplitude in the limit $\Delta \to \sqrt{12g_0}$ is singular, so the uniform soliton theory is not valid for strongly supercritical flows. This occurs because the mass (5.2.2) approaches zero in this limit, but the energy does not.

5.3 Results and discussion

We now compare the uniform soliton theory results (5.2.10), obtained by a mass and energy balance, with numerical solutions for both the forced eKdV equation (2.2.13) and the forced eBBM equation (4.0.2).

Figure 5.1(a) shows the upstream solitary wave amplitude versus the detuning parameter Δ for the KdV equation. Shown are uniform soliton theory, modulation theory and numerical solutions of the forced KdV equation. The forcing function is the hyperbolic secant (3.1.1) with $g_0 = 1.0$ and $W = 0.3$. Modulation theory gives a good comparison over the whole range of Δ. The largest error occurs in the middle of the resonant band, with up to 8% error at $\Delta = 0$. Uniform soliton theory gives a good comparison in the subcritical range and for moderate supercritical flows. For the case $\Delta = 0$, the uniform soliton theory

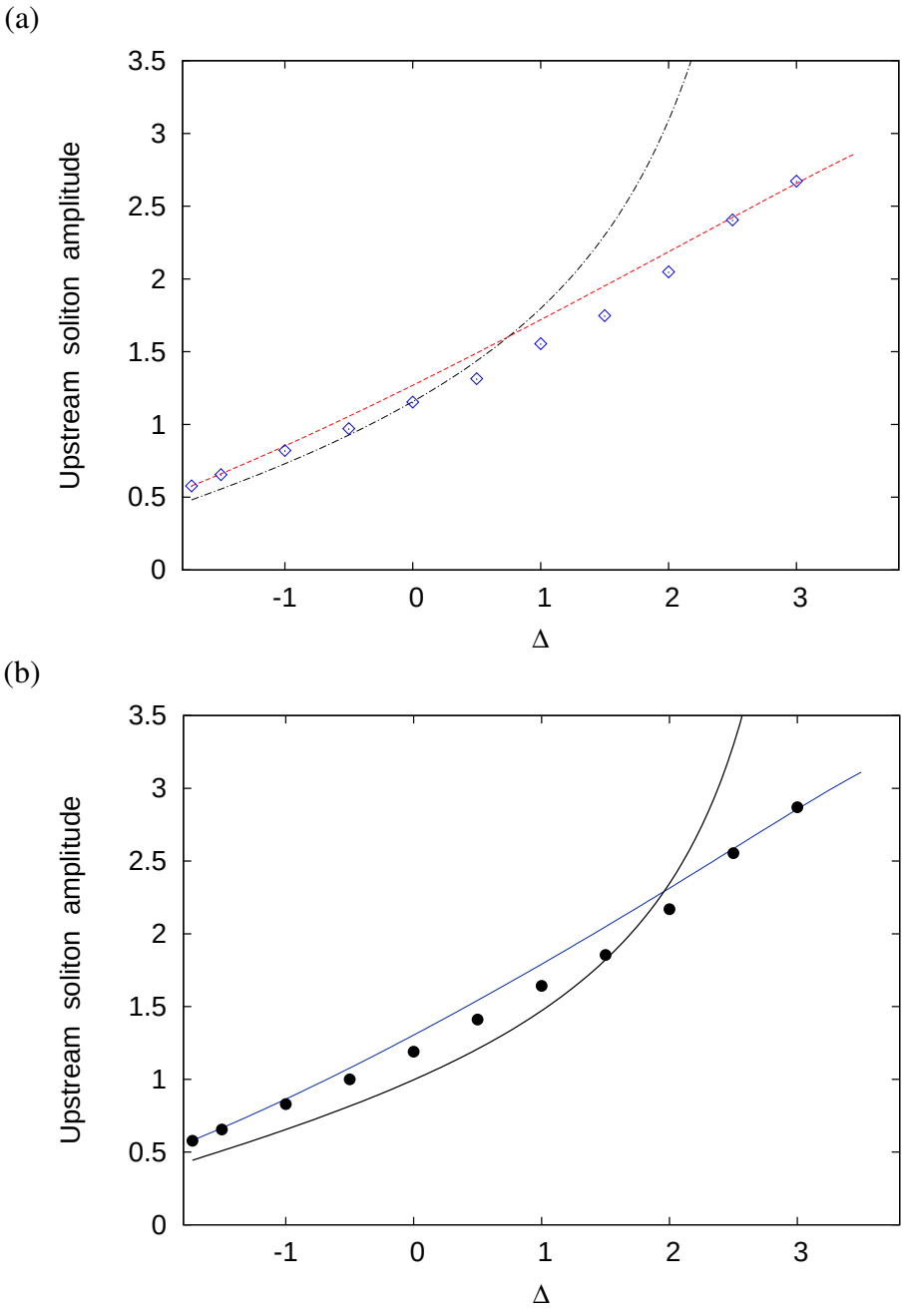

Figure 5.1: The upstream solitary wave amplitude versus the detuning parameter Δ, for surface water waves (2.2.14). Compared are (a) KdV results; uniform solitary wave theory (black dashed dotted line), numerical solutions ($\diamond$) and modulation theory (red dashed line). Also, (b) eKdV results; uniform soliton theory (5.2.10) (black solid line), numerical solutions ($\bullet$) and extended modulation theory (2.3.35) (blue solid line). The forcing function is (3.1.1). The amplitude parameter is $\alpha = 0.15$.

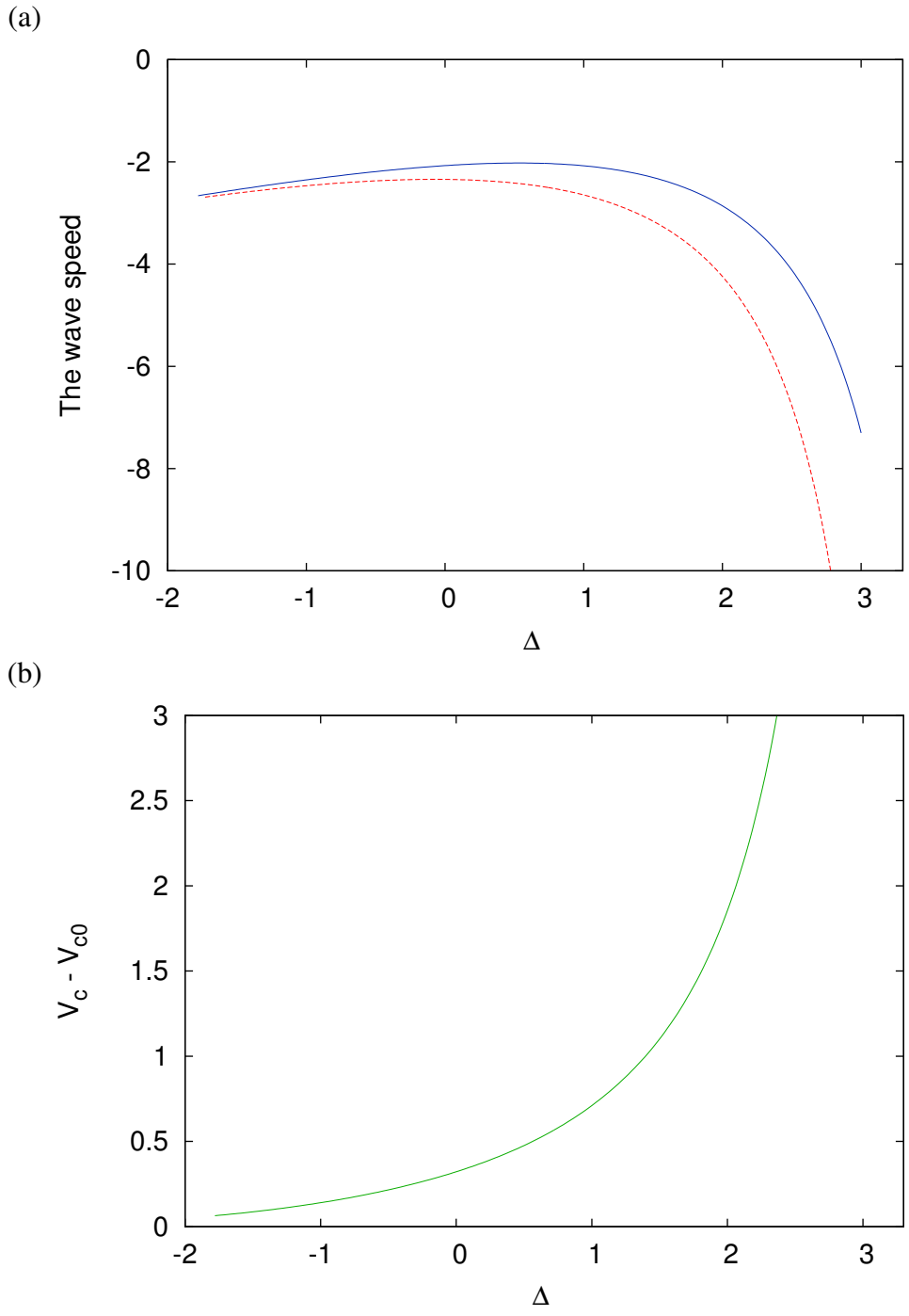

Figure 5.2: The solitary wave speed V_c versus the detuning parameter Δ, for surface water waves (2.2.14). Compared are (a) eKdV (5.2.11) (blue solid line) and KdV (5.2.12) (red dashed line) uniform soliton theories. Also (b) the difference of speed between both models. The amplitude parameter is $\alpha = 0.15$.

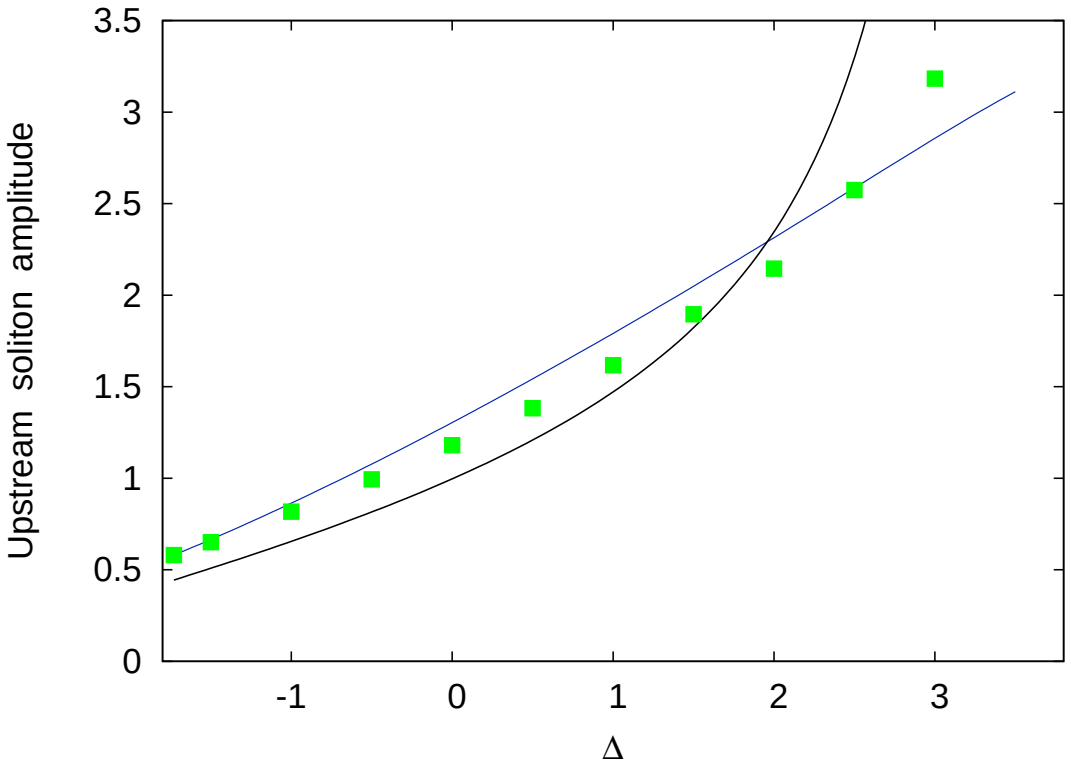

Figure 5.3: The upstream solitary wave amplitude versus the detuning parameter Δ. Compared are uniform soliton theory (5.2.10) (black solid line), extended modulation theory (2.3.35) (blue solid line), for surface water waves (2.2.14) and numerical solutions of the forced eBBM equation, for surface water waves (4.0.3) (■). The forcing is (4.0.5) with $g_0 = 1.0$ and $W = 0.3$. The amplitude parameter is $\alpha = 0.15$.

amplitude $A_c = 1.15$, which agrees well with the numerical solution $A_n = 1.15$, while modulation theory gives $A = 1.25$. However, for strongly supercritical flows uniform soliton theory diverges as there is a singularity at $\Delta = \sqrt{12 g_0}$, at the upper limit of the resonant range.

Figure 5.1(b) shows the upstream solitary wave amplitude versus the detuning parameter Δ for the eKdV equation, for surface water waves (2.2.14). Shown are the uniform soliton theory (5.2.10), extended modulation theory (2.3.35) and numerical solutions of

the forced eKdV equation. The forcing function is the hyperbolic secant (3.1.1) with $g_0 = 1.0$ and $W = 0.3$. The amplitude parameter is $\alpha = 0.15$. The results of extended modulation theory and uniform soliton theory is qualitatively similar to the KdV results. Extended modulation theory provides a good prediction over the whole resonant range but uniform soliton theory is accurate for subcritical flows and loses accuracy for highly supercritical flows. At $\Delta = 0$ the numerical solutions gives the amplitude $A_n = 1.19$, uniform soliton theory gives $A_c = 1.04$ and the extended modulation theory gives $A = 1.29$. For $\Delta \leq 2$, the variation between numerical result and uniform soliton theory is less than 15%.

Figure 5.2(a) shows the wave speed V_c (5.2.11) versus the detuning parameter Δ, for surface water waves (2.2.14). Shown are the uniform soliton theory solutions of the forced KdV and eKdV equations. The amplitude parameter is $\alpha = 0.15$. The eKdV solitary wave speed is higher than the KdV value over all the resonant range. Hence, the eKdV solitary waves travel faster than the KdV solitons. Figure 5.2(b) shows the wave speed difference $V_c - V_{c0}$ versus the detuning parameter Δ, for surface water waves (2.2.14). Compared are V_c the eKdV wave speed (5.2.11) and V_{c0} the KdV wave speed (5.2.12). The difference is larger for highly supercritical case. For subcritical case, the difference is smaller and approaching to zero at the ends of the resonant range.

Figure 5.3 shows the upstream solitary wave amplitude versus the detuning parameter Δ. Shown are the uniform soliton theory (5.2.10), extended modulation theory (2.3.35) for the forced eKdV equation, for surface water waves (2.2.14) and numerical solutions of the forced eBBM equation, for surface water waves (4.0.3). The forcing is the hyperbolic secant (4.0.5) with $g_0 = 1.0$ and $W = 0.3$. The amplitude parameter is $\alpha = 0.15$. At $\Delta = 0$

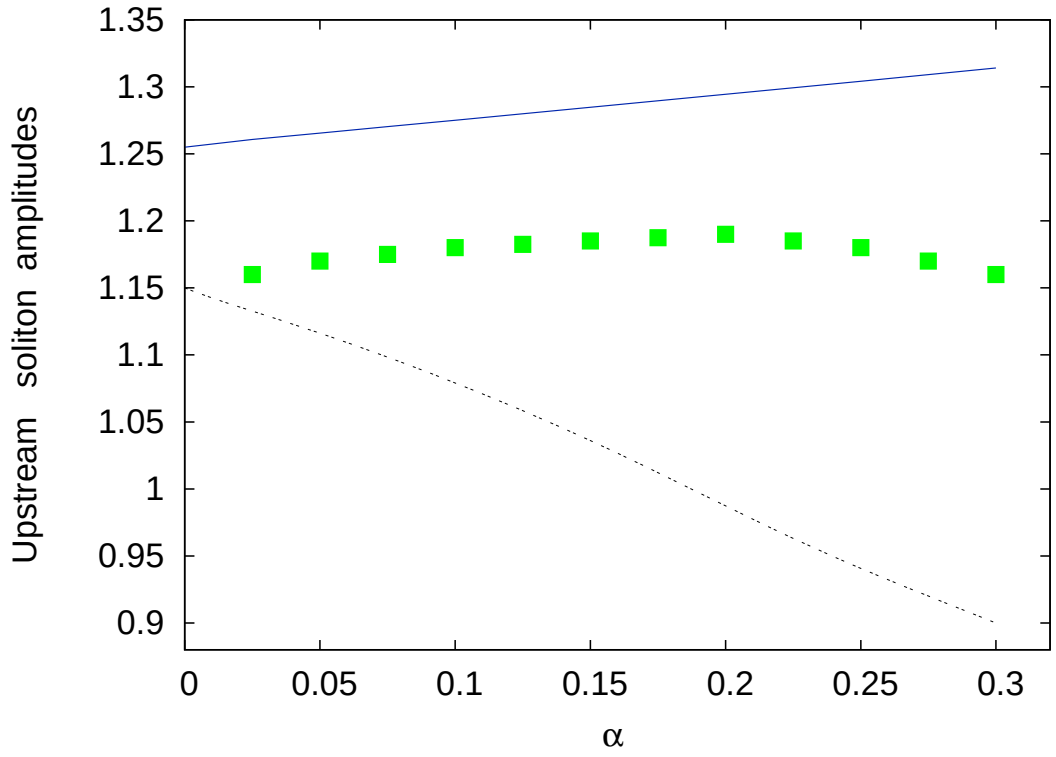

Figure 5.4: Upstream solitary wave amplitude versus the wave amplitude parameter α. Compared are uniform soliton theory (5.2.10) (black dashed line), extended modulation theory (2.3.35) (blue solid line), for surface water waves (2.2.14) and numerical solution of the eBBM model, for surface water waves (4.0.3) (■). The forcing is (4.0.5) with $g_0 = 1.0$ and $W = 0.3$. The detuning parameter is $\Delta = 0$.

the numerical solutions gives $A_{bbm} = 1.18$, uniform soliton theory gives $A_c = 1.04$ and the extended modulation theory gives $A = 1.29$. The variation between the numerical solution and the result of uniform soliton theory is approximatively 18% up to $\Delta = 2$. Hence, the uniform soliton theory agrees well with the eBBM numerical solutions for $\Delta \leq 2$.

Figure 5.4 shows the upstream solitary wave amplitude versus the amplitude parameter α. Compared are uniform soliton theory (5.2.10), extended modulation theory (2.3.35), for surface water waves (2.2.14) and numerical solutions of the forced eBBM

equation, for surface water waves (4.0.3). The forcing is the hyperbolic secant (4.0.5) with $g_0 = 1.0$ and $W = 0.3$. The detuning parameter is $\Delta = 0$. Due to the numerical stability of the eBBM equation we now explore the validity of uniform soliton theory for large wave amplitudes. The figure shows that uniform soliton theory gives that the amplitude decreases as α increases whilst the numerical amplitudes are nearly constant, over this range. Hence, for steeper waves modulation theory is a better approximation than the uniform soliton theory, for exact resonance $\Delta = 0$. Clearly, neglected terms at $O(\alpha^2)$ grow as α increases, reducing the validity of the uniform soliton theory for large α.

5.4 Conclusions

Analytical predictions of the upstream solitary wave amplitude are made using uniform solitary wave theory for the forced eKdV equation. Our uniform soliton theory is based on the conservation laws of mass and energy for the eKdV equation. Comparisons are made with extended modulation theory and with numerical results for both the forced eKdV and eBBM equations. It was shown that uniform soliton theory performs well for subcritical and moderately supercritical flows, but a singularity occurs near the supercritical limit of resonant flow, which invalidates the approximation. Moreover, it was shown that the uniform soliton theory performs poorer than modulation theory for steeper waves.

Chapter 6

Resonant flow over a step

6.1 Introduction

The problem of undular bores generated by the resonant flow over an isolated bottom topography has received much attention by many authors and is relevant in both oceanographic and engineering contexts. Resonant flow over steps, jumps or falls, which also generates unsteady wavetrains, has also been extensively investigated as it is relevant in many physical contexts. Grimshaw et al. (2007b) carried out numerical simulations of the forced KdV equation for resonant flow over a step, and found that upstream and downstream undular bores were generated. Moreover, they showed that an upstream propagating undular bore is generated by a positive step and a downstream propagating undular bore is generated by a negative step. Grimshaw et al. (2007b) and Grimshaw (2010) performed a comprehensive analytical analysis of the steady solutions for flow over a step, based on the forced KdV model. Also, flow over an abrupt step was described by Binder et al. (2006), who considered a "narrow" step with $G(x) = g_o H(x)$ where $H(x)$ is the Heaviside function.

The different ranges of Froude numbers for free surface flow over a step, describing subcritical, transcritical and supercritical flows were studied by Zhang and Zhu (1997) using the forced KdV model. The full Euler equations for resonant flow over an obstacle or step was solved numerically by Zhang and Chwang (2001). They found that upstream advancing solitary waves are generated by the forward step forcing for a positive topography (a bump), whereas the backward step forcing generates the downstream-radiating waves for a negative topography (a hollow). They also found that details of the upstream and downstream undular bores were in broad agreement with modulation theory for the forced KdV equation.

A number of authors have studied problems of free surface flow over a hole, for example, Grimshaw and Smyth (1986) who presented numerical solutions that showed no steady state forms upstream of the topography. Grimshaw et al. (2009b) performed numerical studies of the forced KdV equation for an obstacle with negative polarity. They obtained the two wavetrains generated due to a step down followed by a step up on the downstream side of the hole. Ee et al. (2010) studied resonant flow of a stratified fluid over a hole described by the forced KdV equation. They investigated the effects of the width and the amplitude of the hole on steady solutions. Ee et al. (2011) studied the effect of including an additional cubic nonlinear term to the forced KdV equation (the forced Gardner equation) in some special circumstances. In Section 6.2 the steady state solutions for flow over positive and negative steps are found and the extended modulation theory for these is developed. In Section 6.3 comparisons are made between the extended modulation theory and numerical solutions for the forced eKdV equation. In Section 6.4 conclusions are given.

6.2 The steady-state solution, for flow over a step

The forced eKdV equation (2.2.13) describes resonant flow over topography to second-order. The forcing function $G(x)$ is taken to be

$$G(x) = 0, \qquad x < 0, \qquad \text{and} \qquad G(x) = g_0, \qquad x > Q, \tag{6.2.1}$$

where g_0 is the height of the step. It describes both a positive and a negative step, see Grimshaw et al. (2007b). For the region $0 < x < Q$ the forcing function $G(x)$ varies monotonically. The positive step has $g_0 > 0$ and the negative step has $g_0 < 0$. In order to ensure conservation of mass in the forced eKdV equation (2.2.13), $G(x)$ should return to zero for some $x = x_L >> Q$. Here, x_L is the separation between the front and the rear steps.

The initial condition in the present work is $u(x,0) = 0$ and the higher-order coefficients for surface water waves (2.2.14) are used. The surface elevation is then initially zero when the forcing is switched on. Three distinct solution regions develop as time goes on, a depression downstream of the forcing, a modulated, unsteady, wavetrain which brings the solution back to the mean level of zero and a full or partial undular bore upstream of the forcing, see Figures 6.1, 6.2, 6.3 for examples across the resonant range. In all cases, in the region near the step a hydraulic solution occurs, where the dispersive terms are negligible.

The steady state region over the forcing can be modelled by the non-dispersive limit of the eKdV equation, as the solution is slowly varying in this range. The eKdV equation becomes

$$-u_t - \Delta u_x + 6uu_x - \alpha c_1 u^2 u_x + \alpha c_5 G u_x + \alpha c_6 G_x u + (1 + \alpha c_8 \Delta) G_x = 0. \tag{6.2.2}$$

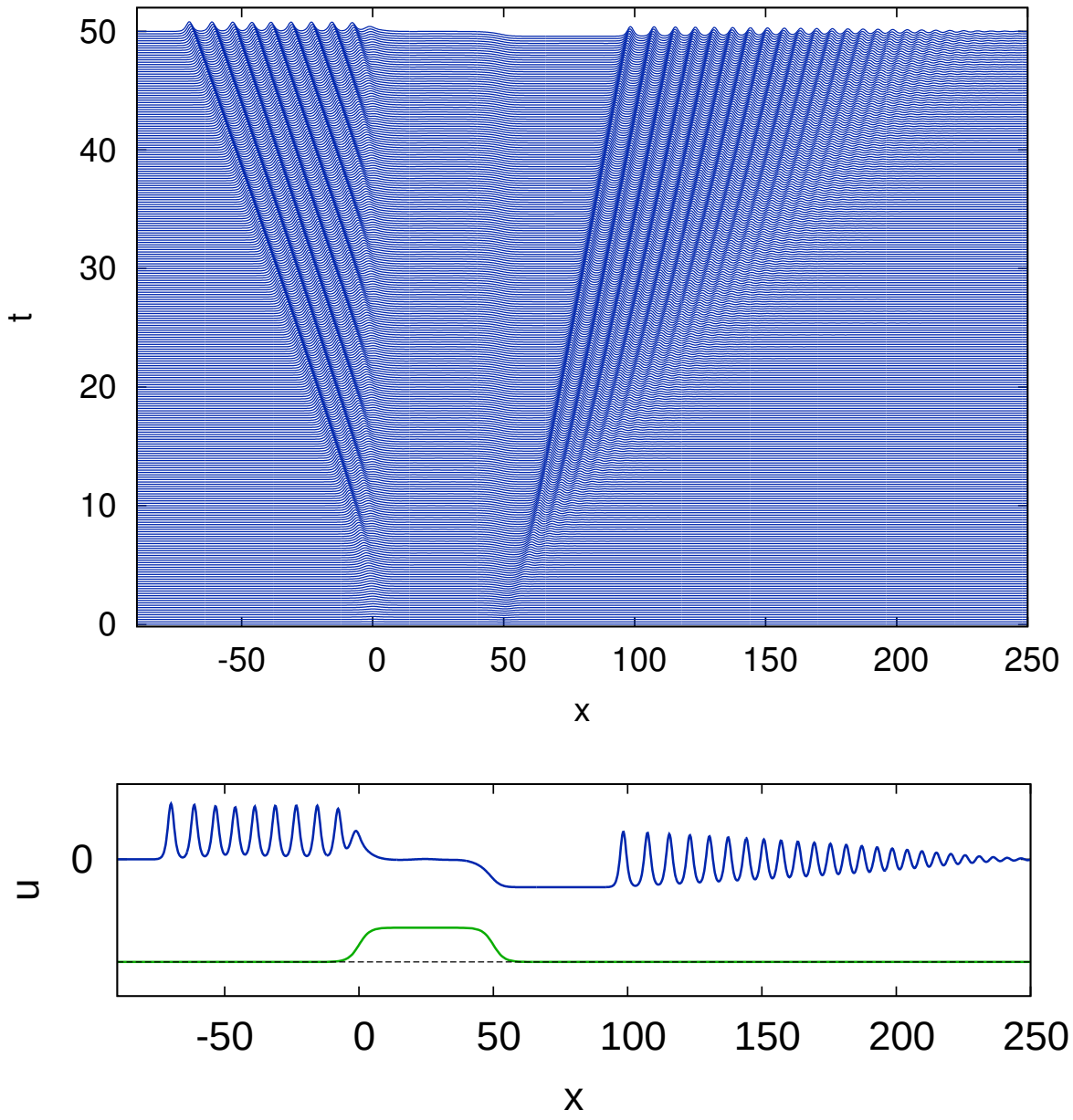

Figure 6.1: Solution of the forced eKdV equation (2.2.13), for surface water waves (2.2.14). Shown is a perspective view in the $x-t$ plane with time up to $t = 50$ (top) and the surface profile u and bathymetry G versus x at $t = 50$ (bottom). The numerical solution of (2.2.13) with the initial condition $u = 0$ is shown. The forcing is (6.3.35) with $g_0 = 0.5$ and $W = 0.3$. The other parameters are $\alpha = 0.15$, $x_L = 50$ and $\Delta = 0$.

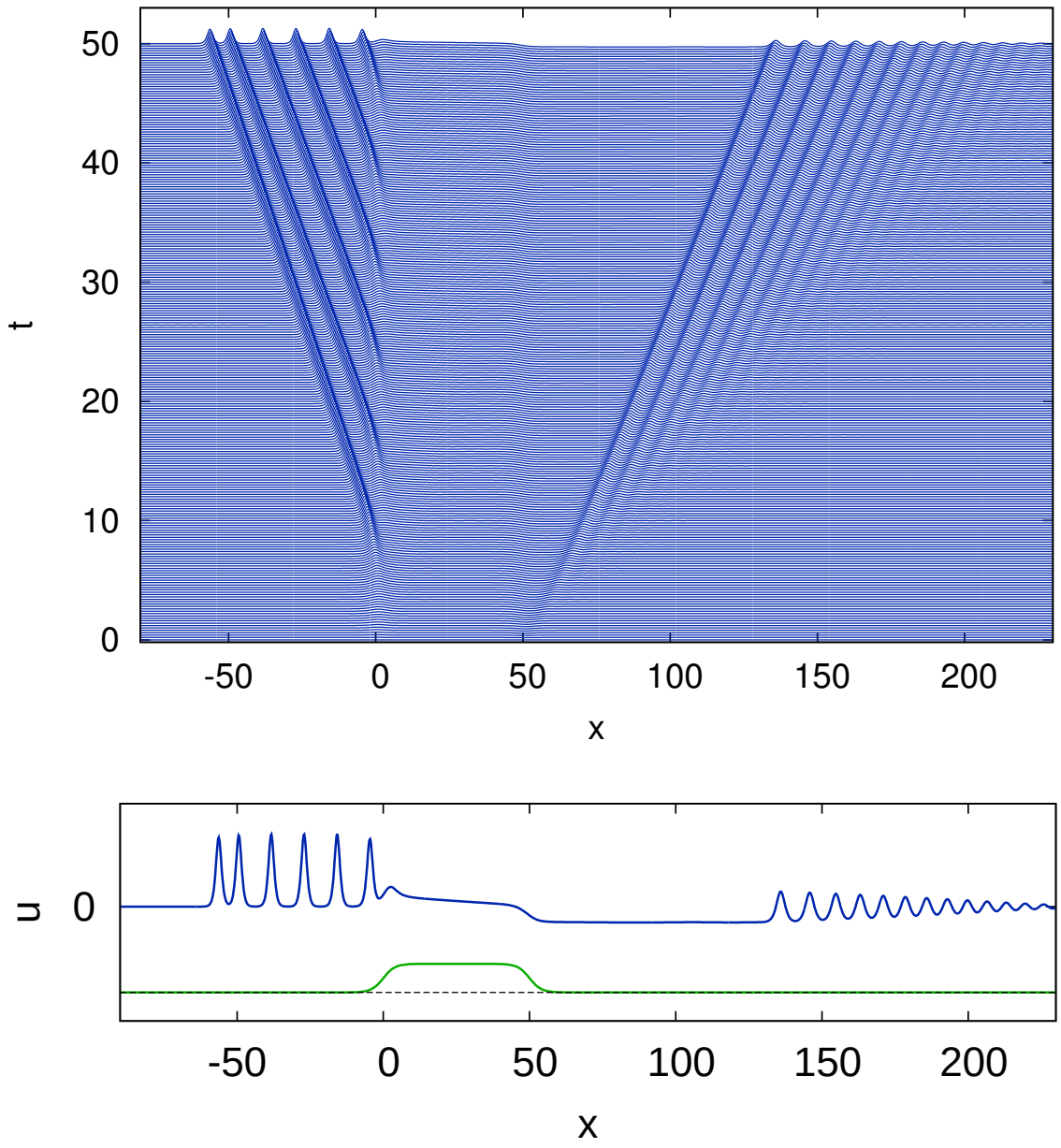

Figure 6.2: Solution of the forced eKdV equation (2.2.13), for surface water waves (2.2.14). Shown is a perspective view in the $x-t$ plane with time up to $t = 50$ (top) and the surface profile u and bathymetry G versus x at $t = 50$ (bottom). The numerical solution of (2.2.13) with the initial condition $u = 0$ is shown. The forcing is (6.3.35) with $g_0 = 0.5$ and $W = 0.3$. The other parameters are $\alpha = 0.15$, $x_L = 50$ and $\Delta = 1$.

Equation (2.2.13) has two steady solutions

$$u_s = \frac{1}{6+\alpha\Delta(M_2-\frac{2}{9}M_1)}\left[\Delta+\alpha\left(\frac{1}{9}M_1[T_c-G]-c_5T_c\right)\pm\sqrt{\Delta^2+12[K_c-G]+2\alpha\Delta F}\right],$$
$$\text{where}\quad M_1=c_1+3c_5+6c_6,\quad M_2=c_5+c_6,\quad T_c=g_o-\frac{1}{12}\Delta^2, \tag{6.2.3}$$
$$\text{and}\quad F=(K_c-G)(M_2-\frac{1}{9}M_1)+\frac{1}{9}M_1(T_c-G)-6c_8G-c_5T_c.$$

Depending on the solution regime different solution branches are chosen. The constant K_c will be determined in the following section. A single solution branch or both solution branches are used, depending on the value of Δ.

Figure 6.1 shows a perspective plot of the numerical solution of the forced eKdV (2.2.13) equation for resonant flow over a step, for critical flow, for surface water waves (2.2.14). Shown are the solution in the $x-t$ plane (top) and the surface profile u and bathymetry G versus x at $t = 50$ (bottom). The numerical solution of (2.2.13) with the initial condition $u = 0$ is shown. The other parameters are $\Delta = 0$ and $\alpha = 0.15$. The forcing function is the hyperbolic tangent (6.3.35). The solution consists of three parts, a steady hydraulic flow over the step, and bores which propagate both upstream and downstream.

Figure 6.2 displays a typical solution of the forced eKdV equation (2.2.13) for super-critical flow over a step, for surface water waves (2.2.14). Shown are a perspective view of the solution in the $x-t$ plane (top) and the surface profile u and bathymetry G versus x at $t = 50$ (bottom). The numerical solution of (2.2.13) with the initial condition $u = 0$ is shown. The other parameters are $\Delta = 1$ and $\alpha = 0.15$. The forcing function is the hyperbolic tangent (6.3.35). Again, the solution consists of three parts, a steady hydraulic flow over the step, the upstream partial undular bore and a full undular bore downstream of the step, whilst Figure 6.3 is for subcritical flow over a step for $\Delta = -0.5$, at time up to $t = 35$.

To match with the upstream and downstream flows, we take the limit of the hydraulic

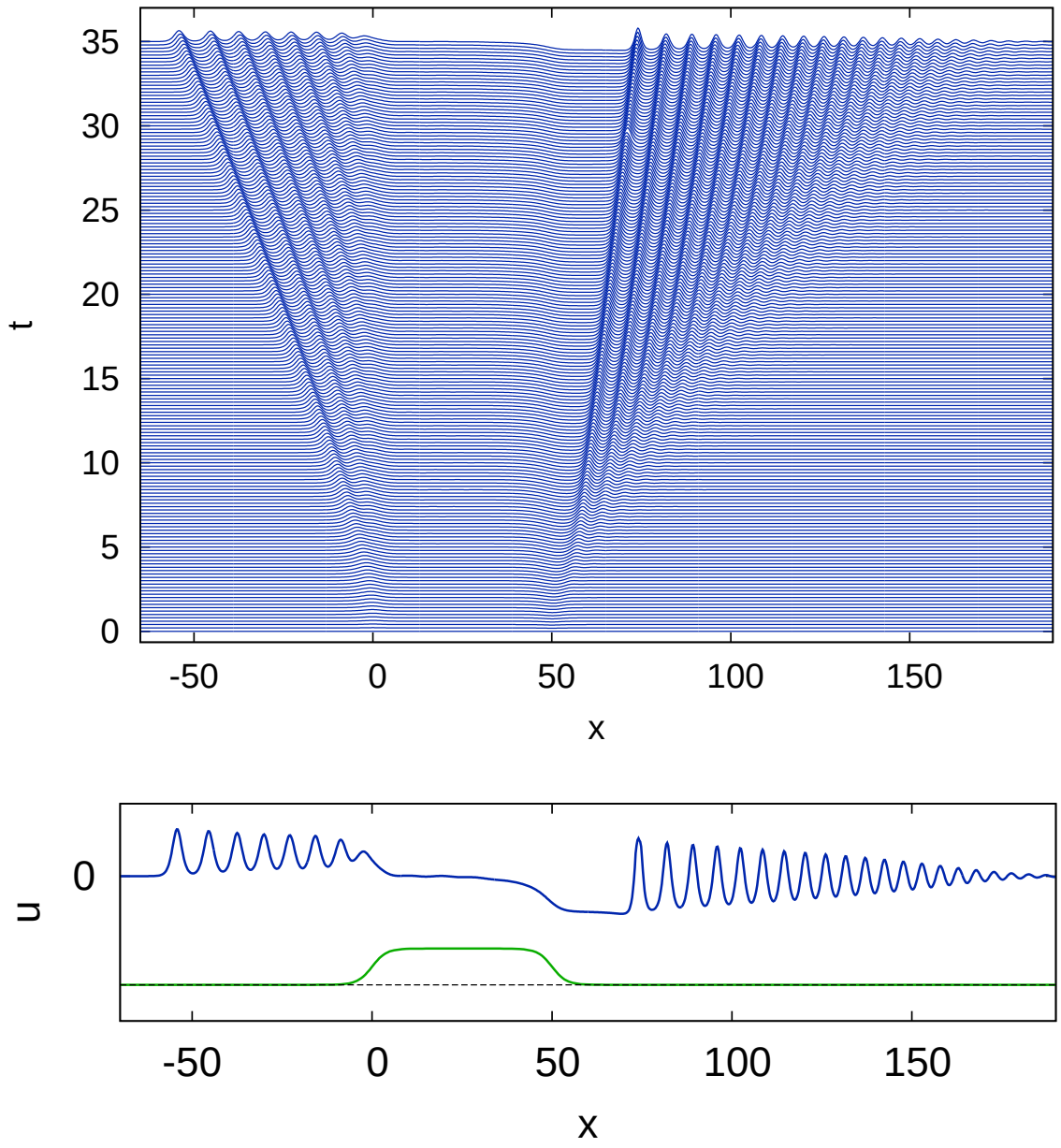

Figure 6.3: Solution of the forced eKdV equation (2.2.13), for surface water waves (2.2.14). Shown is a perspective view in the $x-t$ plane with time up to $t = 35$ (top) and the surface profile u and bathymetry G versus x at $t = 35$ (bottom). The numerical solution of (2.2.13) with the initial condition $u = 0$ is shown. The forcing is (6.3.35) with $g_0 = 0.5$ and $W = 0.3$. The other parameters are $\alpha = 0.15$, $x_L = 50$ and $\Delta = -0.5$.

solution (6.2.3) as $x \to \pm\infty$, giving

$$u_s = u_u \qquad \text{as} \qquad x \to -\infty, \qquad \text{and} \qquad u_s = u_d \qquad \text{as} \quad x \to \infty. \tag{6.2.4}$$

As for an isolated obstacle, the upstream and downstream states (6.2.3) are physically valid when $u_u > 0$ and $u_d < 0$. These requirements give that resonant flow will occur when Δ lies in the range

$$-\sqrt{12|g_0|} + \alpha|g_0|r_1 < \Delta < \sqrt{12|g_0|} + \alpha|g_0|r_1, \quad \text{where} \quad r_1 = 6c_8 - \frac{1}{9}c_1 + \frac{2}{3}c_5 + \frac{1}{3}c_6. \tag{6.2.5}$$

This resonant range is the same as that for an isolated obstacle (2.3.19). To determine the constant K_c, we find the turning points of the long-time unsteady hydraulic solution as considered by Grimshaw and Smyth (1986) and Grimshaw et al. (2007b). Integrating equation (6.2.2) from $-\infty$ to ∞ and applying the boundary conditions (6.2.4) yields

$$-\Delta u_u + 3u_u^2 - \frac{1}{3}c_1\alpha u_u^3 = K_c, \tag{6.2.6}$$

$$-\Delta u_d + \alpha c_5 g_0 u_d + \alpha\Delta^2 \frac{1}{36}\left(\frac{1}{3}c_1 - 2c_5 + 2c_6\right)u_d + 3u_d^2 + (1 + \alpha c_8\Delta)g_0 \tag{6.2.7}$$

$$+\alpha\Delta\left(\frac{1}{6}c_5 - \frac{1}{9}c_1 - \frac{1}{6}c_6\right)u_d^2 = K_c,$$

giving a connection between u_u and u_d. The method of characteristics is used to solve the nonlinear hyperbolic equation (6.2.2) giving

$$\frac{du}{dt} = (1 + \alpha c_8\Delta + \alpha c_6 u)\frac{dG(x)}{dx} \quad \text{on} \quad \frac{dx}{dt} = \Delta - 6u + \alpha c_1 u^2 - \alpha c_5 G(x). \tag{6.2.8}$$

An important question is whether the characteristics reach a turning point where

$$\frac{dx}{dt} = 0, \qquad u = \frac{1}{6}\Delta + \frac{1}{216}\alpha\Delta^2 c_1 - \frac{1}{6}\alpha c_5 G. \tag{6.2.9}$$

Depending on the value of Δ, the upper or lower branch of (6.2.3), or a combination of the two, must be used to construct a physically valid steady state solution. There are three different cases depending on the value of Δ.

A positive step $g_0 > 0$ behaves like the leading edge of an isolated obstacle. So the resonant range is

$$\Delta \leq \sqrt{12 g_0} + \alpha g_0 r_1. \tag{6.2.10}$$

The transition from the resonant to the non-resonant regime occurs at the same Δ value as for an isolated obstacle. For a positive step upstream bores can occur but downstream ones cannot.

The first case is for $\Delta \leqslant \alpha c_5 g_0$. In this case a negative slope is found for all characteristics and $u_d = 0$. Then, from equation (6.2.7), it is readily found that

$$K_c = (1 + \alpha \Delta c_8) g_0. \tag{6.2.11}$$

There are no turning points and the upper branch of (6.2.3) is chosen and the limiting values are

$$u_u = \frac{1}{6 + \alpha\Delta(M_2 - \frac{2}{9}M_1)} \left[\Delta + \alpha \left(\frac{1}{9} M_1 - c_5 \right) \left(g_0 - \frac{1}{12}\Delta^2 \right) + \sqrt{\Delta^2 + 12 g_0 + 2\alpha\Delta M_3} \right],$$
$$u_d = 0, \quad \text{where} \quad M_3 = g_0 \left(6c_8 - \frac{1}{9}c_1 + \frac{2}{3}c_5 + \frac{1}{3}c_6 \right) - \frac{1}{36}\Delta^2 \left(\frac{1}{3}c_1 - 2c_5 + 2c_6 \right). \tag{6.2.12}$$

Upstream, the steady state solution is positive, $u_u > 0$, and this jump is resolved by an undular bore.

The second case is for

$$\alpha c_5 g_0 < \Delta < \sqrt{12 g_0} + \alpha g_0 r_1. \tag{6.2.13}$$

Using equation (6.2.9) and applying the boundary conditions (6.2.4), we find

$$u_d = \frac{1}{6}\Delta + \frac{1}{216}\alpha\Delta^2 c_1 - \frac{1}{6}\alpha c_5 g_0.$$

Then from equation (6.2.7) it can be found that

$$K_c = g_0 - \frac{1}{12}\Delta^2 + \frac{1}{6}\alpha\Delta \left[6c_8 g_0 + c_5 g_0 + \frac{1}{12}\Delta^2 \left(c_5 - c_6 - \frac{1}{3}c_1 \right) \right]. \tag{6.2.14}$$

In this case, there is a turning point and the steady state solution is a combination of both branches of (6.2.3). The values of u_u and u_d are

$$\begin{aligned} u_u &= \frac{1}{6+\alpha\Delta(M_2-\frac{2}{9}M_1)}\left[\Delta+\alpha\left(\frac{1}{9}M_1-c_5\right)\left(g_0-\frac{1}{12}\Delta^2\right)+\sqrt{12g_0+2\alpha\Delta M_4}\right], \\ u_d &= \frac{1}{6}\Delta+\frac{1}{216}\alpha\Delta^2 c_1-\frac{1}{6}\alpha c_5 g_0, \\ \text{where}\quad M_4 &= M_3+c_5g_0-\frac{1}{36}\Delta^2\left(\frac{1}{3}c_1-2c_5+2c_6\right). \end{aligned} \tag{6.2.15}$$

Again, upstream, the solution is positive, $u_u > 0$, and an undular bore occurs. Meanwhile, downstream $u_d > 0$, a rarefaction wave brings the flow back to zero. The solutions for u_u and u_d continuous at $\Delta = \alpha c_5 g_0$, see Figure 6.5.

The third case is for

$$\Delta > \sqrt{12g_0}+\alpha g_0 r_1. \tag{6.2.16}$$

This case is outside of the resonant range so no upstream undular bore occurs as $u_u = 0$. A positive slope is found for all characteristics. Then from equation (6.2.6) it is readily found that $K_c = 0$. There are no turning points and the lower branch of (6.2.3) must be chosen. The values of u_u and u_d are given by

$$\begin{aligned} u_u &= 0, \\ u_d &= \frac{1}{6+\alpha\Delta(M_2-\frac{2}{9}M_1)}\left[\Delta-\alpha c_5\left(g_0-\frac{1}{12}\Delta^2\right)-\frac{1}{108}\alpha\Delta^2 M_1-\sqrt{\Delta^2-12g_0-2\alpha\Delta M_5}\right], \\ \text{where}\quad M_5 &= g_0\left(6c_8-\frac{2}{9}c_1+\frac{4}{3}c_5-\frac{1}{3}c_6\right)+\frac{1}{36}\Delta^2\left(\frac{1}{3}c_1-2c_5+2c_6\right). \end{aligned} \tag{6.2.17}$$

The downstream jump $u_d > 0$ is positive and no undular bore as there is a rarefaction wave. The solution u_u is discontinuous at

$$\Delta = \sqrt{12g_0}+\alpha g_0 r_1,$$

see Figure 6.5.

The negative step $g_0 < 0$ is like the trailing edge of an isolated obstacle. So the resonant range is

$$\Delta > -\sqrt{12|g_0|} + \alpha|g_0|r_1, \tag{6.2.18}$$

the same as an isolated obstacle. For a negative step downstream bores can occur but upstream ones cannot. Similarity, for the negative step, there are also three cases for the local hydraulic solution.

The first case is for $\Delta \geqslant 0$. In this case a positive slope found is for all characteristics and no upstream undular bore occurs, $u_u = 0$. In addition, there are no turning points, and from equation (6.2.6), $K_c = 0$. Hence, the lower branch of (6.2.3) is chosen and the values of u_u and u_d are given by

$$u_u = 0, \tag{6.2.19}$$

$$u_d = \frac{1}{6 + \alpha\Delta(M_2 - \frac{2}{9}M_1)}\left[\Delta - \alpha c_5\left(g_0 - \frac{1}{12}\Delta^2\right) - \frac{1}{108}\alpha\Delta^2 M_1 - \sqrt{\Delta^2 - 12g_0 - 2\alpha\Delta M_5}\right].$$

The upstream solution, $u_u = 0$ so no bore is needed. For the downstream solution $u_d < 0$ and this jump is resolved by an undular bore.

The second case is for

$$-\sqrt{12|g_0|} + \alpha|g_0|r_1 < \Delta < 0. \tag{6.2.20}$$

Using equation (6.2.9) and applying the boundary conditions (6.2.4) and (6.2.6) gives

$$u_u = \frac{1}{6}\Delta + \frac{1}{216}\alpha\Delta^2 c_1, \quad K_c = -\frac{1}{12}\Delta^2 - \frac{1}{648}\alpha\Delta^3 c_1. \tag{6.2.21}$$

There is a turning point and the steady state solution is a combination of both solution

branches (6.2.3). Then, we obtain the values of u_u and u_d as

$$u_u = \frac{1}{6}\Delta + \frac{1}{216}\alpha c_1 \Delta^2, \tag{6.2.22}$$
$$u_d = \frac{1}{6+\alpha\Delta(M_2 - \frac{2}{9}M_1)}\left[\Delta - \alpha c_5\left(g_0 - \frac{1}{12}\Delta^2\right) - \frac{1}{108}\alpha\Delta^2 M_1 - \sqrt{-12g_0 - 2\alpha\Delta M_6}\right],$$
$$\text{where} \quad M_6 = M_5 - \frac{1}{36}\Delta^2\left(c_5 - c_6 + \frac{1}{3}c_1\right).$$

Upstream $u_u < 0$ is negative, so here no undular bore is needed as this jump is resolved by a rarefaction wave. Meanwhile, the downstream solution is also negative $u_d < 0$ and the downstream jump is resolved by an undular bore. The solutions for u_u and u_d are continuous at $\Delta = 0$, see Figure 6.6.

The third case is for

$$\Delta < -\sqrt{12|g_0|} + \alpha|g_0|r_1. \tag{6.2.23}$$

This case is outside of the resonant range, so no undular bore occurs. A negative slope is found for all characteristics. Here, $u_d = 0$, consequently from equation (6.2.6) can be easily found that

$$K_c = (1 + \alpha\Delta c_8)g_0. \tag{6.2.24}$$

There are no turning points and the upper branch of (6.2.3) must be chosen, it is then readily shown that the values of u_u and u_d are given by

$$u_u = \frac{1}{6+\alpha\Delta(M_2 - \frac{2}{9}M_1)}\left[\Delta + \alpha\left(\frac{1}{9}M_1 - c_5\right)\left(g_0 - \frac{1}{12}\Delta^2\right) + \sqrt{\Delta^2 + 12g_0 + 2\alpha\Delta M_3}\right],$$
$$u_d = 0. \tag{6.2.25}$$

Upstream u_u is negative and the jump is resolved by a rarefaction wave. Downstream $u_d = 0$ and so no downstream bore occurs. The solution u_d is discontinuous at $\Delta = -\sqrt{12g_0} + \alpha g_0 r_1$, see Figure 6.6.

The undular bore solution of the eKdV equation (2.3.20) is a modulated cnoidal wave which links the level A behind the bore to the level B in front of the bore. The extent of the bore is

$$\begin{aligned}\Delta-4A-2B-\alpha A^2\left(\frac{8}{3}c_4-\frac{2}{3}c_3-\frac{2}{3}c_1\right)-\alpha B^2\left(\frac{8}{3}c_4-\frac{2}{3}c_3-\frac{1}{3}c_1\right)\\ -\alpha AB\left(16c_4-\frac{4}{3}c_3\right)<\frac{x}{t}<\Delta-12B+6A-\alpha A^2\left(\frac{20}{3}c_4-\frac{1}{3}c_3+\frac{1}{6}c_1\right)\\ -\alpha B^2\left(40c_4-2c_3-2c_1\right)+\alpha AB\left(\frac{4}{3}c_3+\frac{112}{3}c_4\right).\end{aligned} \tag{6.2.26}$$

For a positive step, $A = u_u$ and $B = 0$, and an undular bore occurs upstream $(x < 0)$. Then we find that the extent of the bore is

$$\Delta-4u_u-\alpha u_u^2\left(\frac{8}{3}c_4-\frac{2}{3}c_3-\frac{2}{3}c_1\right)<\frac{x}{t}<max\left\{0,\Delta+6u_u-\alpha u_u^2\left(\frac{20}{3}c_4-\frac{1}{3}c_3+\frac{1}{6}c_1\right)\right\}. \tag{6.2.27}$$

The upstream wavetrain cannot extend beyond the step at $x = 0$. Thus, we obtain the relation for a fully detached upstream undular bore as

$$\Delta+6u_u-\alpha u_u^2\left(\frac{20}{3}c_4-\frac{1}{3}c_3+\frac{1}{6}c_1\right)<0. \tag{6.2.28}$$

Equation (6.2.28) is combined with (6.2.12), (6.2.15) and (6.2.17) to obtain the conditions

$$\begin{aligned}-\sqrt{12g_0}+\alpha g_0 r_1<\Delta<-2\sqrt{g_0(1-\alpha M_7)},\qquad \text{where}\\ M_7=\frac{2}{3}\sqrt{g_0}\left(4c_8+\frac{2}{27}c_1-\frac{2}{9}c_3+\frac{34}{9}c_4+\frac{5}{9}c_5-\frac{2}{9}c_6\right),\end{aligned} \tag{6.2.29}$$

for a full upstream undular bore. The partial undular bore is for

$$-2\sqrt{g_0(1-\alpha M_7)}<\Delta<\sqrt{12g_0}+\alpha g_0 r_1. \tag{6.2.30}$$

The modulus squared, m_0 of the partial bore, is the solution of (2.3.33). We find that the amplitude of the upstream solitary wave by setting mean level β to the upstream limit

u_u of the steady solution, where β is given by (2.3.28). The solitary wave of amplitude $2u_u$ occurs at the leading edge when a mean level of 0.

For a negative step an undular bore lies downstream $(x > Q)$ and $B = u_d$, $A = 0$. The bore occupies the zone

$$max\left\{0, \Delta - 2u_d - \alpha u_d^2\left(\frac{8}{3}c_4 - \frac{2}{3}c_3 - \frac{1}{3}c_1\right)\right\} < \frac{x-Q}{t} < \Delta - 12u_d - \alpha u_d^2\left(40c_4 - 2c_3 - 2c_1\right). \tag{6.2.31}$$

The downstream wavetrain cannot move beyond the step at $x = Q$. The region for a fully detached downstream undular bore can be easily found from (6.2.31) as

$$\Delta - 2u_d - \alpha u_d^2\left(\frac{8}{3}c_4 - \frac{2}{3}c_3 - \frac{1}{3}c_1\right) > 0. \tag{6.2.32}$$

Combining equation (6.2.32) with the criteria (6.2.19), (6.2.22) and (6.2.25), we find the range

$$-\sqrt{3|g_0|} + \alpha|g_0|r_3 < \Delta < \sqrt{12|g_0|} + \alpha|g_0|r_1, \quad \text{where}$$
$$r_3 = \frac{3}{2}c_8 - \frac{7}{36}c_1 - \frac{3}{4}c_3 + 3c_4 - \frac{1}{3}c_5 + \frac{7}{12}c_6, \tag{6.2.33}$$

corresponds to a full downstream bore, whilst a partial bore propagates downstream in the range

$$-\sqrt{12|g_0|} + \alpha|g_0|r_1 < \Delta < -\sqrt{3|g_0|} + \alpha|g_0|r_3. \tag{6.2.34}$$

As for upstream, the modulus squared, m_{0d} of the partial bore, is the solution of (2.3.47). We find the amplitude of the downstream solitary wave by setting $\beta = u_d$. The solitary wave of amplitude $-2u_d$ occurs at the leading edge.

Figure 6.4 shows the parameter ranges in the $\Delta(12g_0)^{-\frac{1}{2}}$ versus $\alpha(\frac{12}{g_0})^{\frac{1}{2}}$ plane for full and partial undular bores, for surface water waves (2.2.14). Shown are (a) Upstream bore

(a)

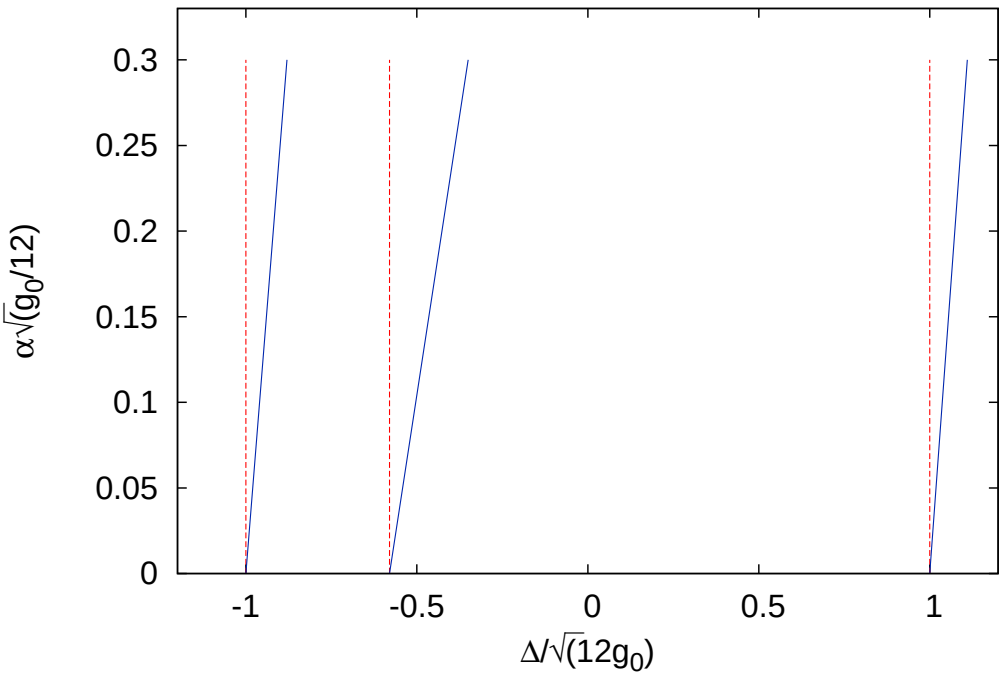

(b)

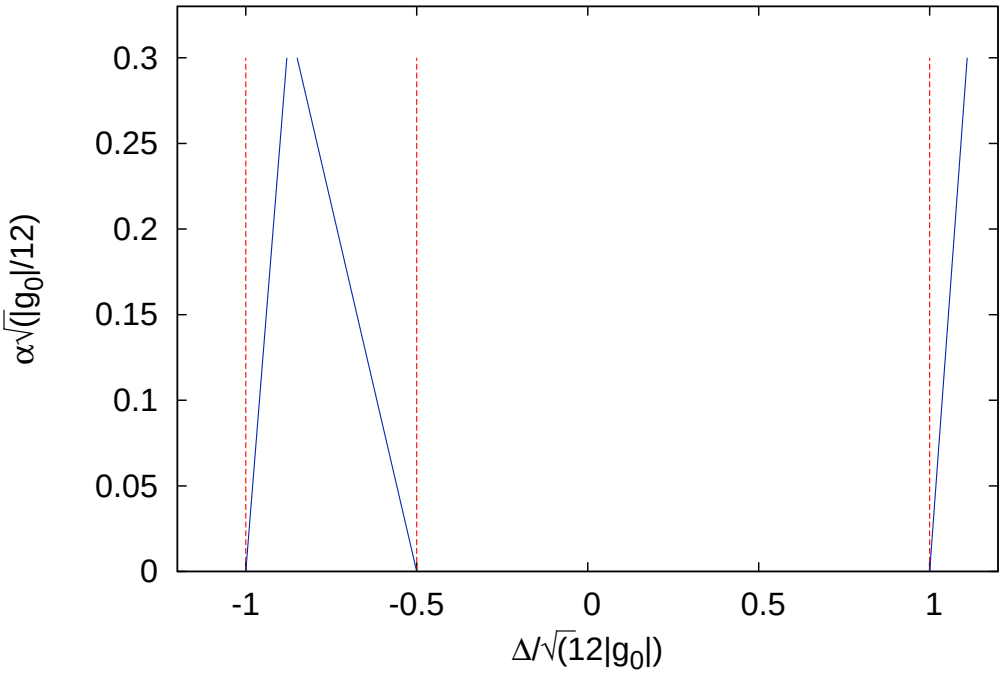

Figure 6.4: The parameter ranges in the $\Delta(12g_0)^{-\frac{1}{2}}$ versus $\alpha(\frac{12}{g_0})^{\frac{1}{2}}$ plane for full and partial undular bores, for surface water waves (2.2.14). Shown are (a) Upstream bore for the ranges (6.2.29) and (6.2.30), and (b) downstream bore for the ranges (6.2.33) and (6.2.34). Compared are eKdV (blue solid line) and KdV (red dashed lines) modulation theory.

for the ranges (6.2.29) and (6.2.30), and (b) downstream bore for the ranges (6.2.33) and (6.2.34). Compared are eKdV and KdV modulation theory. Moving from left to right, the two sets of curves show the subcritical limit of the bore, the transition between the partial and full bore and the supercritical limit of the bore in both figures, one for a full bore and other for a partial bore. The upstream and downstream bores have the same subcritical and supercritical resonant limits; as α increases these limits move toward the supercritical range. A full upstream bore is predicted by KdV theory for strongly subcritical flows and a partial bore for weakly subcritical and all supercritical flows. The transition point in KdV theory between full and partial bores occurs at $\frac{\Delta}{\sqrt{12g_0}} = -0.58$, which not the same point in the localized obstacle. For the downstream bore the transition point in KdV theory between full and partial bores occurs at $\frac{\Delta}{\sqrt{12g_0}} = -0.5$, which like the localized obstacle.

The upstream and downstream undular bore solutions are qualitatively similar to the solutions found for a localized forcing. The wavetrains propagate upstream into the region $x < 0$ and the downstream into the region $x > Q$ from the steps. In the critical case $\Delta = 0$, a partial upstream undular bore occurs, whilst the downstream bore is a full bore. For the subcritical case, the upstream and downstream bores are fully formed. For supercritical cases, a partial upstream undular bore occurs and a full downstream undular bore occurs. Similarly to the isolated obstacle the resonant regimes are slightly different, $-2.44 < \Delta < 2.46$ and $-2.45 < \Delta < 2.45$ for the eKdV and KdV equations, respectively at $\alpha = 0.15$ and $g_0 = 0.5$. The partial upstream bore occurs in the regimes $-1.41 < \Delta < 2.45$ and $-1.36 < \Delta < 2.46$ for the KdV and eKdV equations, respectively. For the full upstream bore, the resonant regimes are $-2.45 < \Delta < -1.41$ and $-2.44 < \Delta < -1.36$ for the KdV and eKdV equations, respectively. The resonant regimes for the full and partial undular bores

upstream are not similar to an isolated obstacle.

However, the resonant regimes, for the full and partial downstream bores are similar to the isolated obstacle at $\alpha = 0.15$ and $g_0 = -0.5$, which are $-1.22 < \Delta < 2.45$ and $-1.25 < \Delta < 2.46$ for a full downstream bore, while the regimes $-2.45 < \Delta < -1.22$ and $-2.44 < \Delta < -1.25$ for a partial downstream bore for the forced KdV and eKdV equations, respectively.

An analysis has been made using the forced eKdV equation to find steady state solutions over positive and negative steps. In the hydraulic limit of a broad step, steady solutions are described for positive g_0 by (6.2.12), (6.2.15) and (6.2.17) and for negative g_0 by (6.2.19), (6.2.22) and (6.2.25). The key parameters of the steady state solution are u_u and u_d, which then generate the undular bore solutions.

Figure 6.5 shows the upstream and downstream steady state solutions over a positive step versus the detuning parameter Δ, for surface water waves (2.2.14), (a) u_u and (b) u_d. Compared are the solutions of the forced eKdV and KdV equations. The other parameters are $\alpha = 0.15$ and $g_0 = 0.5$. The KdV resonant range is $\Delta < 2.45$, while for the eKdV equation it is $\Delta < 2.46$. So the extended resonant range has moved slightly towards the supercritical regime. In Figure 6.5(a), the eKdV steady-state solutions for u_u are greater than the KdV solutions, with the biggest difference for large u_u near the end of the resonant regime. Then, there is a discontinuous jump in u_u to zero, which is beyond the resonant range. For Figure 6.5(b), the eKdV steady state solutions for u_d are also greater than the KdV solutions, for large u_d. As mentioned above, there are three regions, and the steady state is zero for $\Delta < -0.1, 0.0$ for the eKdV and KdV equations, respectively. For positive Δ the eKdV equation u_d values are greater than the KdV results. Outside of the resonant regime, the steady state solutions approaches zero as Δ increases beyond the

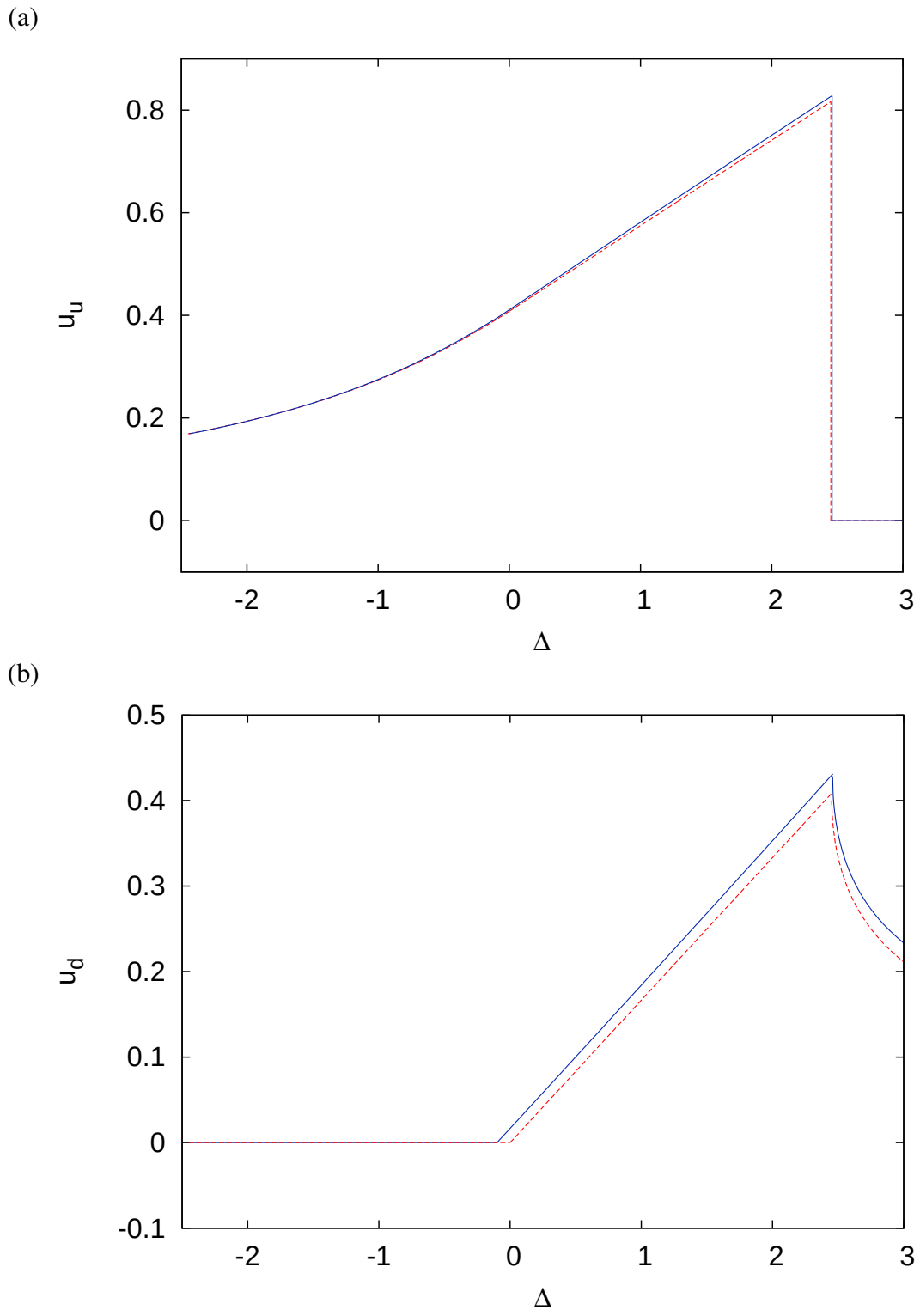

Figure 6.5: Upstream and downstream steady state solutions u_u and u_d over a positive step versus the detuning parameter Δ, for surface water waves (2.2.14). Compared are the forced eKdV (blue solid line) and the forced KdV (red dashed line) equations. The other parameters are $\alpha = 0.15$ and $g_0 = 0.5$.

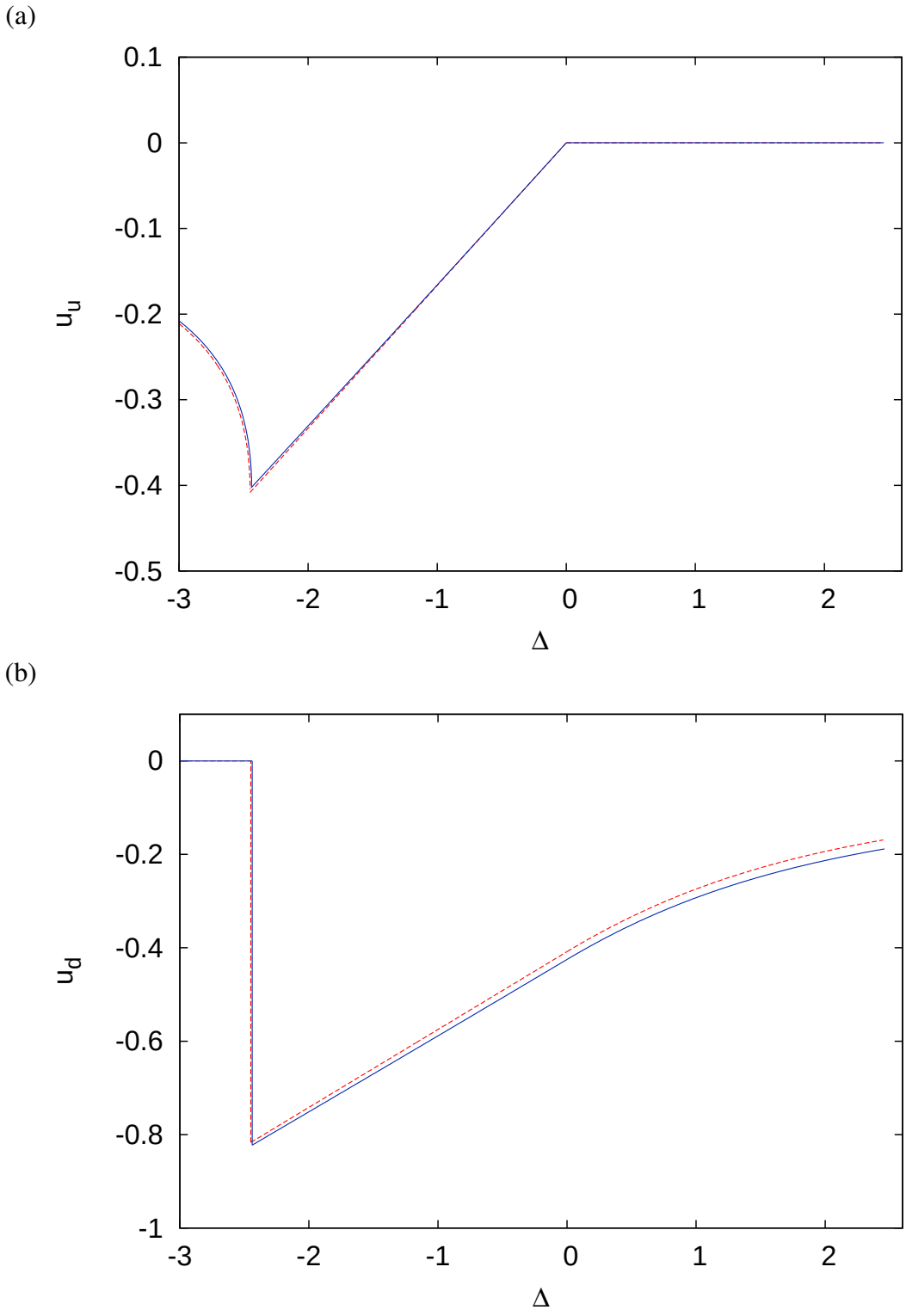

Figure 6.6: Upstream and downstream steady state solutions u_u and u_d over a negative step versus the detuning parameter Δ, for surface water waves (2.2.14). Compared are the forced eKdV (blue solid line) and the forced KdV (red dashed line) equations. The other parameters are $\alpha = 0.15$ and $g_0 = -0.5$.

supercritical limit of resonant flow.

Figure 6.6 shows the upstream and downstream steady state solutions over a negative step versus the detuning parameter Δ, for surface water waves (2.2.14), (a) u_u and (b) u_d. Compared are results for the forced eKdV and KdV equations. The other parameters are $\alpha = 0.15$ and $g_0 = -0.5$. The eKdV resonant range is $\Delta > -2.44$, whilst for KdV it is $\Delta > -2.45$, again a slight move towards the supercritical range. In Figure 6.6(a), there are three regions; the eKdV and KdV upstream steady state solutions u_u are zero for positive Δ. For negative Δ, the eKdV values are slightly larger than the KdV values. Outside of the resonant regime, the solutions are similar for both equations and approach zero as $\Delta \to -\infty$. For Figure 6.5(b), the eKdV steady state solutions for u_d are smaller (but have a large magnitude) than the KdV solutions, with the greatest difference near the end of the resonant regime at $\Delta = 2.46$, and $\Delta = 2.45$ for the eKdV and KdV equations, respectively.

6.3 Comparison with numerical results

Numerical solutions are presented for the behaviour of flow over a step with a finite width. In the present work, we use $g_0 = 0.5$, $W = 0.3$ and $x_L = 50 >> 1$, and the coefficients for surface water waves (2.2.14). The forcing function $G(x)$ as used by Grimshaw et al. (2007b) is

$$G(x) = \frac{g_0}{2}\left[\tanh(xW) - \tanh((x - x_L)W)\right]. \tag{6.3.35}$$

This function represents a step up at $x = 0$ (with $g_0 = 0.5$) and a step down at $x = x_L$ (with $g_0 = -0.5$). So the numerical solutions combine both sets of theoretical results, and represent equations (6.2.12) and (6.2.15) for the upstream solutions over a positive step, and (6.2.19) and (6.2.22) for downstream solutions over a negative step. In the positive

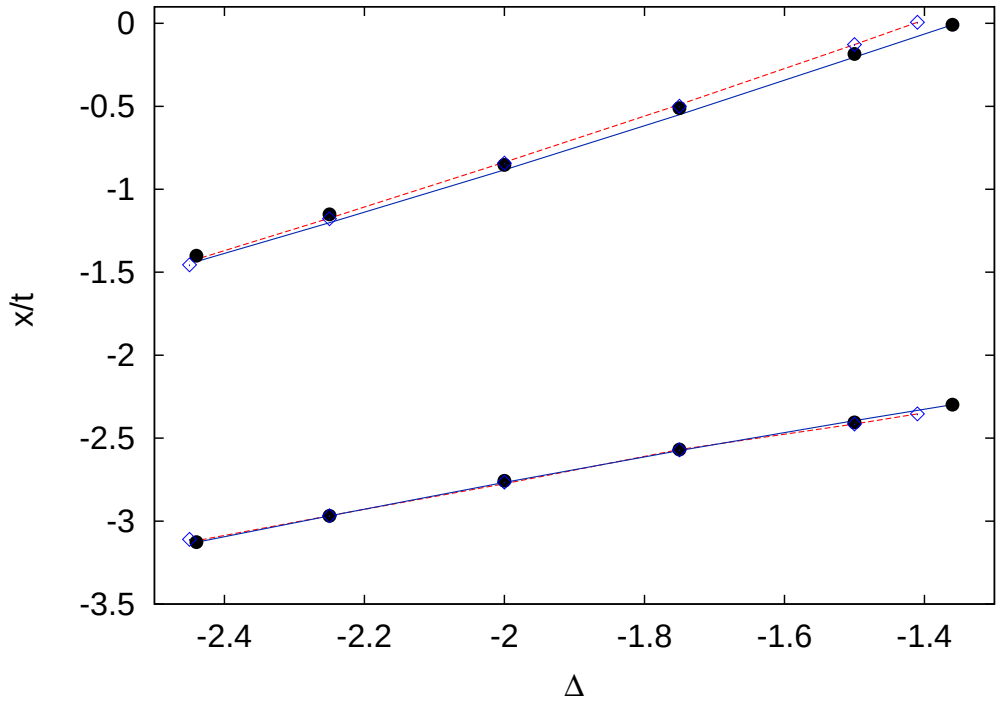

Figure 6.7: Leading and trailing edges of the upstream undular bore versus the detuning parameter Δ, for surface water waves (2.2.14). Shown are modulation theory for the forced eKdV equation (blue solid line) and the forced KdV (red dashed line), and numerical solutions of the forced eKdV ($\bullet$) and KdV ($\diamond$) equations. The forcing is (6.3.35) with $g_0 = 0.5$ and $W = 0.3$. The other parameters are $\alpha = 0.15$ and $g_0 = 0.5$.

step case, a rarefaction wave propagates downstream from $x = 0$, which persists until it reaches $x = 50$ (the end of the step). For the negative step case, a rarefaction wave propagates upstream at $x = Q$, until it reaches $x = 0$. The solutions for the upstream and downstream bores stay separate until $t \approx \frac{50}{|\Delta|}$. For the resonant range of Δ considered here, $-2.44 < \Delta < 2.46$, the solutions stay separate until $t \simeq 20$ for Δ at the ends of the resonant range and for much great times, for values of near zero. At much longer times, as the solutions for the positive and negative steps merge, the solution will approach that for an isolated topography.

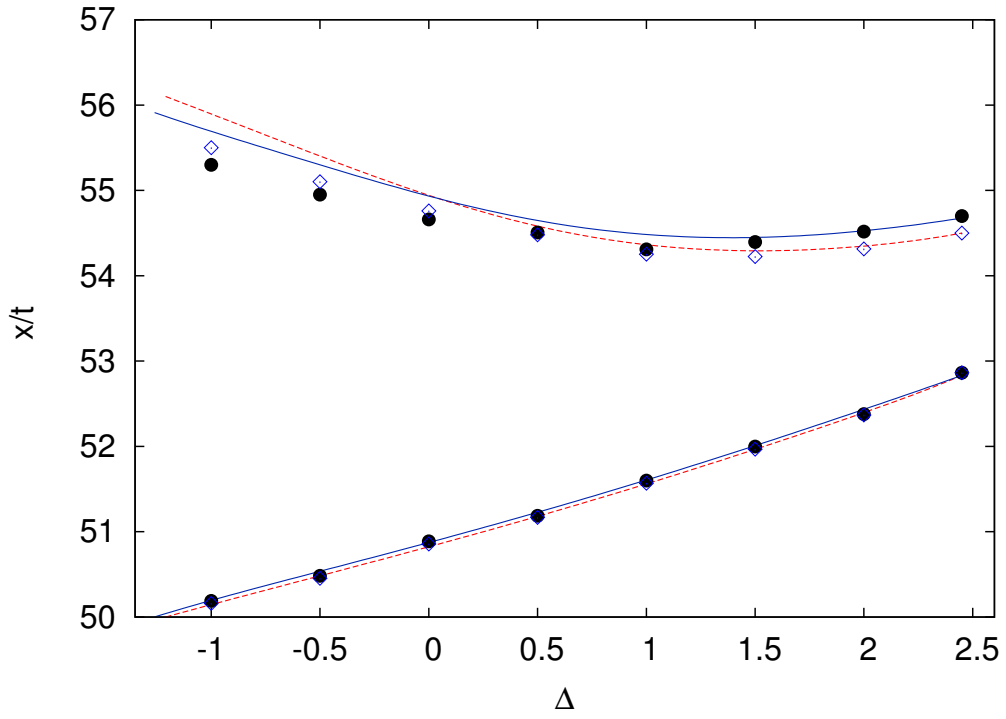

Figure 6.8: Leading and trailing edges of the downstream undular bore versus the detuning parameter Δ, for surface water waves (2.2.14). Shown are modulation theory for the forced eKdV equation (blue solid line) and the forced KdV (red dashed line), and numerical solutions of the forced eKdV ($\bullet$) and KdV ($\diamond$) equations. The forcing is (6.3.35) with $g_0 = 0.5$ and $W = 0.3$. The other parameters are $\alpha = 0.15$ and $g_0 = -0.5$.

Figure 6.7 shows the leading and trailing edges of the upstream undular bore, $\frac{x}{t}$ versus the detuning parameter Δ, for surface water waves (2.2.14). Shown are the numerical solutions and modulation theory solutions of the forced KdV and eKdV equations. The forcing function is the hyperbolic tangent (6.3.35). The other parameters are $g_0 = 0.5$ and $\alpha = 0.15$. For this Figure and Figure 6.8 we define the leading edge to have a larger slope, $\frac{x}{t}$, than that of the trailing edge. Modulation theory shows the eKdV bore is up to 4% narrower than the KdV bore near the end of resonant regime of the full bore. The trailing edge velocity (at which solitary waves occur) for both equations is similar, which are in

good agreement with numerical solutions. The leading edge has zero velocity and is at the forcing when $\Delta = -1.41$ and $\Delta = -1.36$ for the KdV and eKdV cases, respectively. The comparisons with numerical solutions are good and consistent with the differences between the KdV and eKdV modulation theory.

Figure 6.8 shows the leading and trailing edges of the downstream undular bore, $\frac{x}{t}$ versus the detuning parameter Δ, for surface water waves (2.2.14). Shown are the numerical solutions and modulation theory solutions of the forced KdV and eKdV equations. The forcing function is the hyperbolic tangent (6.3.35). The other parameters are $g_0 = -0.5$ and $\alpha = 0.15$. At $\Delta = 0$, the eKdV and KdV values are similar. For negative Δ, the KdV bore extends further, by up to 5% near the end of resonant regime, compared to the eKdV bore. The same effect is seen for an isolated obstacle with a narrower eKdV downstream bore. Unlike a localized obstacle, the eKdV bore is broader than the KdV bore for positive Δ, with a difference of about 4%. The trailing edge has zero velocity and is at the forcing when $\Delta = -1.22$ and $\Delta = -1.25$ for the KdV and eKdV cases, respectively. The velocity of the leading edge (at which linear waves occur) of the eKdV bore is significantly lower for negative Δ and higher for positive Δ compared to the KdV values. The comparisons between the numerical solutions and modulation theory are in excellent over the most of resonant regime with vary up to 6% for subcritical flows cases.

Figure 6.9 shows the upstream solitary wave amplitude versus the detuning parameter Δ, for surface water waves (2.2.14). Shown are the numerical solutions and modulation theory solutions of the forced KdV and eKdV equations. The forcing function is the hyperbolic tangent (6.3.35). The other parameters are $\alpha = 0.15$ and $g_0 = 0.5$. The upstream waves are generated by the step up at $x = 0$, so its given by modulation theory for a pos-

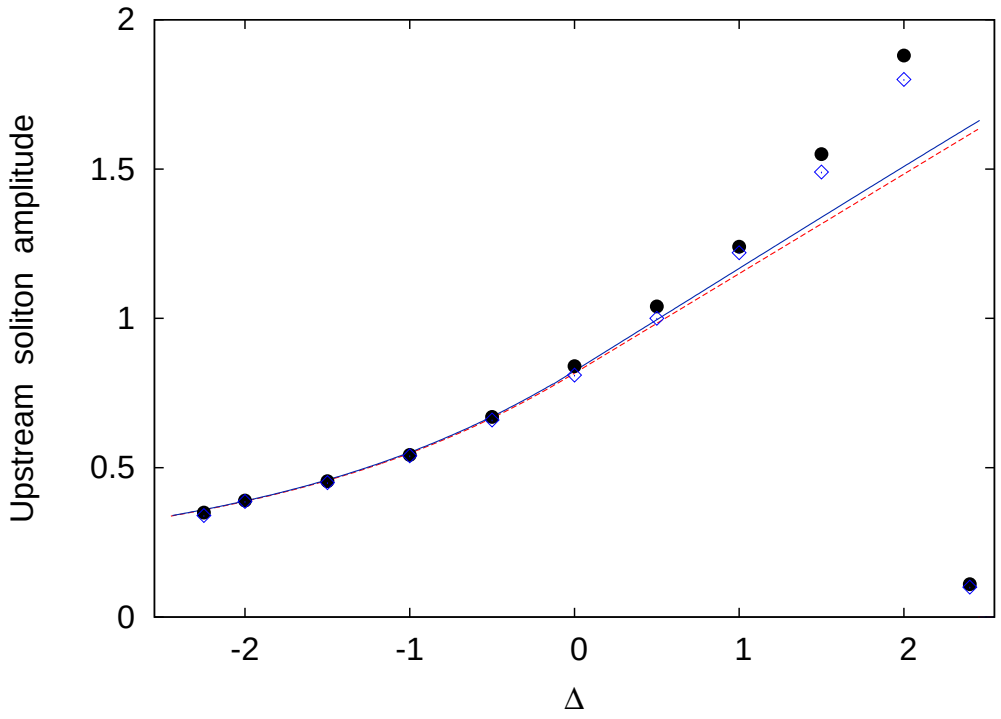

Figure 6.9: Upstream solitary wave amplitude versus the detuning parameter Δ, for surface water waves (2.2.14). Shown are modulation theory for the forced eKdV equation (blue solid line) and the forced KdV (red dashed line), and numerical solutions of the forced eKdV (•) and KdV (⋄) equations. The forcing is (6.3.35) with $g_0 = 0.5$ and $W = 0.3$. The other parameters are $\alpha = 0.15$ and $g_0 = 0.5$.

itive step. The resonant range is $\Delta < 2.46$ and $\Delta < 2.45$ for the eKdV and KdV theories respectively. So the solution is described by the first and second cases for a positive step. The upstream solitary wave amplitudes as predicted by the extended modulation theory are greater than those for the KdV modulation theory over all the resonant regime. The predictions are similar in the subcritical regime, but the difference between the theoretical predications increases in the supercritical regime, with a difference of 3% at $\Delta = 2.46$. The variations between the numerical and theoretical results are small for the strongly subcritical case and the middle of the resonant band, but are slightly larger in supercriti-

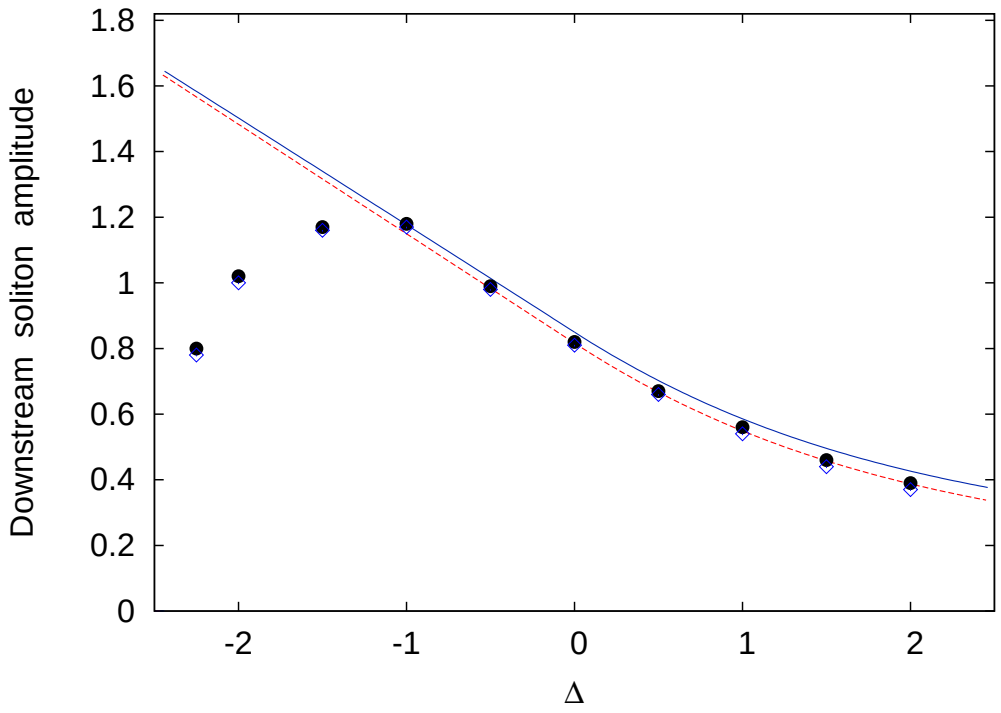

Figure 6.10: Downstream solitary wave amplitude versus the detuning parameter Δ, for surface water waves (2.2.14). Shown are modulation theory for the forced eKdV equation (blue solid line) and the forced KdV (red dashed line), and numerical solutions of the forced eKdV $\bullet$ and KdV ($\diamond$). The forcing is (6.3.35) with $g_0 = 0.5$ and $W = 0.3$. The other parameters are $\alpha = 0.15$ and $g_0 = -0.5$.

cal case, with errors up to 19%, due to the increasing amplitude of the upstream solitary waves. There are also quantitative differences between the numerical results. Note that the numerical solitary wave amplitudes drop quickly, to a near zero amplitude, beyond the resonant band. The upstream solitary wave amplitudes are consistently larger for the forced eKdV equation. For example at $\Delta = 2$, the upstream solitary wave amplitudes are 1.88 and 1.79 for eKdV and KdV models, respectively, with differences of about 5%.

Figure 6.10 shows the downstream solitary wave amplitude versus the detuning parameter Δ, for surface water waves (2.2.14). Shown are numerical solutions and modulation theory solutions for the forced KdV and eKdV equations. The forcing function is

the hyperbolic tangent (6.3.35). The other parameters are $\alpha = 0.15$ and $g_0 = -0.5$. The downstream waves are generated by the step down at $x = 50$ so are given by modulation theory for the negative step, the resonant range is $\Delta > -2.44, -2.45$ for the eKdV and KdV models, respectively. This Figure gives both the first and second cases for a negative step. The downstream solitary wave amplitude as predicted by the eKdV theory is higher than the KdV theory prediction for all values of Δ. There are variations between the theories, with a maximum difference of 9%. The theoretical and numerical results are in agreement in the supercritical case. The difference between the theoretical and numerical results is small for the middle of the resonant band, but for the subcritical regime, the difference increases, with difference up to 6% at $\Delta = -1.22$. As $\Delta \to -2.44$ the solution approaches the edge of the resonant range, beyond which no undular bore occurs. The theory predicts a step change in the amplitude, but the numerical calculations show a smooth change to zero. The numerical results for the forced eKdV and KdV equations are slightly different. The downstream solitary wave amplitude given by the extended equation is greater than for the KdV equation, for example at $\Delta = 2$, the downstream solitary wave amplitude for the forced eKdV equation is 0.39, while the forced KdV equation value is 0.37, with a difference of to 5%.

As for a localized obstacle, the change in amplitude, as predicted by the extended theory, in comparison with the KdV theory is very consistent with the numerical results for both the upstream and downstream wavetrains. Also, the extent of bores vary with the detuning parameter Δ at the resonant regime. Note that the upstream undular bore is formed over a positive step, while the downstream is formed over a negative step.

6.4 Conclusions

We have extended previous studies on resonant flow over a step by considering all the higher-order terms associated with the forced eKdV equation. The results show that an upstream propagating undular bore is generated over a positive step formed by a elevation upstream of the step, and a downstream propagating undular bore is generated over a negative step formed by a depression downstream of the step. Numerical solutions have been found for the obstacle (6.3.35) for both a positive and a negative step. Good agreement was obtained between the theoretical and numerical solutions of the eKdV equation. We have shown that the eKdV predictions for upstream solitary wave amplitudes are higher than the KdV results in supercritical cases, as the amplitudes became large. For the downstream solitary wave amplitudes the differences are not so large as for the upstream case. The eKdV bores are narrower than the KdV ones, both upstream and downstream by up to 4%. The widths of the bores predictions are confirmed by the numerical solutions of the forced eKdV equation.

Chapter 7

Conclusions and future work

This thesis has considered the flow of a fluid over both an isolated topography and a step in the long wavelength, weakly nonlinear limit. Our model is the eKdV equation, which includes higher-order nonlinear, dispersive and nonlinear-dispersive terms beyond the KdV approximation. The basic premise is that the solution contains a locally steady solution that connects the upstream and downstream undular bores over an obstacle or a step. The numerical results from the forced eKdV equation agree very well with the analytical results, and the present results differ to those of the forced KdV equation, for steeper waves. Numerical calculations are presented for transcritical, supercritical and subcritical flows over the obstacle or step.

In Chapter 2 we extended the modulation theory for the forced KdV equation, describing flow over an isolated obstacle, by considering all the higher order nonlinear, dispersive and nonlinear-dispersive terms one-order beyond the KdV approximation. We developed higher-order theoretical predictions to describe the upstream and downstream solitary wave amplitudes and also the width of the bores.

In Chapter 3 we compared the extended modulation theory results from Chapter 2

with the results for the forced KdV equation, for flow over an isolated obstacle. The extended modulation theory gives upstream and downstream solitary wave amplitudes predictions that are higher than the KdV theory. We also compared the theoretical results with numerical simulations of the forced eKdV equation. Generally, the eKdV equation predicts higher upstream solitary wave amplitudes than the KdV model for supercritical flows, and the downstream solitary wave amplitudes also higher for subcritical flows. There is a very good comparison with the numerical results and variations between the eKdV and KdV equations increase for steeper waves.

In Chapter 4 numerical solutions of the forced eBBM equation were also obtained and compared with the extended modulation theory. The motivation for this is that the eBBM equation is asymptotically equivalent to the eKdV equation but stable for steeper waves (α large). The agreement between theory and numerical results is excellent for the upstream solitary wave amplitudes for $\alpha \leqslant 0.25$. However, there is more variation for downstream solitary wave amplitudes, with the eBBM numerical amplitudes significantly lower. It is concluded that the eBBM model is satisfactory for waves of low to moderate steepness. Hence the eBBM equation is extremely useful in numerical studies, due to its superior numerical stability properties.

In Chapter 5 we apply uniform soliton theory to the eKdV model as an alternative way to predict the upstream solitary wave amplitudes. This alternative technique based on the assumption of uniform solitary waves is compared with extended modulation theory and it is found that a good comparison exists for subcritical and moderately supercritical flows.

In Chapter 6 we calculate the higher-order modulation theory for flow over a step. The theory is derived for both positive and negative steps. The results show that an upstream

propagating undular bore is generated over a positive step formed by a elevation upstream of the step, and a downstream propagating undular bore is generated over a negative step formed by a depression downstream of the step. Quantitative agreement is found with numerical solutions. The eKdV equation predicts larger upstream solitary wave amplitudes than the KdV equation, for supercritical flows as the waves are steeper. Also, the width of the bores is lower than for KdV bores.

In summary, we have analytically and numerically demonstrated that the simulations from both the forced eKdV equation and extended modulation theory agree and show that differences occur, compared to the forced KdV equation. The extended modulation theory is to be preferred to KdV modulation theory as the higher-order terms better model steeper waves.

This work gives some indications on the usefulness of the eKdV equation, and offers some options, for future work. We have considered higher-order coefficients appropriate for shallow water waves. Other sets of higher-order coefficients, such as for internal waves could also be derived for the forced full eKdV equation and investigated to determine the effect of higher-order coefficients in other experimental and observational scenarios. It is hoped that this theoretical and numerical study will encourage additional experimental investigations of the flow regimes to better understand the differences between KdV and experimental results.

The extended modulation theory results rely on the use of an asymptotic transformation, which introduces errors at $O(\alpha^2)$. It would be of great interest to use the method of El (2005), which allows the determination of the leading and trailing edges of undular bores corresponding to non-integrable equations. The method could be applied to the

eKdV equation to obtain exact expressions for the solitary wave amplitudes and the width of the bores, in flow regimes when full undular bores occur. However, the application of the method of El (2005) to the problem of partial bores is uncertain and would require extensive investigation to determine if it could be applied, as the partial bore is cut-off at $m = m_0$, rather than at the linear wave edge.

Appendix A

The numerical schemes

A.1 The forced eKdV equation

The forced eKdV equation (2.2.13) numerical is solved using an extension to the classical leapfrog method of Zabusky and Kruskal (1965). It is

$$\begin{aligned} u_i^{j+1} &= u_i^{j-1} - \frac{\Delta t}{\Delta x}\left(\Delta - 6u_i^j + c_1\alpha\left(u_i^j\right)^2\right)\left(u_{i+1}^j - u_{i-1}^j\right) + \frac{\Delta t}{\Delta x^3}\left(u_{i+2}^j - 2(u_{i+1}^j - u_{i-1}^j) - u_{i-2}^j\right) \\ &+ \alpha\frac{\Delta t}{\Delta x^3}\left[c_2\left(u_{i+1}^j - u_{i-1}^j\right)\left(u_{i+1}^j - 2u_i^j + u_{i-1}^j\right) + c_3\left(u_{i+2}^j - 2(u_{i+1}^j - u_{i-1}^j) - u_{i-2}^j\right)u_i^j\right] \\ &+ c_4\alpha\frac{\Delta t}{4\Delta x^5}\left(u_{i+4}^j - 2u_{i+3}^j - 2u_{i+2}^j + 6u_{i+1}^j - 6u_{i-1}^j + 2u_{i-2}^j + 2u_{i-3}^j - u_{i-4}^j\right) \\ &+ c_5\alpha\frac{\Delta t}{\Delta x}\left(u_{i+1}^j - u_{i-1}^j\right)\left(G(x)_i^j\right) + c_6\alpha 2\Delta t u_i^j\left(\frac{dG(x)}{dx}\right)_i^j + c_7\alpha 2\Delta t\left(\frac{d^3G(x)}{dx^3}\right)_i^j \\ &+ 2\Delta t(1 + c_8\alpha\Delta)\left(\frac{dG(x)}{dx}\right)_i^j \end{aligned} \tag{A.1.1}$$

Note that we use a superscript to denote the time level and a subscript to denote the spatial location. Also, the derivatives G_x and G_{xxx} are obtained using analytical expressions instead of from finite-difference approximations. The scheme has truncation error $O(\Delta t^2, \Delta x^2)$ and is stable for small $\Delta t = O(\Delta x^5)$. Typical values used in our computations are the time step $\Delta t = 1 \times 10^{-3}$ and the space step $\Delta x = 4 \times 10^{-3}$. The boundary conditions

used are

$$u_i^j = 0 \quad (j = -3,\ldots,0; \quad i = N+1,\ldots,N+4),$$

on the domain $x = [-L, L]$. The computational domain is large with $L = 600$.

A.2 The forced eBBM equation

Marchant (1999b) used an implicit, three level, finite difference scheme with second-order accuracy. If the solution at time $t = t_j$ is

$$u_i^j = u(t_j = j\Delta t, x_i = i\Delta x), \quad i = 1,\ldots,N,$$

then the implicit finite difference scheme for the forced eBBM equation (4.0.2) is

$$\begin{aligned}
&c_4\alpha^2\frac{1}{\Delta x^4}\left(u_{i+2}^{j+1}+u_{i-2}^{j+1}\right)-\alpha\left(c_4\alpha\frac{4}{\Delta x^4}+\frac{(1-\alpha\Delta)}{\Delta x^2}\right)\left(u_{i+1}^{j+1}+u_{i-1}^{j+1}\right)\\
&+\left(1+c_4\alpha^2\frac{6}{\Delta x^4}+2\alpha\frac{(1-\alpha\Delta)}{\Delta x^2}\right)u_i^{j+1}=c_4\alpha^2\frac{1}{\Delta x^4}\left(u_{i+2}^{j-1}+u_{i-2}^{j-1}\right)\\
&-\alpha\left(c_4\alpha\frac{4}{\Delta x^4}+\frac{(1-\alpha\Delta)}{\Delta x^2}\right)\left(u_{i+1}^{j-1}+u_{i-1}^{j-1}\right)+\left(1+c_4\alpha^2\frac{6}{\Delta x^4}+2\alpha\frac{(1-\alpha\Delta)}{\Delta x^2}\right)u_i^{j-1}\\
&-\frac{\Delta t}{\Delta x}\left(1+\alpha\Delta+6\alpha u_i^j+c_1\alpha^2\left(u_i^j\right)^2\right)\left(u_{i+1}^j-u_{i-1}^j\right)-2\Delta t\alpha(1+c_8\alpha\Delta)\left(\frac{dG(x)}{dx}\right)_i^j\\
&-\alpha^2\frac{\Delta t}{\Delta x^3}\left[c_2\left(u_{i+1}^j-u_{i-1}^j\right)\left(u_{i+1}^j-2u_i^j+u_{i-1}^j\right)+c_3\left(u_{i+2}^j-2(u_{i+1}^j-u_{i-1}^j)-u_{i-2}^j\right)u_i^j\right]\\
&-c_5\alpha^2\frac{\Delta t}{\Delta x}\left(u_{i+1}^j-u_{i-1}^j\right)\left(G(x)_i^j\right)-c_6\alpha^2 2\Delta t u_i^j\left(\frac{dG(x)}{dx}\right)_i^j-c_7\alpha^2 2\Delta t\left(\frac{d^3G(x)}{dx^3}\right)_i^j\\
&i=1,\ldots,N
\end{aligned} \tag{A.2.2}$$

Here, a superscript is used to denote the time level and a subscript to denote the spatial location, where Δt is the time step and Δx is the space step. This scheme is stable for $c_4 > 0$ (as for surface water waves) as no high frequency waves are propagated, while for $c_4 < 0$ the scheme is only stable for very small values of Δt. The boundary conditions used are

$$u_i^j = 0 \quad \forall j, \quad i = -1, 0, N+1, N+2.$$

The space grid points in our computations were separated by $\Delta x = 5 \times 10^{-2}$ and the time step by $\Delta t = 5 \times 10^{-2}$. Also, the accuracy of the numerical method is $\mathrm{O}(\Delta t^2, \Delta x^2)$.

References

Akylas, T. R. (1984). On the excitation of long nonlinear water waves by a moving pressure distribution. *Journal of Fluid Mechanics*, **141**:455–466.

Albalwi, M. D., Marchant, T. R., and Smyth, N. F. (2017). Higher-order modulation theory for resonant flow over topography. *Physics of Fluids*, **29**:077101.

Apel, J., Holbrock, J., Liu, A., and Tsai, J. (1985). The Sulu Sea internal soliton experiment. *Journal of Physical Oceanography*, **15**:1625–1651.

Apel, J. R., Ostrovsky, L. A., Stepanyants, Y. A., and Lynch, J. F. (2007). Internal solitons in the ocean and their effect on underwater sound. *The Journal of the Acoustical Society of America*, **121**:695–722.

Arvelyna, Y. and Oshima, M. (2007). New Application of Wavelet Transform for Internal Wave Detection SAR and Optical Image: A Case Study in Japan Waters. *In OCEANS 2007-Europe* , **IEEE**:1–6.

Baines, P. (1977). Upstream influence and Long's model in stratified flows. *Journal of Fluid Mechanics*, **82**:147–159.

Baines, P. G. (1981). Satellite observations of internal waves on the Australian north-west shelf. *Australian Journal of Marine and Freshwater Research*, **32**:457–463.

Baines, P. G. (1979). Observation of stratified flow over two-dimensional obstacles in fluid of finite depth. *Tellus*, **31**:351–371.

Baines, P. G. (1984). A unified description of two-layer flow over topography. *Journal of Fluid Mechanics*, **146**:127–167.

Baines, P. G. (1995). *Topographic effects in stratifed flows*. Cambridge University Press, Cambridge.

Benjamin, T. B., Bona, J. L., and Mahony, J. J. (1972). Model equations for long waves in nonlinear dispersive systems. *Proceedings of the Royal Society of London A: Mathematical, Physical and Engineering Sciences*, **272**:47–78.

Binder, B. J., Blyth, M. G., and Balasuriya, S. (2015). Steady free-surface flow over spatially periodic topography. *Journal of Fluid Mechanics*, **781**:R3.

Binder, B. J., Dias, F., and Vanden-Broeck, J.-M. (2006). Steady free-surface flow past an uneven channel bottom. *Theoretical and Computational Fluid Dynamics*, **20**:125–144.

Bona, J., Pritchard, W., and Scott, L. (1985). Numerical schemes for a model of nonlinear dispersive waves. *Journal of Computational Physics*, **60**:167–186.

Boussinesq, J. (1871). Théorie de l'intumescence liquide appelée 'onde solitaire' ou de 'translation', se propageant dans un canal rectangulaire. *Comptes Rendus Academie Sciences Paris*, 72:755–759.

Boussinesq, J. (1877). *Essai sur la th'eorie des eaux courantes*. Acad'emie des Sciences de l'Institut de France, M'emoires pr'esent'es par divers savants (**ser 2**) 23:1-680.

Burde, G. I. (2011). Solitary wave solutions of the high-order KdV models for bi-directional water waves. *Communications in Nonlinear Science and Numerical Simulation*, **16**:1314–1328.

Chen, C. Y. (2007). An experimental study of stratified mixing caused by internal solitary waves in a two-layered fluid system over variable seabed topography. *Ocean Engineering*, **34**:1995–2008.

Chen, H.-H. and Liu, C.-S. (1978). Nonlinear wave and soliton propagation in media with arbitrary inhomogeneities. *Physics of Fluids*, **21**:377–380.

Choi, H. and Kim, H. (2016). The hyperbolic relaxation systems for the forced KdV equations with hydraulic falls. *European Journal of Mechanics-B/Fluids*, **58**:20–28.

Choi, J., Lin, T., Sunb, S., and Whang, S. (2010). Supercritical surface waves generated by a negative or oscillatory forcing. *Discrete and Continuous Dynamical Systems-Series B*, **14**:1313–1335.

Choi, J., Sun, S., and Whang, S. (2008). Supercritical surface gravity waves generated by a positive forcing. *European Journal of Mechanics B/Fluids*, **27**:750–770.

Cole, S. L. (1985). Transient waves produced by flow past a bump. *Wave Motion*, **7**:579–587.

Craik, A. D. (2004). The origins of water waves theory. *Annual Review of Fluid Mechanics*, **36**:1–28.

Darrigol, O. (2003). The spirited horse, the engineer, and the mathematician: Water waves in nineteenth-century hydrodynamics. *Archive for History of Exact Sciences* , **58**:21–95.

Davis, R. E. and Acrivos, A. (1967). Solitary internal waves in deep water. *Journal of Fluid Mechanics*, **29**:593–607.

Driscoll, C. F. and O'Neil, T. M. (1976). Modulational instability of cnoidal wave solutions of the modified Korteweg-de Vries equation. *Journal of Mathematical Physics*, **17**:1196–1200.

Ee, B., Grimshaw, R., Chow, K., and Zhang, D.-H. (2011). Steady transcritical flow over an obstacle: Parametric map of solutions of the forced extended Korteweg-de Vries equation. *Physics of Fluids*, **23**:046602.

Ee, B., Grimshaw, R., Zhang, D.-H., and Chow, K. (2010). Steady transcritical flow over a hole: Parametric map of solutions of the forced Korteweg-de Vries equation. *Physics of Fluids*, **22**:056602.

El, G. and Hoefer, M. (2016). Dispersive shock waves and modulation theory. *Physica D: Nonlinear Phenomena*, **333**:11–65.

El, G. A. (2005). Resolution of a shock in hyperbolic systems modified by weak dispersion. *Chaos: An Interdisciplinary Journal of Nonlinear Science*, **15**:037103.

El, G. A., Grimshaw, R. H., and Smyth, N. F. (2006). Unsteady undular bores in fully nonlinear shallow-water theory. *Physics of Fluids*, **18**:027104.

El, G. A., Grimshaw, R. H., and Smyth, N. F. (2009). Transcritical shallow-water flow past topography: finite-amplitude theory. *Journal of Fluid Mechanics*, **640**:187–214.

El, G. A. and Grimshaw, R. H. J. (2002). Generation of undular bores in the shelves of slowly-varying solitary waves. *Chaos: An Interdisciplinary Journal of Nonlinear Science*, **12**:1015–1026.

El, G. A., Grimshaw, R. H. J., and Kamchatnov, A. M. (2007). Evolution of solitary waves and undular bores in shallow-water flows over a gradual slope with bottom friction. *Journal of Fluid Mechanics*, **585**:213–244.

El, G. A., Grimshaw, R. H. J., and Tiong, W. K. (2012). Transformation of a shoaling undular bore. *Journal of Fluid Mechanics*, **709**:371–395.

Fermi, E., Pasta, J., and Ulam, S. (1955). Studies of nonlinear problems. *Document LA-1940*, **46**:490–502.

Fornberg, B. and Whitham, G. B. (1978). A numerical and theoretical study of certain nonlinear wave phenomena. *Proceedings of the Royal Society of London A: Mathematical, Physical and Engineering Sciences*, **289**:373–403.

Gardner, C. S., Greene, J. M., Kruskal, M. D., and Miura, R. M. (1967). Method for solving the Korteweg-de Vries equation. *Physical Review Letters*, **19**:1095.

Gong, L. and Shen, S. (1994). Multiple supercritical solitary wave solutions of the stationary forced Korteweg-de Vries equation and their stability. *SIAM Journal on Applied Mathematics*, **54**:1268–1290.

Gourlay, T. P. (2010). Hydrodynamic effects on fast monohulls or catamarans travelling through the critical speed in shallow water. *ANZIAM Journal*, **51**:C137–C154.

Grimshaw, R. (2003). *Internal solitary waves*. Environmental Stratified Flows, Springer US.

Grimshaw, R. (1970). The solitary wave in water of variable depth. *Journal of Fluid Mechanics*, **42**:639–656.

Grimshaw, R. (2010). Transcritical flow past an obstacle. *The ANZIAM Journal*, **52**:2–26.

Grimshaw, R. and Maleewong, M. (2013). Stability of steady gravity waves generated by a moving localised pressure disturbance in water of finite depth. *Physics of Fluids*, **25**:076605.

Grimshaw, R. and Maleewong, M. (2015). Critical control in transcritical shallow-water flow over two obstacles. *Journal of Fluid Mechanics*, **780**:480–502.

Grimshaw, R., Maleewong, M., and Asavanant, J. (2009a). Stability of gravity-capillary waves generated by a moving pressure disturbance in water of finite depth. *Physics of Fluids*, **21**:082101.

Grimshaw, R. and Pelinovsky, E. (2002). Interaction of a solitary wave with an external force in the extended Korteweg-de Vries equation. *International Journal of Bifurcation and Chaos* , **12**:2409–2420.

Grimshaw, R., Pelinovsky, E., and Poloukhina, O. (2002a). Higher-order Korteweg-de Vries models for internal solitary waves in a stratified shear flow with a free surface. *Nonlinear Processes in Geophysics*, **9**:221–235.

Grimshaw, R., Pelinovsky, E., Stepanyants, Y., and Talipova, T. (2006). Modelling internal solitary waves on the Australian North West Shelf. *Marine and Freshwater Research*, **57**:265–272.

Grimshaw, R., Pelinovsky, E., and Talipova, T. (2007a). Modelling internal solitary waves in the coastal ocean. *Surveys in Geophysics*, **28**:273–298.

Grimshaw, R., Pelinovsky, E., and Talipova, T. (1997). The modified Korteweg-de Vries equation in the theory of large-amplitude internal waves. *Nonlinear Processes in Geophysics*, **4**:237–250.

Grimshaw, R., Pelinovsky, E., Talipova, T., and Kurkina, O. (2010). Internal solitary waves: propagation, deformation and disintegration. *Nonlinear Processes in Geophysics*, **17**:633–649.

Grimshaw, R., Pelinovsky, E., and Tian, X. (1994). Interaction of a solitary wave with an external force. *Physica D: Nonlinear Phenomena*, **77**:405–433.

Grimshaw, R., Zhang, D., and Chow, K. (2009b). Transcritical flow over a hole. *Studies in Applied Mathematics*, **122**:235–248.

Grimshaw, R., Zhang, D., and Chow, K. (2007b). Generation of solitary waves by transcritical flow over a step. *Journal of Fluid Mechanics*, **587**:235–254.

Grimshaw, R. H. J., Chan, K. H., and Chow, K. W. (2002b). Transcritical flow of a stratified fluid: The forced extended Korteweg-de Vries model. *Physics of Fluids*, **14**:755.

Grimshaw, R. H. J. and Smyth, N. F. (1986). Resonant flow of a stratified fluid over topography. *Journal of Fluid Mechanics*, **169**:429–467.

Gurevich, A. V. and Pitaevskii, L. P. (1974). Nonstationary structure of a collisionless shock waves. *Soviet Journal of Experimental and Theoretical Physics*, **38**:291–297.

Hammack, J. L. and Segur, H. (1974). The Korteweg-de Vries equation and water waves. Part 2. Comparison with experiments. *Journal of Fluid Mechanics*, **65**:289–314.

Hanazaki, H. (1992). A numerical study of nonlinear waves in a transcritical flow of stratified fluid past an obstacle. *Physics of Fluids A: Fluid Dynamics*, **10**:2230–2243.

Hasegawa, A. and Tappert, F. (1973). Transmission of stationary nonlinear optical pulses in dispersive dielectric fibers. I. Anomalous dispersion. *Applied Physics Letters*, **23**:142–144.

Helfrich, K. and Melville, W. (2006). Long nonlinear internal waves. *Annual Review of Fluid Mechanics*, **38**:395–425.

Hirota, R. (1973). Exact envelope-soliton solutions of a nonlinear wave equation. *Journal of Mathematical Physics*, **14**:805.

Hirota, R. (1972). Exact solution of the sine-Gordon equation for multiple collisions of solitons. *Journal of the Physical Society of Japan* , **33**:1459–1463.

Hirota, R. (1971). Exact solution of the Korteweg-de Vries equation for multiple collisions of solitons. *Physical Review Letters*, **27**:1192–1194.

Holloway, P., Pelinovsky, E., Talipova, T., and Barnes, B. (1997). A Nonlinear model of internal tide transformation on the Australian North West Shelf. *Journal of Physical Oceanography*, **27**:871–896.

Huang, D. B., Sibul, O. J., Webster, W. C., Wehausen, J. V., Wu, D. M., and Wu, T. L. (1982). Ships moving in the transcritical range. *Proceedings Conference on Behaviour of Ships in Restricted Waters, Varna*, **2**:26–1–26–10.

Kamchatnov, A., Kuo, Y., Lin, T., Horng, T., Gou, S., Clift, R., El, G., and Grimshaw, R. (2013). Transcritical flow of a stratified fluid over topography: analysis of the forced Gardner equation. *Journal of Fluid Mechanics*, **736**:495–531.

Kamchatnov, A., Kuo, Y., Lin, T., Horng, T., Gou, S., Clift, R., El, G., and Grimshaw, R. (2012). Undular bore theory for the Gardner equation. *Physical Review E*, **86**:036605.

Karczewska, A., Rozmej, P., and Infeld, E. (2014a). Shallow-water soliton dynamics beyond the Korteweg-de Vries equation. *Physical Review E*, **90**:012907.

Karczewska, A., Rozmej, P., and Rutkowski, . (2014b). A new nonlinear equation in the shallow water wave problem. *Physica Scripta*, **89**:054026.

King, A. C. and Bloor, M. I. (1987). Free-surface flow over a step. *Journal of Fluid Mechanics*, **182**:193–208.

Korteweg, D. J. and de Vries, G. (1895). On the change of form of long waves advancing in a rectangular canal, and on a new type of long stationary waves. *Philosophical Magazine*, **39**:422–443.

Lagrange, J. (1781). Mmoire sur la thorie du mouvement des fluides. Nouv. Mem. Acad. *Acadmie de Berlin, Mmoires, also in Lagrange 18671892*, **4**:695748.

Lagrange, J. (1786). Sur la mani‘ere de rectifier deux entroits des Principes de Newton relatifs ‘a la propagation du son et au mouvement des ondes. *Nouveaux mmoires de l’Acadmie royale des sciences et belles-lettres de Berlin, anne*, **5**:591609.

Lamb, H. (1997). *Hydrodynamics*. Cambridge University Press, Cambridge.

Lamb, K. and Yan, L. (1996). The evolution of internal wave undular bores: Comparisions of a fully nonlinear numerical model with weakly nonlinear theory. *Journal of Physical Oceanography*, **26**:2712–2734.

Lee, S. and Whang, S. (2015). Trapped supercritical waves for the forced KdV equation with two bumps. *Applied Mathematical Modelling*, **39**:2649–2660.

Lee, S. J., Yates, G. T., and Wu, T. Y. (1989). Experiments and analyses of upstream-advancing solitary waves generated by moving disturbances. *Journal of Fluid Mechanics*, **199**:569–593.

Luke, J. C. (1967). A variational principle for a fluid with a free surface. *Journal of Fluid Mechanics*, **27**:395–397.

Marchant, T. (1999a). Asymptotic solitons of the extended Korteweg-de Vries equation. *Physical Review E*, **59**:3745–3748.

Marchant, T. and Smyth, N. (2012). Approximate techniques for dispersive shock waves in nonlinear media. *Journal of Nonlinear Optical Physics and Materials*, **21**:1250035.

Marchant, T. and Smyth, N. (1991). Initial-boundary value problems for the Korteweg-de Vries equation. *Journal of Applied Mathematics*, **47**:247–264.

Marchant, T. R. (2004). Asymptotic solitons for a third-order Korteweg-de Vries equation. *Chaos, Solitons & Fractals*, **22**:261–270.

Marchant, T. R. (2008). Undular bores and the initial-boundary value problem for the modified korteweg-de vries equation. *Wave Motion*, **45**:540–555.

Marchant, T. R. (1999b). Coupled Korteweg-de Vries equations describing, to high-order, resonant flow of a fluid over topography. *Physics of Fluids*, **11**:1797–1804.

Marchant, T. R. (2000). Solitary wave interaction for the extended BBM equation. *Proceedings of the Royal Society of London A: Mathematical, Physical and Engineering Sciences*, **456**:433–453.

Marchant, T. R. (2002a). Asymptotic solitons for a higher-order modified Korteweg-de Vries equation. *Physical Review E*, **66**:046623.

Marchant, T. R. (2002b). Higher-order interaction of solitary waves on shallow water. *Studies in Applied Mathematics*, **109**:1–17.

Marchant, T. R. and Smyth, N. F. (1990). The extended Korteweg-de Vries equation and the resonant flow of a fluid over topography. *Journal of Fluid Mechanics*, **221**:263–287.

Marchant, T. R. and Smyth, N. F. (2002). The initial boundary problem for the Korteweg-de Vries equation on the negative quarter-plane. *Proceedings of the Royal Society of London A: Mathematical, Physical and Engineering Sciences*, **458**:857–871.

Marchant, T. R. and Smyth, N. F. (2006a). An undular bore solution for the higher-order Korteweg-de Vries equation. *Journal of Physics A: Mathematical and General*, **39**:L563–L569.

Marchant, T. R. and Smyth, N. F. (1996). Soliton interaction for the extended Korteweg-de Vries equation. *Journal of Applied Mathematics*, **56**:157–176.

Marchant, T. R. and Smyth, N. F. (2006b). Undular bore solution of the Camassa-Holm equation. *Physical Review E*, **73**:057602.

Matsutani, S. and Tsuru, H. (1991). Reflectionless quantum wire. *Journal of the Physical Society of Japan*, **60**:3640–3644.

McIntyre, M. E. (1972). On Long's hypothesis of no upstream influence in uniformly stratified or rotating flow. *Journal of Fluid Mechanics*, **52**:209–242.

Mei, C. C. (1986). Radiation of solitons by slender bodies advancing in a shallow channel. *Journal of Fluid Mechanics*, **162**:53–67.

Melville, W. K. and Helfrich, K. R. (1987). Transcritical two-layer flow over topography. *Journal of Fluid Mechanics*, **178**:31–52.

NASA (2003). Internal waves in the Sulu Sea. *http://earthobservatory.nasa.gov/IOTD/view.php?id=3586*, **1**:July.

NASA (2006). Internal waves in the Tsushima Strait. *http://earthobservatory.nasa.gov/IOTD/view.php?id=7230*, **21**:December.

Newton, I. (1687). *Philosophi naturalis principia mathematica (Translation by Andrew Motte 1995)*. New York: Prometheus Books.

Olver, P. J. (1979). Euler operators and conservation laws of the BBM equation. *Mathematical Proceedings of the Cambridge Philosophical Society*, **85**:134–160.

Ostrovsky, L. A. and Stepanyants, Y. A. (2005). Internal solitons in laboratory experiments: comparison with theoretical models. *Chaos: An Interdisciplinary Journal of Nonlinear Science*, **15**:037111.

Peregrine, D. (1966). Calculations of the development of an undular bore. *Journal of Fluid Mechanics*, **25**:321–330.

Perel'man, T., Fridman, A., and El'yashevich, M. (1974). A modified Korteweg-de Vries equation in electrohydrodynamics. *Soviet physics, Journal of experimental and theoretical physics*, **39**:643–646.

Porter, V. A. and Smyth, N. F. (2002). Modelling the morning glory of the Gulf of Carpentaria. *Journal of Fluid Mechanics*, **454**:1–20.

Rayleigh, L. (1876). On Waves. *Philosophical Magazine*, **1**:257–279.

Ruderman, M. S., Talipova, T., and Pelinovsky, E. (2008). Dynamics of modulationally unstable ion-acoustic wavepackets in plasmas with negative ions. *Journal of Plasma Physics*, **74**:639–656.

Russell, J. S. (1844). Report on waves; rept. fourteenth meeting of the British association for the advancement of science. *John Murray, London*, pages 311–390.

Shen, S. (1995). On the accuracy of the stationary forced Korteweg-de Vries equation as a model equation for flows over a bump. *Quarterly of Applied Mathematics*, **53**:701–7195.

Smyth, N. and Holloway, P. (1988). Hydraulic jump and undular bore formation on a shelf break. *Journal of Physical Oceanography*, **18**:947–962.

Smyth, N. F. (1988). Dissipative effects on the resonant flow of a stratified fluid over topography. *Journal of Fluid Mechanics*, **192**:287–312.

Smyth, N. F. (1987). Modulation theory solution for resonant over topography. *Proceedings of the Royal Society of London A: Mathematical, Physical and Engineering Sciences*, **409**:79–97.

Smyth, N. F. (1990). Formation of one dimensional waves for resonant flow in a channel. *Pure and Applied Geophysics*, **133(4)**:619–633.

Sprenger, P. and Hoefer, M. (2017). Shock waves in dispersive hydrodynamics with nonconvex dispersion. *SIAM Journal on Applied Mathematics*, **77**:26–50.

Stoker, J. J. (1957). Water Waves. The mathematical theory with applications. Intersecience, New York.

Su, C. H. and Gardner, C. S. (1969). Korteweg-de Vries equation and generalisations III. Derivation of the Kortwewg-de Vries equation and Burgers equation. *Journal of Mathematical Physics*, **10**:536–539.

Thews, J. G. and Landweber, L. (1935). The influence of shallow water on the resistance of a cruiser model. *United States Experimental Model Basin, Navy Yard, Washington*, **Report No. 408**.

Thews, J. G. and Landweber, L. (1936). A thirty-inch model of the S. S. Clairton in shallow water. *United States Experimental Model Basin, Navy Yard, Washington*, **Report No. 414**.

Vanden-Broeck, J.-M. (1987). Free-surface flow over an obstruction in a channe. *The Physics of fluids*, **30**:2315–2317.

Vassilev, V. M., Djondjorov, P. A., Hadzhilazova, M. T., and Mladenov, I. M. (2011). Traveling wave solutions of the Gardner equation and motion of plane curves governed by the mKdV flow. *AIP Conference Proceedings*, **1404**:86–93.

Watanabe, S. (1984). Ion acoustic soliton in plasma with negative ion. *Journal of the Physical Society of Japan*, **53**:950–956.

Whitham, G. (1965a). A general approach to linear and non-linear dispersive waves using a Lagrangian. *Journal of Fluid Mechanics*, **22**:273–283.

Whitham, G. (1965b). Non-linear dispersive waves. *Proceedings of the Royal Society of London A: Mathematical, Physical and Engineering Sciences*, **283**:238–261.

Whitham, G. B. (1974). *Linear and nonlinear waves*. Wiley New York.

Wu, D. M. and Wu, T. L. (1982). Three-dimensional nonlinear long waves due to moving surface pressure. *Proceedings of 14th Symposium on Naval Hydrodynamics, Washington, DC .National Academy Press*, pages 103–125.

Wu, T. Y. (1987). Generation of upstream advancing solitons by moving disturbances. *Journal of Fluid Mechanics*, **184**:75–99.

Zabusky, N. J. and Kruskal, M. D. (1965). Interaction of solitons in a collisionless plasma and the recurrence of initial states. *Physical Review Letters*, **15**:240–243.

Zakharov, V. E. (1968). Stability of periodic waves of fnite amplitude on the surface of a deep fluid. *Journal of Applied Mechanics and Technical Physics*, **9**:190–194.

Zakharov, V. E. and Shabat, A. B. (1972). Exact theory of two-dimensional self-focusing and one-dimensional self-modulation of waves in nonlinear media. *Journal of Experimental and Theoretical Physics*, **34**:62–69.

Zhang, D. H. and Chwang, A. T. (1996). Numerical study of nonlinear shallow water waves produced by a submerged moving disturbance in viscous flow. *Physics of Fluids*, **8**:147–155.

Zhang, D. H. and Chwang, A. T. (2001). Generation of solitary waves by forward- and backward-step bottom forcing. *Journal of Fluid Mechanics*, **432**:341–350.

Zhang, H. P., King, B., and Swinney, H. (2007). Experimental study of internal gravity waves generated by supercritical topography. *Physics of Fluids*, **19**:096602.

Zhang, Y. L. and Zhu, S. P. (1997). Subcritical, transcritical and supercritical flows over a step. *Journal of Fluid Mechanics*, **333**:257–271.